THE EFFECTS OF MULTIPLE UNLOADING EXPOSURES ON BONE PROPERTIES IN THE FEMUR OF ADULT MALE RATS

A Thesis

by

DERRICK SCOTT MORGAN

Submitted to the Office of Graduate Studies of
Texas A&M University
in partial fulfillment of the requirements for the degree of

MASTER OF SCIENCE

May 2012

Major Subject: Mechanical Engineering

THE EFFECTS OF MULTIPLE UNLOADING EXPOSURES ON BONE PROPERTIES IN THE FEMUR OF ADULT MALE RATS

A Thesis

by

DERRICK SCOTT MORGAN

Submitted to the Office of Graduate Studies of
Texas A&M University
in partial fulfillment of the requirements for the degree of

MASTER OF SCIENCE

Approved by:

Chair of Committee,	Harry A. Hogan
Committee Members,	Susan Bloomfield
	Richard Malak
Head of Department,	Jerry Caton

May 2012

Major Subject: Mechanical Engineering

ABSTRACT

The Effects of Multiple Unloading Exposures on Bone Properties in the Femur of Adult Male Rats. (May 2012)

Derrick Scott Morgan, B.S., Baylor University;

M.S., Baylor University

Chair of Advisory Committee: Dr. Harry A. Hogan

NASA goals include long-term International Space Station (ISS) missions and the ambitious objective of eventually sending astronauts to Mars. Unfortunately, exposure to unloading due to microgravity during spaceflight has been shown to cause detrimental health effects on bone. Therefore, NASA is seeking a ground-based animal model to study the long-term effects of unloading on bone in order to better insure the health and mission capability of astronauts. The hindlimb unloaded (HU) rat model was used to study the effects of multiple unloading exposures and aging on bone properties. Six month old, adult, male Sprague-Dawley rats were separated into the following groups: baseline (BL, sacrificed when received at 6 months age), aging cage control (AC, normal weight-bearing cage activity), 1HU7 (unloaded for 1 month starting at 7 months of age and allowed to recover for 3 months), 1HU10 (normal cage activity until 10 months of age, unloaded for 1 month, recovered for 2 months), and 2HU10 (unloaded for 1 month at 7 months of age, allowed to recover for 2 months, unloaded again for 1 month at 10 months of age, followed by 2 months of recovery). Every 28 days a subset of animals (n=15) were euthanized and both femurs were excised. A peripheral quantitative computed tomography (pQCT) scanner was used to collect densitometric and geometric properties at the right and left femoral neck and at the left femoral midshaft. Mechanical testing (axial and lateral compression of the femoral neck and 3pt bending of the

midshaft) was performed at each location and strength indices based on pQCT parameters were calculated.

Femoral neck properties decreased due to HU but recovered with respect to increase over HU, BL, and AC by the end of the recovery periods. Femoral midshaft properties were relatively unaffected, but did show slight decreases for older animals at month 10, which recovered during the two month recovery period. Femoral neck geometry exhibited increased endocortical resorption and periosteal apposition of the cortical shell which suggests that trabecular bone plays an important role in how the total bone is affected by HU. Densitometric properties were affected less by HU with respect to BL than were mechanical strength values. Results suggest that femoral neck is more affected by unloading than midshaft, particularly for multiple exposures of unloading. Also, aging does not appear to be a critical factor for bone loss due to HU for either femoral neck or midshaft.

NOMENCLATURE

vBMD	Volumetric Bone Mineral Density
BMC	Bone Mineral Content
FN	Femoral Neck
FD	Femur Diaphysis
TD	Tibia Diaphysis
HU	Hindlimb Unloaded
BL	Baseline
AC	Aging Cage Control
MNCS	Minimum Cross-Sectional Area
EM	Elastic Modulus
pQCT	Peripheral Quantitative Computed Tomography
μCT	Micro Computed Tomography
PBS	Phosphate Buffered Saline
ROI	Region of Interest
SSI	Structural Strength Index
BSI	Bending Strength Index
CSI	Compressive Strength Index
ISS	International Space Station

TABLE OF CONTENTS

LIST OF FIGURES

Page

LIST OF TABLES

Page

INTRODUCTION

Rationale

The human skeleton has evolved to perform numerous bodily functions necessary for survival beyond its obvious structural uses, including mineral homeostasis and hematopoiesis as well as locomotion and vital organ protection (1). The skeleton's ability to perform all of these functions comes from the unique properties of bone. Bone serves as the primary structural foundation and support structure of the body by being stiff and strong, while maintaining enough elasticity to absorb the energy from locomotion. This allows the long bones found in the arms and legs as well as the spinal vertebrae to serve as part of the body's shock absorption system. Also, the impressive strength of healthy bone makes it an ideal material for protecting vital organs by forming the rib cage, spine, and cranium.

In order to maintain proper function the human body must maintain mineral and electrolyte thresholds in a process known as homeostasis, and bone serves as a natural reservoir for these necessary minerals. When needed, the body can temporarily reclaim the stored resources in order to maintain the overall homeostasis of the organism. Also, hematopoiesis, the generation of blood cell components, takes place in the bone marrow found within bones. The bone marrow creates a steady supply of components so that new blood cells can be formed throughout the day in order for proper blood flow and function. Finally, bone provides a firm vantage point for muscles to attach to by way of tendons, in order to provide the mechanical leverage that allows for normal locomotion of the body.

This thesis follows the style of the Journal of Bone and Mineral Research (JBMR).

However, the most important characteristic of bone is its ability to adapt to changes and stresses placed upon it in order to make its structure and properties more appropriate for the typical daily loading it experiences (2). The mechanical strength of bone varies depending on site and location in the body as well as its size, mass distribution, geometry, and internal architecture (3-6). A feedback control system interprets the strain distribution placed on the skeleton from loads and adapts bone tissue to strengthen areas with high strain distributions, while removing bone from areas with low strain distributions (1). For instance, exercise studies in children have shown significant bone gains due to increased activity and stresses on the skeletons of the youths as they develop (7-9).

Unfortunately, there are factors, including disease and environmental effects, which can cause severe deterioration of bone strength and parameters. Osteoporosis is one such disease which is characterized by a severe weakening of an individual's bones that causes them to fail and fracture more easily. According to the National Osteoporosis Foundation, approximately 10 million people have the condition, with another 34 million currently at risk. It is estimated that half of all women over 50 and a quarter of all men will break a bone due to osteoporosis (10). Fractures of the hip are most concerning since they incur the greatest morbidity, mortality, and cost compared to other bone fractures in men and women (11). Currently, areal bone mineral density (aBMD) at the hip by dual-energy X-ray absorptiometry (DXA) is the key clinical measure used in the osteoporotic fracture prediction model (FRAX) used by the World Health Organization (WHO) (11).

Microgravity as experienced during long duration spaceflight is an environmental factor which can greatly affect bone. It has been shown that spaceflight can disrupt bone growth, induce bone loss, and result in impaired material and mechanical properties for growing animals (12). Lang et. al. showed substantial decreases in aBMD and volumetric bone mineral density (vBMD) by CT for International Space Station (ISS)

astronauts at the hip and spine (13). This loss of BMD will eventually lead to fracture risk even in otherwise healthy astronauts, but BMD is not always accurate at predicting the strength of bone (14). Therefore, these microgravity effects have become a serious concern for the overall health of NASA astronauts performing long-duration space missions, such as on the ISS, and a high priority needs to be placed on determining the full effects of microgravity exposure on bone and how it correlates with BMD.

NASA HRP

In early 2004, NASA developed the Human Research Program (HRP) with the objective of using research to develop procedures to better understand and ameliorate the negative effects of the space environment on the health and performance of astronauts (15). NASA's mission directorates are four fold:

1) Enable a safer, more secure, efficient, and environmentally friendly air transportation system
2) Direct the identification, development, and validation of exploration systems and technologies
3) Explore the earth-sun system, our own solar system, and the universe beyond
4) Extend the duration and boundaries of human space flight to create new opportunities for exploration and discovery (15)

Lately, NASA's exploration goals have been increasingly sophisticated and ambitious including, until recently, returning to the Moon, potentially establishing a research station there, traveling to Mars, and continuing to expand our exploration further into the solar system. Even though the lunar goals have been put on hold, there is still continuing research relevant to the ISS and to Mars exploration missions at some point in the future. In order to ensure the full health and peak productivity of the astronauts on missions, the purview of HRP includes a number of concerns for long term space travel including:

environmental factors, habitability, human factors, medical capabilities, physiology, psychological and behavioral health, and space radiation (15). The HRP is broken up into six elements consisting of the International Space Station Medical Project, Space Radiation, Human Health Countermeasures, Exploration Medical Capability, Behavioral Health and Performance, and Space Human Factors and Habitability to address the various concerns (15).

Under the Human Health Countermeasures element, the applicable topics for this thesis are "Risk of Bone Fracture" and "Risk of Early Onset Osteoporosis Due to Spaceflight." During long term missions, such as to Mars, the astronauts may encounter situations where they could experience high impact forces relative to those experienced in transit. This, coupled with a potential reduction in bone strength due to microgravity, may result in situations with an increased Factor of Risk (FOR). Factor of Risk or Risk of Bone Fracture is defined as the ratio between the applied force vector to the bone and the fracture load of the bone (15). NASA currently measures bone strength by aBMD with DXA, the standard methods as recommended by WHO. Average BMD over a series of long duration (4-6 month) missions declines by 1-2 % per month, but it remains unclear if this BMD loss has a lower limit or if the lower gravities on the Moon and Mars could mitigate the bone loss. Therefore, it is necessary for NASA to have a thorough knowledge of the loss and recovery dynamics that microgravity and disuse have on bone strength and the factor of risk.

Another potential bone risk for astronauts on long term missions is the potential for early onset osteoporosis. As mentioned above, osteoporosis is characterized by a severe weakening of the bone which usually occurs due to aging. Extrinsic factors, such as microgravity during spaceflight, can potentially accelerate the aging-related bone loss and cause the condition to occur at a much younger age. With as much as 2% mineral loss per month in microgravity, the impact on aging bone is not yet known and could potentially put astronauts who have performed long duration missions at long-term risk.

Knowledge Gaps

Currently, NASA has a series of knowledge gaps for both bone fracture risk and early onset osteoporosis risk that need to be addressed. Most importantly, NASA is seeking "integrated nutritional, exercise, and/or pharmaceutical countermeasures that can be used to mitigate microgravity induced bone loss." (15) However, technologies to diagnosis fractures in-flight, monitor net bone calcium changes, and monitor skeletal adaptations in order to determine whether there is a plateau in bone loss, gender effects, and changes in bone turnover are still in development. General scientific knowledge gaps include determining the risk of vertebral compression fractures, whether bone strength is completely recovered with the recovery of BMD, what the potassium; magnesium; and phosphorus changes are in relation to cardiovascular issues and bone loss; and what loads are applied to bone in-flight and during extra-vehicular activities (EVA) and if they increase the risk of fracture (15).

Significance

On Earth, individuals with osteoporosis accumulated an estimated two million fractures and $19 billion in costs in 2005; and these figures are expected to increase to three million fractures and $25.3 billion in costs by 2025 (10). It is known that spaceflight can disrupt bone growth, induce bone loss, and result in impaired material and mechanical properties which, coupled with disuse atrophy, could lead to osteoporosis later in life (16,10). Therefore, understanding the causes of osteoporosis, how it can be treated, and how bone functions under different environmental conditions is important both to NASA and to the entire healthcare industry. Intervention methods, such as pharmaceuticals and exercise regimens, are currently being studied; therefore, it is doubly important to gather data on how bone responds to environmental effects and how it recovers and adapts to stimuli. Long duration missions to Mars and beyond our solar system will be possible only if the health of the astronauts participating in those missions can be protected for both the journey into space and the return to Earth.

Ground-based animal models have the advantage of simulating osteoporotic changes while on Earth so that bone strength and properties can be evaluated in a controlled manner. Experiments on Earth are flexible and can be scheduled and modified more easily than in space. The duration of the experiment can be varied with multiple time points measured within a single experiment. This makes Earth-based experiments more cost effective; they can be matched with space-flight experiments and they avoid environmental complications such as hyper-gravity during spaceflight takeoff (17). Finally, destructive mechanical tests can be performed on the bone samples of ground-based animal models to provide an accurate measure of the bone strength beyond calculated values. Thus, these models can be used to study both the effects of microgravity on bone and osteoporotic changes, as well as potential treatments and loss and recovery patterns.

Objectives

This study will use the hindlimb unloaded rat model, a well-established, ground-based analogue, to observe the effects of age and simulated weightlessness on the various densitometric, structural, and calculated properties of bone. The study will investigate bone strength and parameter changes due to hindlimb unloading by focusing on the femur in order to compare the results to astronaut data collected by NASA. Choosing the femur also allows for CT scans and destructive mechanical tests to be performed at the femoral neck (hip) and to make direct comparisons. This can be done only with animal models and not clinically. The study will be pursued as outlined by:

1. Characterize the effects of multiple exposures of simulated microgravity and age on the mechanical, densitometric, and geometric properties of the femoral neck and femur midshaft.
2. Compare the loss and recovery characteristics for densitometric properties, bone geometry, measured mechanical strengths, and calculated mechanical strengths.

3. Determine the effects of prior HU exposure and age upon the loss and recovery characteristics (at both sites and for all variables).
4. Compare and contrast the loss and recovery responses at the femoral neck and the femur midshaft.
5. Compare mechanical properties of the femoral neck for two different loading configurations (axial and lateral).

Hypotheses

H1: Initial HU will exacerbate the effects of the second HU with larger reductions in vBMD and strength, and slower recovery or even incomplete recovery.

H2: The older animals will be more negatively affected by HU and have greater reductions in BMC, vBMD, and strength when compared to younger animals subjected to HU.

H3: Femoral neck strength and properties will be more severely affected by multiple HU exposures than will the femur midshaft.

BACKGROUND

Bone Physiology and Structure

General Bone Physiology

Bone consists primarily of a fibrous protein called collagen, calcium phosphate crystals, and water with lesser quantities of other proteins, polysaccharides, and other living cells (18). These components together create a composite material which has unique properties for dealing with compression, torsional, and tension forces generated by the body.

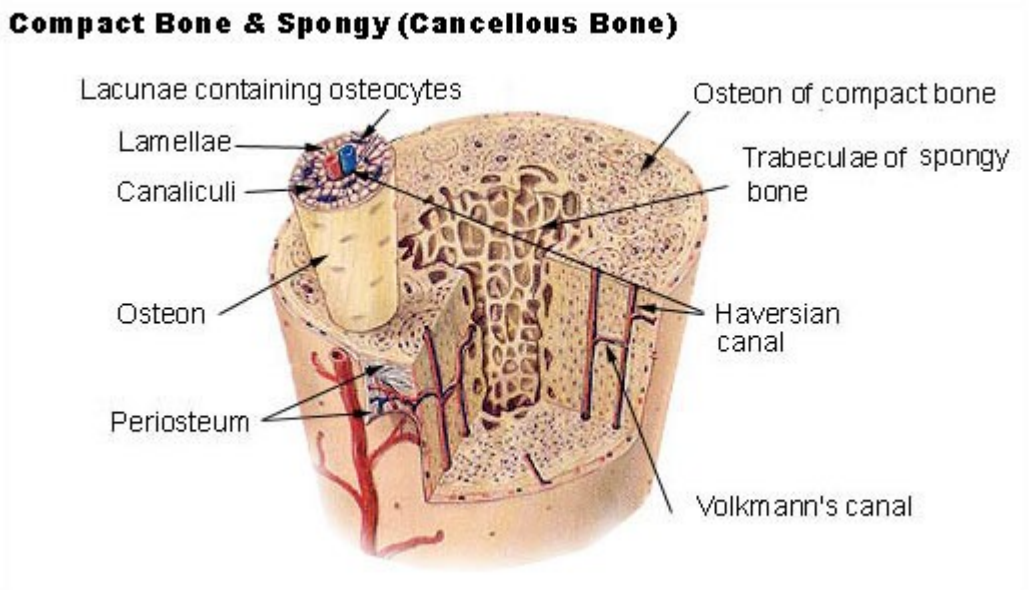

Fig. 1. General anatomy of bone showing compact bone, trabecular bone, osteocytes, Haversian canals, and Volkmann's canals. (19)

There are a number of different types of bone cells with each having a function to play in the growth, development, and maintenance of bone over the course of the lifetime of the

organism. Osteoclasts are bone resorbing cells which aggressively remove bone in order to remodel the structure to adapt to changes in the stress/strain environment. Osteoblasts on the other hand, are bone forming cells which follow behind the osteoclasts and lay down new layers of bone. Occasionally, osteoblasts become trapped within a new layer of bone which transforms the trapped osteoblast into an osteocyte. These osteocytes are believed to play a significant role in the sensing of mechanical stresses and strains. Finally, bone-lining cells cover the outer surfaces of bones and control the movements of ions between the rest of the body and the bone (18).

Cortical vs. Cancellous

On a macro level, bone consists of two different types of tissue referred to as cortical (or compact) bone and trabecular (or cancellous) bone (Figs. 1-2). All bone is porous and

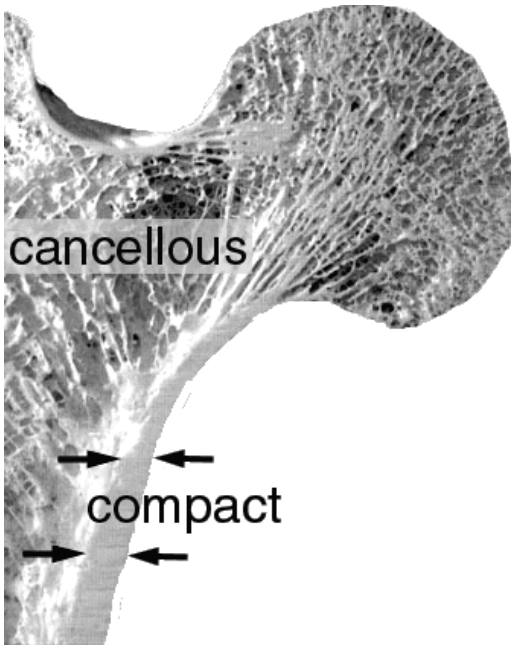

Fig. 2. Compact (Cortical) and Cancellous (Trabecular) bone found in the proximal femur. (20)

can range in porosity from zero to one hundred percent, but the majority of bone is either very porous or not, with little intermediate levels (21). For example, cortical bone is

dense with a low porosity ranging from 5-10% in humans; major porosities are Haversian canals, Volkmann's canals, and resorption cavities found within a low porosity, strong cortex that provides structural support (Fig. 1) (21).

Trabecular bone, however, has a high porosity ranging from 75-95% with a matrix formed by a variable arrangement of struts and plates referred to as "trabeculae." The tissue space around trabecular bone is filled with bone marrow (21). Both types of bone have adaptable, dynamic structures where cortical bone can become more porous like trabecular bone, depending on the mechanical stimuli.

Haversian Systems

Haversian systems, consisting of Haversian canals, Volkmann's canals, and resorption cavities, form in the cortical bone of humans as osteoclasts move forward breaking down older bone. During this process they leave behind a cylindrical resorption cavity approximately 200 micro-meters in diameter (18,21). The osteoblasts immediately move in to begin laying down new bone in the canal, but the osteoclasts continue to break down the older bone in the layers around the osteoblasts. This process leaves cylindrical layers in the bone with central canals (Haversian canals), which are occupied by blood vessels and nerves.

Haversian canals are approximately 50 microns in diameter and are generally aligned with the long axis of the bone (21). Volkmann's canals are also formed by osteoclasts, but are smaller and travel in a transverse direction, perpendicular to Haversian canals. These canals also contain blood vessels and nerves but their primary purpose is to connect Haversian canals to each other and the outside surface of the bone. The

formation of these structures results from the remodeling process that bone is continuously using to adapt to environmental changes (18).

Remodeling and Shape

Bone modeling alters the overall shape of the bone and is how bone develops during the growth process in young animals, but re-modeling affects all surfaces of the bone and is critical to the upkeep of the skeletal structure throughout life (18). Both of these processes are controlled by the activities of the osteoclasts and osteoblasts, which focus on adapting the mechanical strength to the environment while minimizing mass. For instance, long bones are usually circular in shape and hollow in the mid-shaft with expanded ends filled with trabecular bone. This provides a stiff, strong structure which is resistant to distortions due to forces at the joints. Even though a thinner tube minimizes mass while maintaining strength, a thinner tube-shape is limited by the possibility of buckling (18). A careful balance of geometric properties is maintained to provide an ideal level of strength based upon environmental mechanical stimuli. This ability of bone to sense the mechanical stresses and strains placed upon it and modify its structure to better withstand these strains is referred to as Wolff's Law (21).

Bone material properties and formation rates depend on both mechanical stimuli and the age and health of the individual. For instance, remodeling rates in adults can be substantially increased by different events, including changes in the mechanical loading of the skeleton (21). However, these adaptations primarily come from changes in the material properties instead of skeletal geometry changes. This suggests that increasing cortical bone strength and stiffness through remodeling is nearly impossible due to the density of the cortical bone not leaving many large voids to be filled by osteoblast remodeling activity. Therefore, it is much easier to reduce cortical bone strength than to increase it through mechanical loading (21). In children, though, skeletal geometry is not

set until the growth plates fuse. Exercise intervention studies have shown significant bone gains in young individuals, with little return beyond bone preservation for adults with a mature skeleton (7,22,9,23-25,8,26). Therefore, during longitudinal growth, particularly during puberty, increased mechanical loading can cause significant bone modeling and structural changes including altered geometry for children, while more modest changes are observed in the mature adult skeleton (7,9,23,27). It is adaptations like these which result in the different shapes and strengths of bone throughout the body.

Anatomy of the Femur

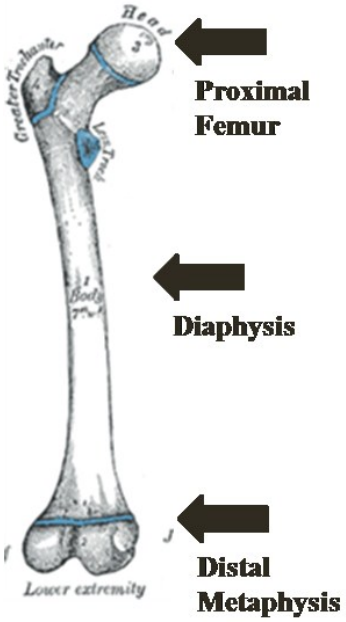

Fig. 3. Illustration of a human femur. (28)

The femur is the longest and strongest bone in the human body and consists of three main sections. The proximal femur in humans is closest to the head and is specially

formed to fit and articulate at the hip joint. The diaphysis or mid-shaft forms the main length of the bone, and the distal metaphysis forms the lower area of the femur including the condyles (Fig. 3).

The proximal femur induces the acetabular hip joint which allows for proper movement in most mammals. It is a "mixed site" which refers to it being a region that consists of a cortical bone shell surrounding trabecular bone. The hip is a ball-and-socket joint that connects with the (lesser and greater trochanters, the femoral neck) femoral head which

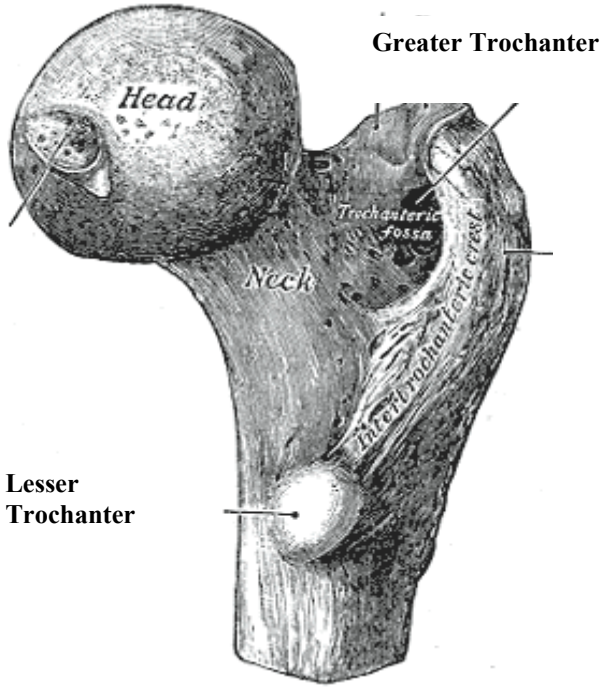

Fig. 4. Illustration of the proximal femur of a human. The structures present are the head, neck, greater trochanter, lesser trochanter, and a proximal section of the shaft. (28)

rotates in the pelvis during locomotion (Fig. 4). The location of the proximal femur

subjects the joint to a unique selection of body forces and loading conditions, which can be as high as 8-10 times the weight of the body being supported. Thus, the femoral neck is anisotropic and must behave differently depending on the loading directions and conditions. Due to its critical use in movement, degenerative diseases such as osteoarthritis and osteoporosis can have profound effects on movement and function at the proximal femur.

The diaphysis, or mid-shaft, is the main shaft of the femur which lays between the proximal femur and the distal femur metaphysis). It is a long, generally circular shaped tube consisting entirely of cortical bone. The shaft is strong and stiff which allows it to effectively serve as a structural support and to transmit body forces.

Rat vs. Human Bone

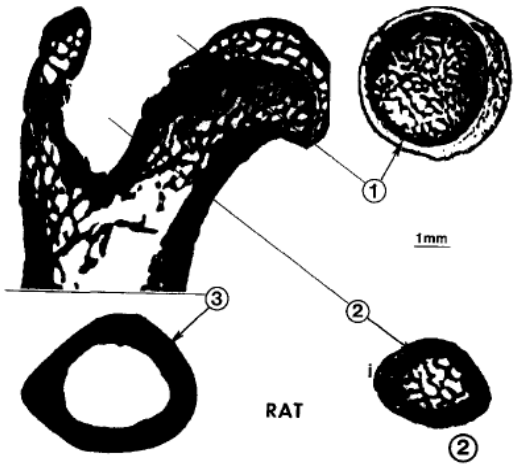

Fig. 5. Microradiograph of a rat proximal femur with cross-sections through (1) the head, (2) the neck, and (3) the shaft regions. (29)

There are important differences between rat and human bone, as well as site-specific differences that should be noted. Primarily, rats lack a Haversian system, Haversian remodeling, and osteons that are found in normal human cortical bone (29). Also, bone growth and modeling processes which occur in rat skeletons are not found in adult human skeletons (30). Interestingly, osteopenia does not cause hip fractures in rats, likely due to their proximity to the ground and the different proximal femur structure from the human hip (30).

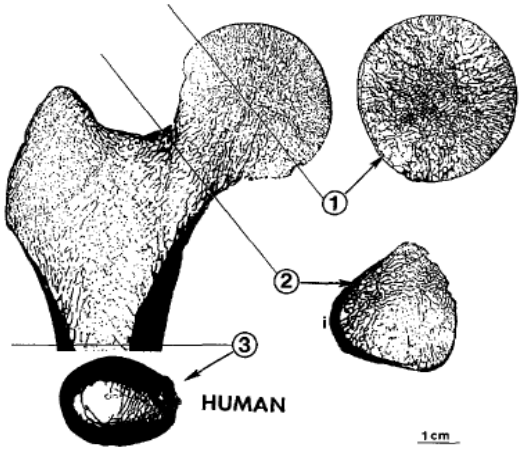

Fig. 6. Microradiograph of a human proximal femur with cross-sections through (1) the head, (2) the neck, and (3) the shaft regions. (29)

At the femoral neck, humans have much more trabecular bone and there is a substantial difference in the shape of the proximal femur as compared to rats (Fig. 5) (29,31). Bagi et. al. have shown circular or oval cross sections with uniform cortical shell thicknesses in rat femoral necks as compared to humans, which have roughly triangular shaped femoral necks with non-uniform cortical shells (Figs. 5-6). Also, the amount of cortical bone at the proximal femur is considerably larger in rats, with 72.5% of the total neck consisting of cortical bone which is 500 times higher than humans who are at approximately 12.5% cortical (29). Lastly, the applied loads during normal movement at

the proximal femur are different due to the up-right posture of humans as compared to the quadrupedal motion of rats.

One important similarity between rat and human bone is that cortical bone loss originates from the endocortical surface for both species (30). This is important for comparisons between human bone and rat bone at the midshaft, which consists primarily of cortical bone for both species.

Mechanical Testing Theory for Bone

Bone can generally be treated as an irregularly shaped structural material which can be subjected to the standard regimen of mechanical engineering tests used to determine material properties. Mechanical testing to failure can provide load and deflection curves, which can then be used to calculate stress, strain, energy absorption, and other mechanical properties. These results can be compared with the densitometric data acquired from pQCT scanning in order to determine the correlation between actual mechanical strength and strengths estimated from CT scanning.

Load deformation curves generated from mechanical tests typically consist of a linear region during the beginning of the test where elastic deformation is occurring, followed by yielding and a non-linear section of the curve where plastic deformation occurs until ultimate failure. Elastic deformation occurs when an applied force is not large enough to cause permanent deformation. In other words, the material returns to its original shape. Materials tested into the plastic deformation region of the curve will not return to their original shape and are permanently deformed or broken after testing. Bone, however, does not have a true linear region due to viscoelastic effects; fluids in the bone matrix cause some energy to be lost, but treating it as a linear elastic material serves as a good approximation (32).

Three-Point Bend Testing

Three-point bending tests are one of the standard ways to test the strength of structural materials. It is especially useful for rodent bones since their small size and irregular geometry make it difficult to machine specimens capable of being tensile or compressively tested accurately (32). A three-point bend test is performed by supporting

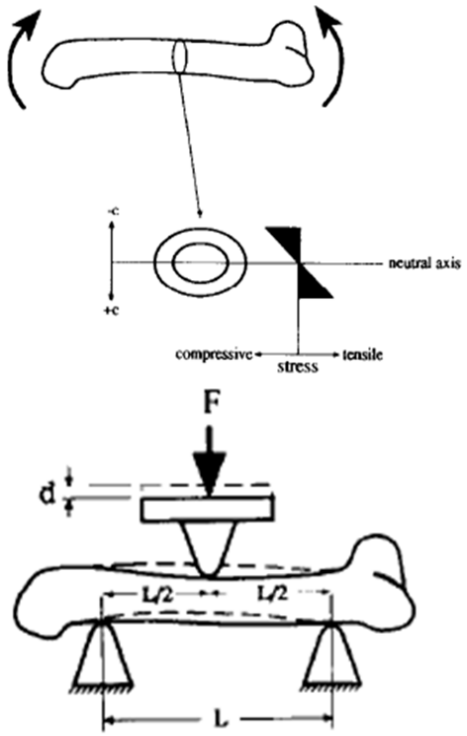

Fig. 7. Three-Point bending tests approximate the midshaft of the bone as a hollow cylinder. When the test is performed, the applied load generates compressive and tension forces within the bone. The typical test setup places the bone between a span length and a quasi-static load is applied at the center. (32)

both ends of the long bone across two spans while an anvil applies a load at the center of the specimen (Fig. 7). The applied load generates compressive stresses on one side of the

bone and tensile stresses on the other. Since the bone shape is approximated as a hollow, circular tube, the highest stresses are found at the outermost surface of the specimen. Three-point bending tests on rodent bones have two primary limitations. First, the span length should be approximately 16 times the thickness of the specimen in order to prevent the displacement from being caused by shear stresses instead of direct loading. This is extremely difficult in rodent bone specimens due to their small size. Therefore, Turner and Burr recommend using a span length between 15 to 20 mm for male rats in order to guarantee that most (85-90%) of the flexure occurs due to bending (32). Also, three-point bending tests create high shear stresses at the anvil due to the single loading point. However, the test is simple and the four-point bending test requires equal loading at its two anvil loading points which is very difficult due to the irregular shape of bones. Therefore, three-point bending tests are more commonly used to test the material strength of long bones (32).

Values for stress, strain, toughness, and modulus of elasticity can be calculated for three-point bending tests using the following equations developed for beam theory

$$\sigma = \frac{Mc}{I} = \frac{FLc}{4I} \qquad \varepsilon = \frac{12cd}{L^2}$$

$$E = \frac{FL^3}{d48I} \qquad I = i_c + Ad^2$$

$$u = \frac{0.75 * Energy\ Absorbed * APdia^2}{L * CSMI}$$

where the variables are defined as:

σ - stress

ε – strain

E - Modulus of Elasticity (Young's Modulus),

I - polar moment of inertia

u – toughness

F – force

L – span length

c – radius of the bone

d – max deflection at bone center

A – cross sectional area of the bone

Energy Absorbed – area under the force/displacement curve

APdia – anterior/posterior diameter

CSMI – cross sectional moment of inertia

It should be noted that these equations are most effective for the linear, pre-yield region of the force-displacement curve. Once yielding occurs, strain is much more difficult to calculate and the stress is no longer a simple product of strain and elastic modulus. Also, there is some deformation due to shear strain during the test. Both of these conditions, yielding plus the deformation due to shear strain, causes an over-estimation of the calculated strain and an under-estimation of the calculated elastic modulus. Therefore, total and post-yield calculations of these properties assume that the stress-strain relationship is still linear and only provides an estimate of the true strain and elastic modulus (32-34).

Axial Compression

An axial compression test (Fig. 8) on the femoral neck is one way to test the combined strength of the cortical and trabecular bone at a primary weight-bearing site in the skeleton. The axial loading direction simulates a single leg stance similar to the stance found during normal locomotion, which can be a fracture mechanic in humans, though, this is rare. Unfortunately, due to the complex geometry at the proximal femur, the femoral neck is placed under a variety of loading conditions during the test including bending, shear, and compression. This combined stress state generates irregular fracture cross-sections and makes calculation of intrinsic data extremely difficult. Therefore, only maximum load achieved during the test and the stiffness (linear region of the load-deflection curve) are reported.

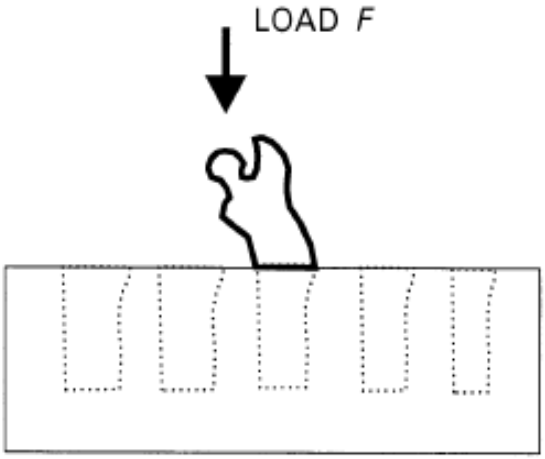

Fig. 8. Typical setup for an axial compression test of the proximal femur. The shaft is secured to prevent specimen movement and a load is quasi-statically applied at the femoral head until failure. (35)

The axial compression test is conducted by cementing, either through embedding or mechanically gripping, the proximal half of the femoral shaft up to the lesser trochanter (Fig. 8). A computer controlled, quasi-statically applied load is applied at the femoral head and parallel to the femoral shaft until failure at the neck occurs. The computer gathers the maximum load and deflection during the test in order to generate a force-deflection curve.

Lateral Compression

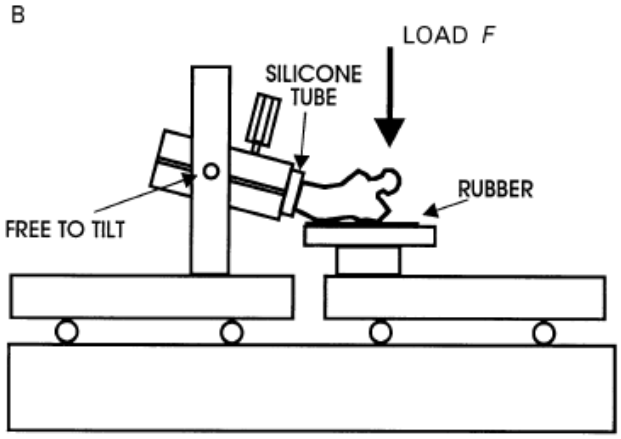

Fig. 9. Setup for a lateral compression test of a proximal femur. The shaft is clamped in a free-tilt base and the load is applied to the femoral head in a different direction from the axial test. (35)

A lateral compression test (Fig. 9) is another way to test the mixed properties of cortical and trabecular bone at the proximal femur site. However, a different loading direction is used in order to study the strength in a "fall stance." By testing the neck laterally, an approximation of the types of forces generated by a typical human fall onto the lateral hip can be applied. However, this model is limited by its quasi-static loading, which has a much slower loading rate than a typical fall (36). Also, the same geometry issues for the axial compression test are also present in the lateral test. The bone's irregular geometry creates a complex loading condition with bending, shear, and compression forces that make the calculation of intrinsic material properties difficult. Therefore, lateral tests also provide data on only maximum force and stiffness.

The lateral test is performed by mechanically clamping the proximal shaft of the femur up to the lesser trochanter between two pivoting supports which prevent a moment from

being applied to the shaft (Fig. 9). The lateral side of the bone is angled down 10 degrees from the horizon which approximates the position of a human femur when it strikes the ground during a fall. The proximal half is allowed to rest on a soft surface while a quasi-statically applied load is placed on the femoral head and perpendicular to the horizon until fracture occurs.

Literature Review

Current research involving astronauts by Lang et al. has determined that astronauts on long duration missions to the International Space Station (ISS) lost spinal bone at a rate of 0.8-0.9% per month and hip bone at a rate of 1.2-1.5% per month (13). They also developed strength indices based upon previous finite element modeling and utilizing geometric and vBMD properties of bone found by CT scanning. After calculating bending and compressive strength indices and observing the changes in cortical and trabecular bone mass in the hip of newly returned astronauts, the Lang group predicted that long-duration spaceflight may result in a substantial reduction of bone strength (13). Additionally, Carpenter et al. also used QCT scanning of the hip on ISS astronauts before launch and after return to study changes in density and structure. Trabecular BMD values did not return to pre-launch levels even after 2-4.5 years of recovery (37). Crew members lost as much as 14% of the trabecular BMD at the femoral neck (37).

Bloomfield et al confirmed these results with an animal model by looking at site and compartment specific changes in bone due to hind limb unloading of rats. The bone properties in cancellous (trabecular) rich sites such as the femoral neck were adversely affected by unloading (14). However, unloading produced few changes in cortical bone mass, geometry, and mechanical properties but increases in ultimate load and stiffness at the tibial midshaft after unloading (14). Mosekilde et al. found similar results during an immobilization study; reporting that the immobilization induced a significant loss of strength at both femoral metaphyses but not at the diaphysis. A study on the effects of simulated weightlessness on bone properties in rats performed by Martin et al. also

generated similar results. The results suggested that unloading, as well as time, affected the mass and composition of the femur, but neither suspension or time alone had a significant effect at the midshaft (38).

Another study by Lang et al. focusing on the proximal femur and the effects of reloading after spaceflight revealed that astronauts subjected to partial skeletal disuse on missions lasting 4-6 months showed substantial losses in bone mass at the proximal femur along with cortical thinning and declining strength index estimates (39). However, no changes in overall tissue volume or cross-sectional area were observed which indicated that cortical thinning was occurring at the endosteal side of the cortical shell and lead to the decline in strength estimates. After reloading, expansion on the periosteal side of the cortical shell was seen and believed to be an adaptive measure to preserve bone strength for normal loading conditions. However, fall loading conditions are substantially more traumatic due to their sudden, high loading rates and the periosteal expansion may not be sufficient to counteract these higher forces. The Lang group noted that reloading caused increases in cross-sectional area and cortical volume values which had lower vBMD than the bone observed pre-spaceflight indicating slower vBMD recovery. Also, after one year of recovery, strength indices had still not returned to pre-flight levels (39).

Further studies have researched the differences between axial and lateral loading of the femoral neck for humans. For instance, Keyak et al. studied the reduction in proximal femoral strength due to long-duration spacelight for astronauts. Finite element models were generated from QCT data taken pre-launch and after return to Earth. Based on the model, astronauts lost significant levels of max force to failure during the unloading period. Performing the analysis in the lateral direction showed a max loss of 24% in ultimate load while the analysis of axial testing calculated max losses of 20-30% (40). Furthermore, an earlier study by Keyak et al. on the effect of loading conditions (axial or lateral) on the femoral neck fracture load revealed that the greatest applied force and lowest fracture load occurred for lateral testing (41).

Jamsa et al studied the mechanical properties of the femoral neck in mice with fall and stance loading conditions. The fall (or lateral) loading forces were slightly higher than the axial; however, the pQCT parameters correlated with the mechanical properties in the axial condition but not as well in the lateral (35). A second study by Jamsa et al. noticed significantly lower cross-sectional area, BMC, and BMD at the femoral neck for mice during an immobilization study (42). The femoral neck was shown to be a more sensitive indicator of bone loss than the diaphyseal femur because three-point bending tests of the femur were not as significant as axial and lateral femoral neck tests (42). However, in this case the force to failure in the lateral direction was lower compared to the axial (42).

Other factors can affect the strength of bone beyond disuse including hormone deficiency, exercise, diet, muscle strength, and use of anti-resorptive pharmaceuticals to combat osteoporosis (31,43,16,44-46). However, aging also affects bone and its response to external stimuli such as disuse. Perrien et al. observed the effects of extreme age on the skeletal response to disuse in rats. Significant reductions in cortical BMD and increased porosity of the cortical bone was observed for 32 month old rats while trabecular volume and architecture only changed for the 6 month old rats (47). Perrien suggests that the site of bone loss due to disuse changes with age (47).

Thomsen et al. reported rats losing bone at the femoral neck with age, but also showed that the greatest loses in biomechanical strength occurred at the femoral neck and distal femur metaphysis compared to the femur diaphysis (midshaft) (48). These results suggest sites with mixed cortical and cancellous bone such as those found in the proximal and distal femur are indeed affected by age. The Thomsen results also suggest that there is a correlation between age and bone loss during unloading and Dehority et al suggested that the mechanisms of bone loss during disuse appeared to be age-dependent after studying bone and hormonal changes during unloading of male rats (49). The

research of Bloomfield, Dehority, and others indicates that the bone loss of young and skeletally mature animals have different loss kinetics during disuse (44,14,49,50). Human bone also appears to have different growth and loss kinetics depending on the age of the individual as seen in the age and exercise studies mentioned in the Remodeling and Shape section (22,23,8,25,7,9,24,27,26).

Ideally, geometric and pQCT based strength estimates can be developed to eliminate the need for mechanical testing all together by calculating accurate measurements of mechanical strength. This is especially important for determining the bone strength of astronauts since it not feasible to perform mechanical testing on their limbs after a return to normal loading. Cheng et al tried to assess proximal femur strength by observing the relationship between BMD and femoral geometry in human cadavers. Their results showed that BMD measured at the trochanter was a significantly better predictor of femoral strength than BMD measurements taken at the femoral neck (51). Their study also indicated that cortical area was a better computed predictor of bone strength than BMD (51).

Since bone strength depends on the loading directions, materials, and the geometry of the bones involved, a significant reduction of BMD and material properties is an important medical complication for future long-duration space flight missions due to the increase in fracture risk for healthy astronauts (14,13,52,53). Other studies have done some research on the effects of disuse on bone loss, the effects of age on loss, and the effects of both disuse and age on bone loss. However, there are no other animal studies which have looked at multiple exposures to unloading. Since aging astronauts can perform multiple missions with long term exposures to unloading, it is important to fully characterize how these factors may affect the astronauts over their lifetimes.

HU Rat Model

One important approach to research and understand bone loss due to spaceflight and countermeasures is to utilize ground-based animal models. Seen in Fig. 10, the hindlimb unloaded rat model is a well-established, ground-based analogue which provides data for the design of spaceflight experiments and for studying the effect of microgravity on the skeletal system (14,2). Tail harnesses are used to elevate the animals (rats or mice) hindquarters, removing the gravitational loading without immobilizing the limb, and simulating the physiological conditions which occur during microgravity exposure (Fig. 10). These include differential muscle atrophy, cephalad fluid shift, freedom to move, eat, and groom using the forelimbs, and unloading of the hindlimbs without paralysis so that the animal can recover from unloading, and normal weight gain in growing rats or minimal weight loss in adult animals (17). Unloading on Earth causes a number of changes in bone. For instance, it causes changes in many of the mineral and matrix components including calcium, collagen, and hydroxyproline and causes large effects on the mass of bones due to the reduced mechanical loading of the hindlimbs. Unloading generates lower stresses and strains, causes the skeleton to require less bone mass to maintain normal structural integrity, and can cause a delay in bone growth (2). Osteoblasts and bone formation rates are suppressed which indicates that other factors, including age, may affect how an individual responds to unloading.

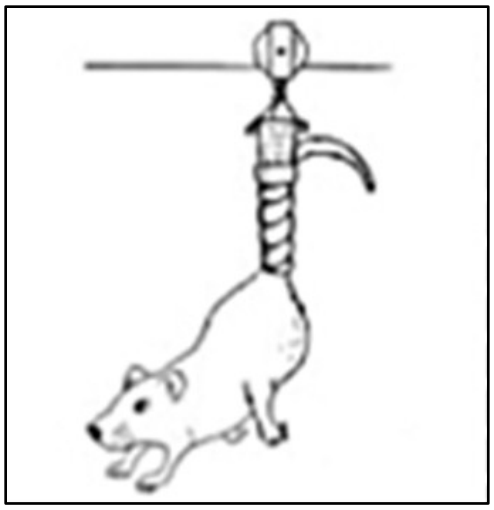

Fig. 10. Graphic of a hindlimb unloaded rat. A harness is attached to the tail and used to lift the hindlimbs of the rat while still allowing the forelimbs to bear weight. The rat is still capable of moving due to the pulley attached to the tail harness. Also, the angle of head tilt downward provides a good imitation of the fluid shift experienced by astronauts during spaceflight.

METHODS

Study Design

This study was designed to observe the effects and dynamics of unloading and recovery on the densitometric and mechanical properties of rat bone in order to generate a ground-based model for how human bone reacts during spaceflight. The development of this research is important to support astronaut crew health and performance during and after space exploration missions. NASA is specifically seeking "novel research that defines the precise relationship between long-term recovery of bone mineral density and bone strength/quality, including the effects of multiple spaceflights." The long-term health consequences for astronauts who perform extended and/or multiple spaceflights remain unclear; therefore, utilizing this form of animal study is important since bone strength cannot be directly measured on living humans to assess bone health. (15)

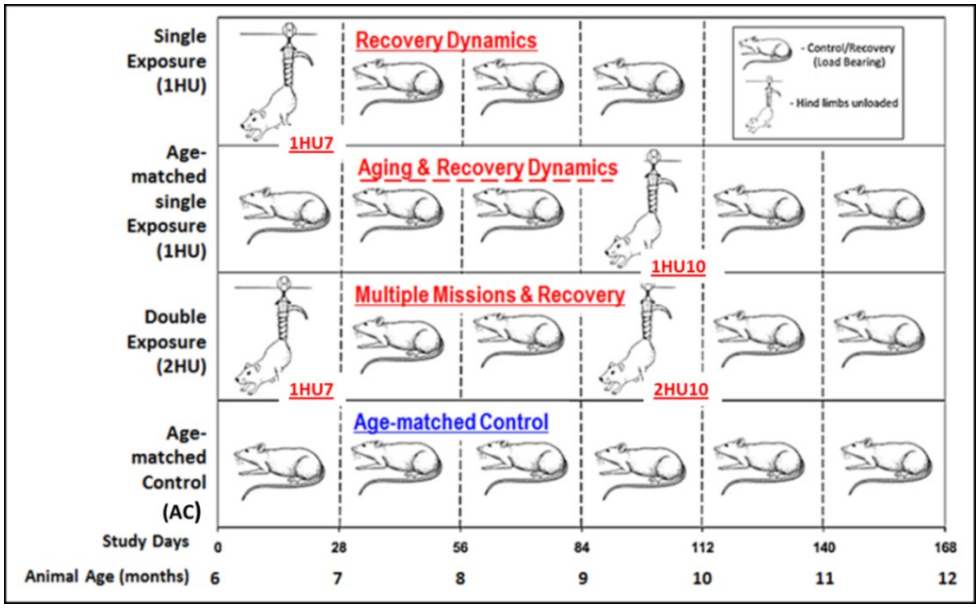

Fig. 11. Study design showing graphically the different groups (1HU7, 1HU10, 2HU10, AC), hindlimb unloading periods, recovery periods, age of the animals in months, and the days in the study.

Experiment 1

The study was broken up into different experiments focusing on various aspects of the recovery dynamic from long-term space missions. The initial experiment observed the discordant recovery dynamic of bone once weight bearing had been returned to normal, with a particular emphasis on the precise relationship between bone mineral content (BMC, reflecting total bone mass), BMD, and bone strength during recovery. Six month old adult male Sprague-Dawley rats were separated into three groups: baseline (BL), age matched cage control (CC), and hindlimb unloaded (HU). The baseline group consisting of 15 animals (n = 15) was sacrificed at the start of the experiment. The HU group was hindlimb unloaded for 28 days, re-ambulated, and allowed to recover for 84 days. A sample (n = 15) of animals was sacrificed at each 28 day point for both the HU group as well as the matched CC group for a total study time of 112 days. It was hypothesized that:

1) BMC will recover completely by 28 to 56 days after HU.
2) BMD will not recover as fast, or as extensively, as BMC.
3) Bone strength will not recover as fast, or extensively, as BMC or BMD.
4) The strongest predictors of bone strength at the end of HU, and also after recovery from HU, will be a combination of BMC, BMD, and bone organic matrix (collagen) parameters (15).

The results of this experiment can be viewed in Joshua Kupke's thesis titled: Characterization of the Femoral Neck Region's Response to the Rat Hindlimb Unloading Model Through Tomographic Scanning, Mechanical Testing, and Estimated Strengths (54).

Experiment 2

The second experiment (Fig. 11), which this thesis will focus on, followed a similar study design as the first experiment by once again using six-month-old male Sprague-

Dawley rats separated into groups consisting of BL, AC, and HU. The purpose of this phase was to study the effects of multiple missions, which for the ground-based rat HU model consisted of using two successive HU exposures as shown in Fig. 11. In order to fully ascertain the effects of an initial HU on a second HU, another HU group must be included. Specifically, another group of animals was exposed to a single HU that was matched to start at the same time as the second HU for the double-HU group. This group is designated 1HU10 in Fig. 11. Including this group also made possible assessment of the effects of age-at-onset upon the response to a single HU, plus recovery. The BL group was sacrificed at the beginning of the study. The HU group of animals was divided into three subcategories labeled 1HU7, 1HU10, and 2HU10. The 1HU7 animals were subjected to 28 days of HU beginning on day 0 followed by 84 days of recovery. A second HU began at day 84 for another 28 days followed by a second 56 day recovery period for the 2HU10 group. The 1HU10 animals were subjected to a single 28 day HU beginning on day 84 to match the second HU in the 2HU10 group. Samples (n = 15) from all HU groups and the AC group were euthanized at each 28 day time point as done in the previous phase. A graphic summary of this timeline can be seen above in Fig. 11.

Tail Suspension

Before the animals could be tail suspended, custom made harnesses were built to support their weight. The harnesses consisted of cloth, tape, wire, and a hook which is then adhered to each rat's tail by cyanoacrylate glue. The rats were first sedated with a ketamine dexmedetomidine cocktail, an anesthetic, before beginning the harnessing procedure. Each animal's tail was thoroughly cleaned with anti-bacterial cleanser to remove any debris and dead skin cells and then dried with acetone to provide a better surface for the adhesive to bond to. Once dry, the tails were sprayed with an adhesive Quick-Drying Tape Adherents Q.D.A. (Cramer®, Gardner, KS), and the harness was coated with the cyanoacrylate adhesive (Amazing Goop) before being carefully positioned on the tail. The harness was positioned along the lateral edges of the tail and approximately three to seven millimeters from the base in order to provide the rat

freedom of movement. The cyanoacrylate was allowed to set and each animal was given four mL of saline before the animals were woken from the anesthesia with a reversal agent (Atipamezole, 1 mg/kg). As the animals were regaining consciousness, the harnesses were loosely hung in the HU cages from a suspension wire for 24 hours to allow the animals to acclimate to their new condition and to recover from the anesthetic. After the acclimation period, the hindquarters were fully raised into the HU position so that the hindlimbs were no longer weight bearing and the head was tilted down approximately 30 degrees. Swivels attached to the guide-wire and connected to the harness hooks allowed for full freedom of movement, while stops on the guide-wire prevented hindlimb contact with the cage walls. During HU, each animal was provided with food and water and was observed multiple times per day to check on tail health and cleanliness, while ensuring that the animals remained fully unloaded for the 28-day period.

Bone Removal and Preservation

At each 28 day time point, 15 animals were sacrificed to provide mechanical testing specimens at multiple time points. The rats were anesthetized with ketamine, pQCT scanned following the procedures described below, and euthanized in agreement with the experiment's AUP and IRB approval. After sacrifice, the right and left femora were excised and carefully cleaned of soft tissue, while ensuring that damage to the midshaft and femoral neck, which could create stress concentrations and premature failure during mechanical testing, was avoided. The right femur was cut in half at the diaphysis so that the distal half could be used for organic matrix assays and histomorphometry. The right proximal femur and the left whole femur were wrapped in gauze, soaked in phosphate buffered saline (PBS), and stored in separate vials in a -20° C freezer for preservation. The specimens were removed from the freezer only for CT scanning and for axial mechanical testing of the right proximal femur or three-point bend testing of the left femur, followed by lateral mechanical testing of the left proximal femur half. The right

proximal femurs and left midshafts experienced two freeze-thaw cycles, while left proximal femurs experienced three freeze-thaw cycles.

Tomography Scanning

A Stratec XCT-Research M peripheral quantitative computed tomography (pQCT) scanner (XCT Research M Stratec; Norland Corp., Fort Atkinson, WI) with a 0.071 X 0.071 X 0.5 mm voxel size was used to study the densitometric and architectural changes of the bone *ex vivo*. Before scanning, the machine was calibrated with a hydroxyapatite cone phantom simulating normal bone properties to ensure precision measurements.

The left femur midshafts were scanned first so that three-point bending mechanical testing could occur before scanning both the right and left proximal femurs. A specimen which aligned the femur along the axis of the scanner's gantry was fixed into place and filled with PBS to maintain normal hydration of the bone (Fig. 12 A).

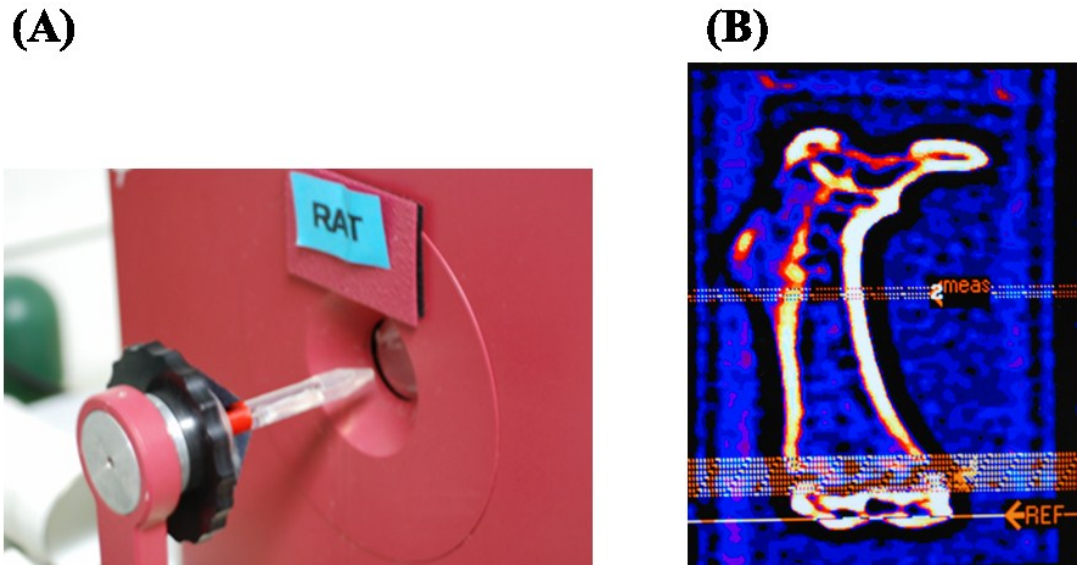

Fig. 12. (A) Femur prepared for pQCT scanning. (B) pQCT scout scan showing placement of scan lines to scan the femur metaphysis and the midshaft.

A femur was placed into the holder with the anterior side facing down and an initial scout view was taken of the whole femur to determine slice position through the use of a reference line placed at the distal end (Fig. 12B). Scans were generated using contour mode 3 to determine the outer edge of the bone with peel mode 2 to distinguish between cortical and cancellous bone. Two scan slices were then taken at the diaphysis (midshaft) and densitometric data including total, cancellous, and cortical volumetric bone mineral density (vBMD), bone mineral content (BMC), area, and cross-sectional moment of inertia (CSMI). Total, or integral, results consist of both the cancellous bone and the cortical bone which surrounds it (Fig. 13). The cortical results consist of only the cortical shell, seen in Fig. 13 as the white outline around the colored cancellous bone, while the cancellous results consist of only the inner cancellous bone inside the cortical shell.

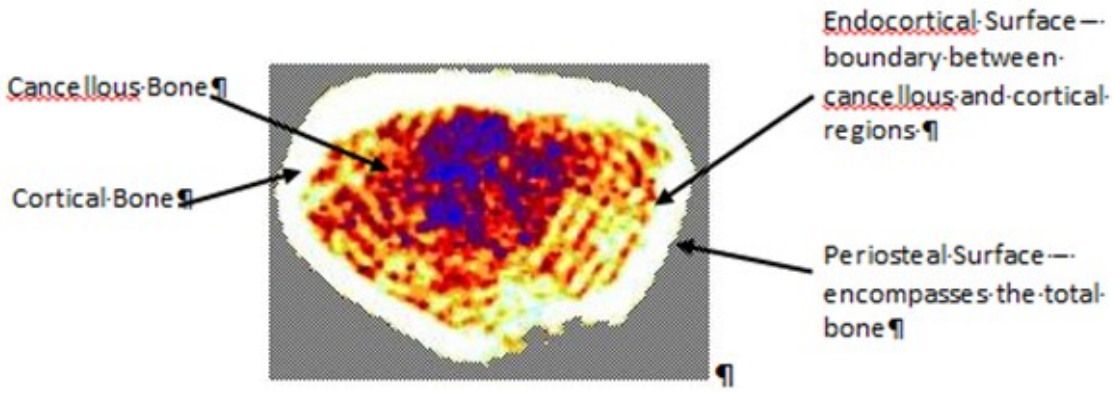

Fig. 13. Image of a pQCT scan of bone at the femur metaphysis. This figure is used to illustrate a pQCT scan which clearly shows the cortical shell surrounding the inner trabecular bone. Total or integral bone consists of this entire area, cortical bone consists of only the cortical shell, and trabecular bone consists of only the cancellous bone within the cortical shell.

A sample of cross-sectional scans corresponding to the scout view of Fig. 12B is shown in Fig. 14. These include the five scans at the distal metaphysis (panels A-E), which

were not used in this study, plus the three scans at the midshaft (panels F-H), which were used in this study.

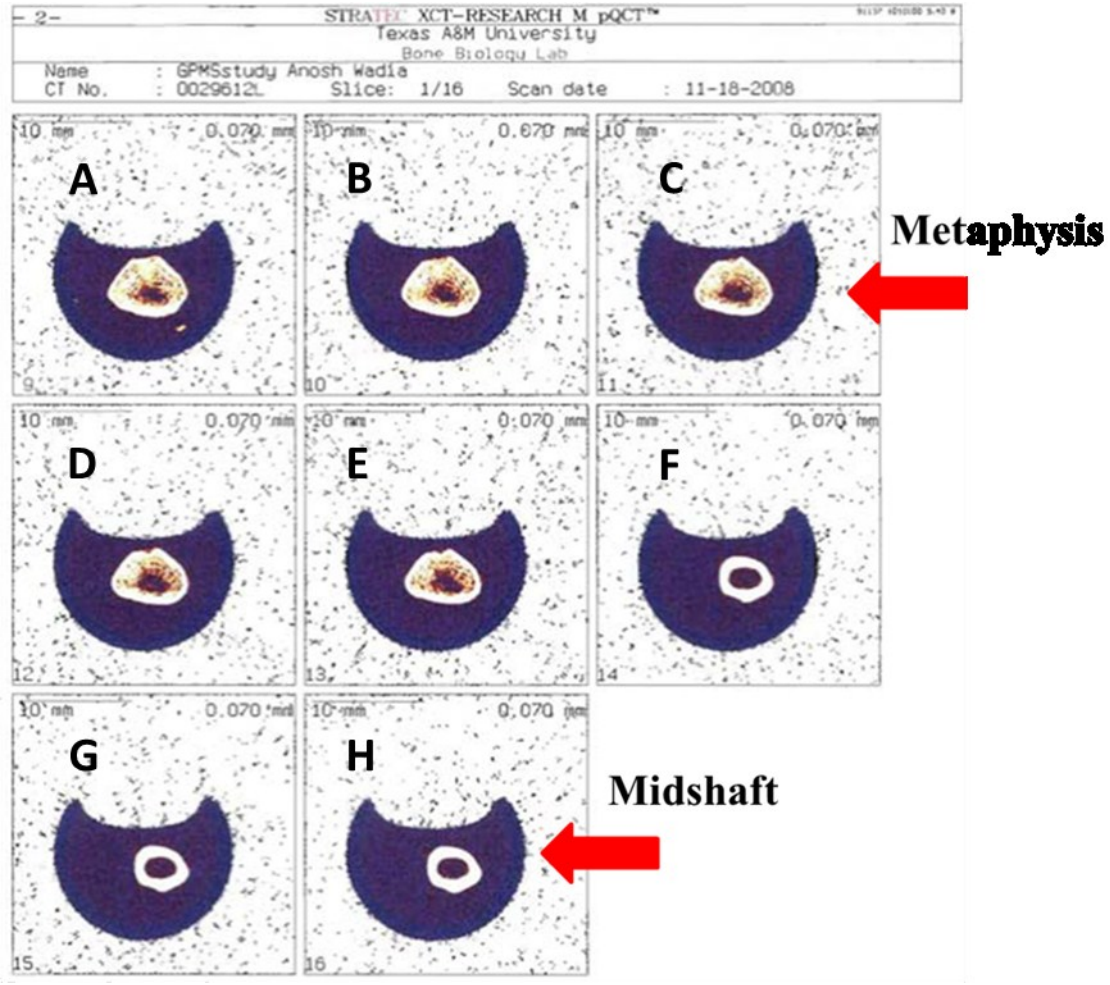

Fig. 14. Typical pQCT scan slices of the femur showing multiple scans at the metaphysis (5) and at the midshaft (3). The metaphysis has a thin cortical shell made of dense bone shown as a white ring around a large amount of lower density trabecular bone inside the shell shown in red. The midshaft has a thicker cortical shell with little to no trabecular bone present.

After three-point bend mechanical testing was completed on the left femurs, left and right proximal femurs remained to be scanned. Two proximal femur molds were built to

position both the right and left necks along the axis of the scanner's gantry. Each specimen was carefully placed into either a right or left mold and wrapped in saline soaked gauze to maintain preservation. Three slices were chosen in the neck region of both the right and left proximal femurs (Fig. 15). Densitometric and geometric property data was collected and averaged for the three slices.

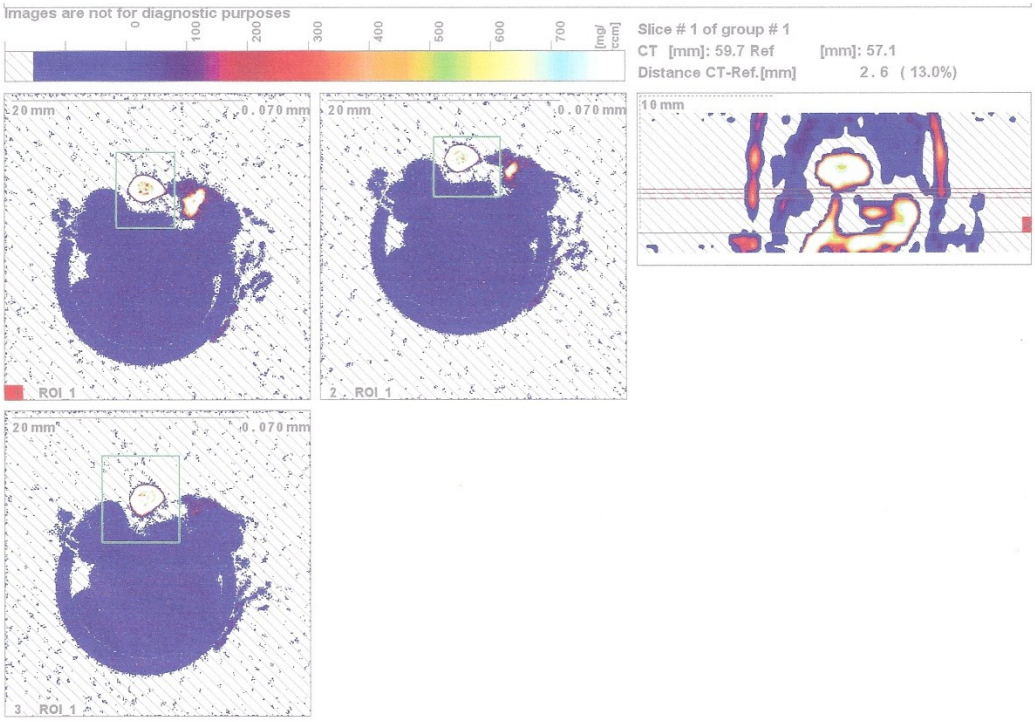

Fig. 15. A typical femoral neck pQCT scan. The figure on the right displays scan line placement while the three figures on the left display the slices associated with each scan line.

Mechanical Testing: Femur Midshaft

The femurs were removed from the freezer, thawed, and an Instron 3345 Mechanical Testing System was used to perform the three-point bend testing of the left femurs. The bones were placed anterior side down across two aluminum span supports 15 mm apart

and loaded by a descending hammer which contacted at the midshaft until fracture (Fig. 16). The Instron machine provided a quasi-static load at a rate of 2.54 mm/min (0.1 in/min) during the test and the load was measured with a 1000 N load cell. A linear variable displacement transducer (LVDT) was used to collect sensitive displacement measurements at the loading site and the data was recorded at 10 Hz.

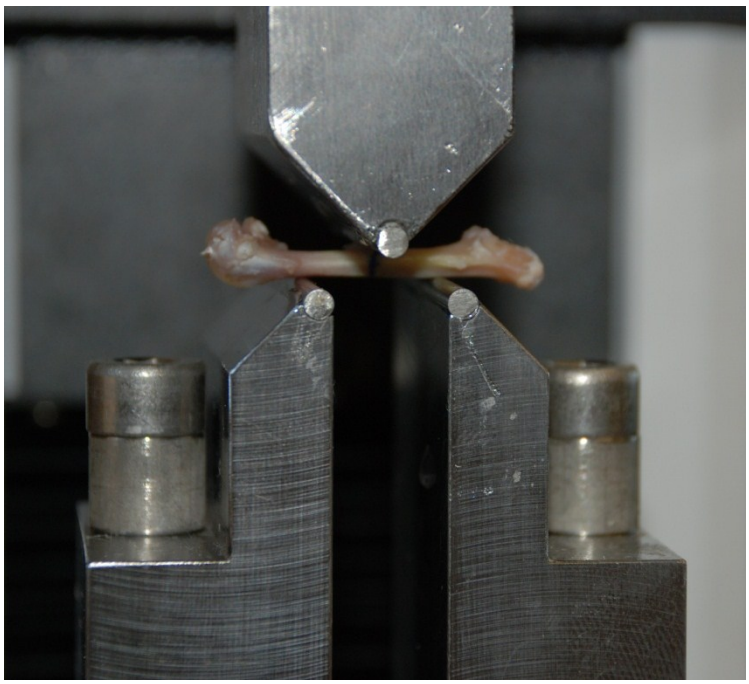

Fig. 16. Three-point bending test of the femur at the midshaft. The specimens are placed across a span of 15 mm and tested at the midshaft by a hammer which descends at a constant rate of 2.54 mm/min until failure.

Mechanical Testing: Femoral Neck

Following the initial mechanical testing of the left femurs and subsequent proximal femur scanning, the Instron machine was used again to perform mechanical testing to failure for each proximal femur. Two different loading stances, axial and lateral, were used to test the mechanical strength.

Axial Testing

For axial testing, which simulates a single leg stance, a rigid metal testing fixture with holes of various sizes to accommodate different femoral shaft sizes was used to keep the main axis of the femoral shaft vertical. Each hole was notched to fit the lateral ridge of the femur shaft to ensure a secure fit and to ensure that the vertical alignment was maintained throughout the test. The proximal femur was then positioned so that a flat cylindrical platen was set over the femoral head and in a direction parallel to the femoral shaft (Fig. 17). A quasi-static load was applied to the femoral head via the cylindrical platen at a rate of 2.54 mm/min until the specimen fractures.

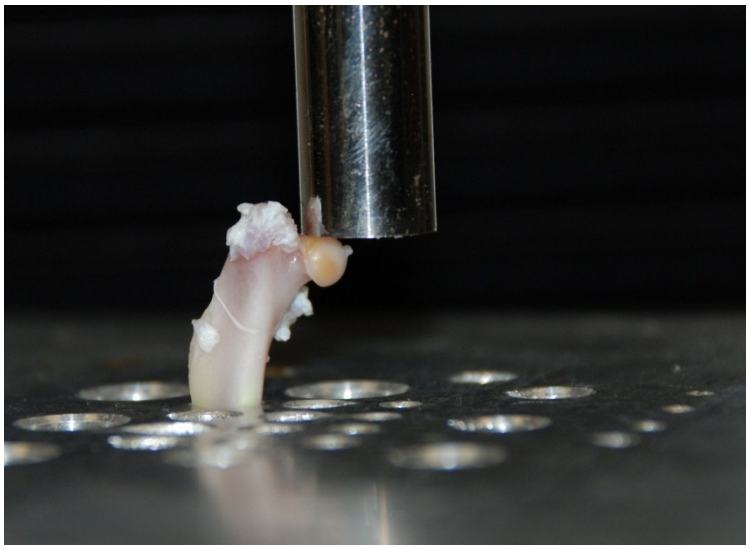

Fig. 17. Axial femoral neck test. The specimen is placed in a machined jig at the base and positioned under a platen. The platen presses down on the femoral head to produce loading forces on the neck at a constant rate of 2.54 mm/min until failure.

Lateral Testing

Lateral testing, which simulates a typical biped fall stance, utilized a testing fixture which rotated the bone approximately 100 degrees. The fixture also featured an adjustable clamp to fit the different femoral shaft sizes and to provide a secure fit. The femur was supported by a pair of bearings at the clamp to stop any moment from occurring in the femoral shaft. Also, the surface of the fixture was covered with a soft rubber to focus the breaking force in the neck region instead of on the greater trochanter (Fig. 18). The femoral head was again aligned under a flat, cylindrical platen which provided a quasi-static load at a rate of 2.54 mm/min.

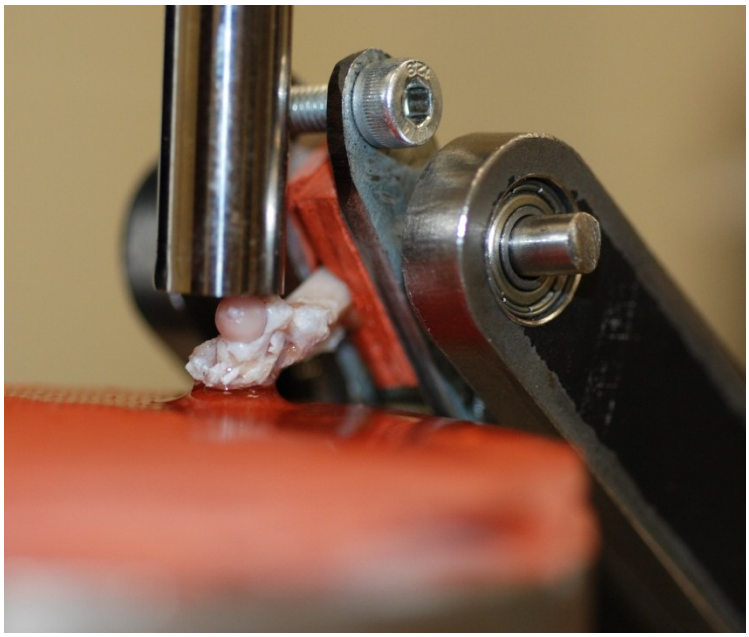

Fig. 18. Lateral femoral neck test. The specimen is clamped at the base in a machined jig and positioned under a platen. The platen presses down on the femoral head to produce loading forces on the neck, which have a different loading direction than the axial test, at a constant rate of 2.54 mm/min until failure.

Data Analysis

Data acquired from pQCT scanning was imported into Microsoft Excel for analysis, each animal was separated into their respective groups, and each group was averaged to form a single time point. The averages were plotted to show longitudinal data over the course of the experiment in order to observe trends from hindlimb unloading and the recovery periods. All properties including total vBMD, BMC, area, cortical and trabecular vBMD, BMC, and area, as well as cross-sectional moments of inertia (maximum, minimum, and polar) were analyzed and plotted for the left femur midshafts and the femoral necks. The average cortical thickness was determined by assuming the total area provided by the pQCT scanner was a circle and calculating the radius. The radius for the endocortical area was determined in the same manner. The endocortical radius was subtracted from the total radius to calculate the thickness of the cortical shell. Image files showing the attenuation values of each voxel were also collected from the pQCT scanner. Utilizing a method developed by Joshua Davis(55) in accordance with a an analysis developed by Cory et al.(56), MS Excel was used to analyze each file through conditional formatting to form an image of the cross-sectional slice taken by the CT scanner. The attenuation values were converted to elastic modulus values by the following method. A set of axes were generated and the centroid of the slice was calculated. Using the polar moments of inertia and the width provided by the scanner for each slice, an elastic modulus weighted bending strength index (BSI) was calculated with the following equations and used as a non-destructive, calculated measure of bone strength.

$$I_x + I_y = \left(\sum (E * X^2) + \sum (E * Y^2)\right) * \frac{0.007^2}{18600}$$

$$BSI = \frac{I_x + I_y}{W}$$

The mechanical testing data were analyzed using a custom MatLab program called DatMeT 3.0 which was developed by Scott Bouse, a previous student in the Texas A&M Bone Biomechanics Lab. The force and displacement data were imported into the program and plotted to show force vs. displacement curves for each specimen. DatMeT was used to calculate extrinsic mechanical properties including stiffness (N/mm), ultimate force (N), yield force (N), and energy to yield (N-mm), ultimate force (N-mm), and failure (N-mm).

The specimen curves were selected and the linear region, ultimate force, and break point were chosen by the user (Fig. 19). The program then automatically calculated the extrinsic properties and produced an Excel file with the data. The values for each time point were averaged and plotted to generate longitudinal curves showing the changes in the extrinsic properties due to the hindlimb unloading and the recovery periods.

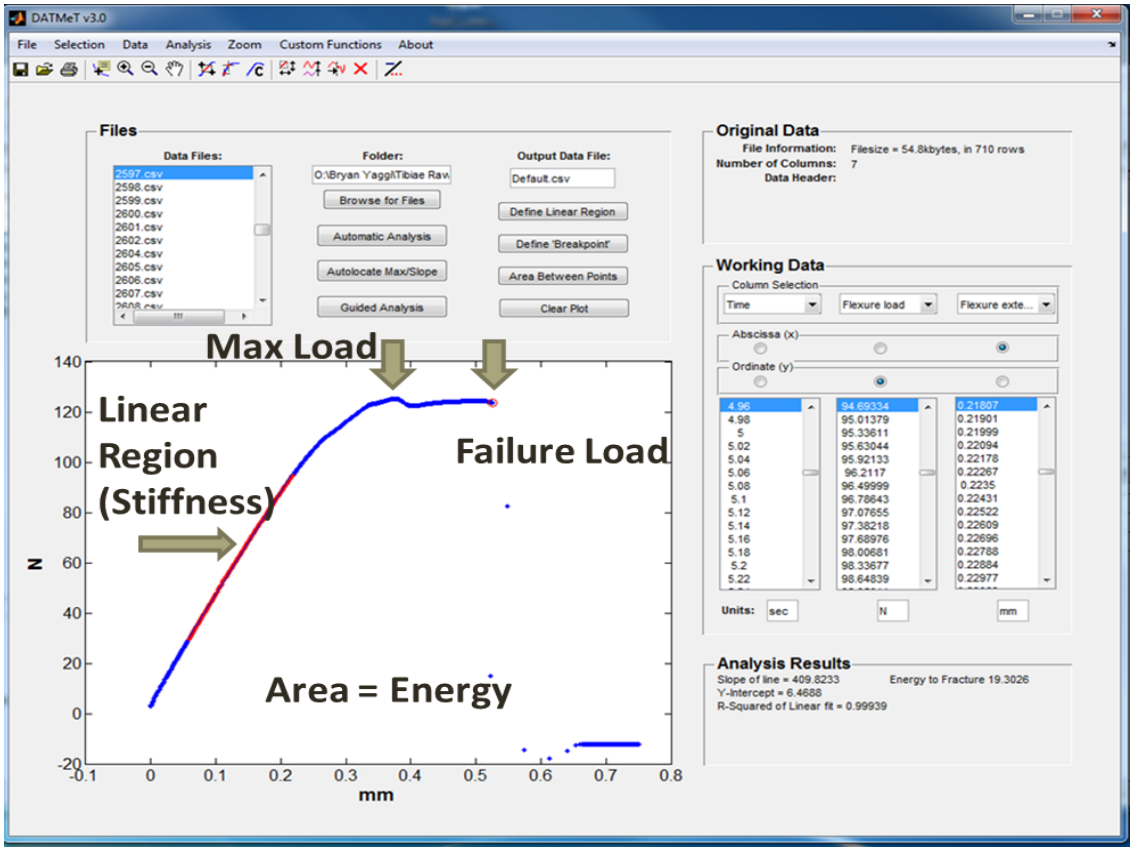

Fig. 19. An example of DatMet being used to analyze mechanical testing data collected from the Instron testing machine. The load displacement curve is graphed in blue and the linear region is highlighted in red. The failure point has been chosen and is depicted by the red circle. Once the user has defined these, the program calculates the stiffness, yield point, and energies and generates an Excel file with these values clearly labeled (see Appendix). An example of the Excel file can be seen in the Appendix.

Statistical Analysis

Stastical analyses were performed on all data (densitometric, geometric, mechanical testing, and calculated strengths) using SPSS (IBM, Armonk, New York) at a p-value of 0.5. The data collected both from pQCT scanning and mechanical testing is end-point data, meaning the data was collected *ex-vivo* after the animal was euthanized. Due to the variability of having different animal groups providing data at different times, a two-sample t-test was deemed appropriate and used between data points of interest to observe any statistically significant differences. Normality was assumed among the groups but equal variances were not.

Recovery can be defined a number of different ways; a recovery value can be compared to the original baseline values at the beginning of the study, with respect to age-matched cage control values, or to recovery values seen at the end of each HU period. Therefore, the t-tests were performed with respect to BL, to AC, and to HU to fully observe the recovery dynamic after suspension.

RESULTS

The results of the pQCT scanning, mechanical testing, and statistical analyses are presented in the following way. Absolute values with statistical symbols are shown by tables at the beginning of each section while data shown as a percentage of baseline value are displayed graphically. The right femoral neck pQCT data are presented in this section of the document, while the left femoral neck pQCT data is presented in the Appendix. Both sets of data are very close in magnitudes and trends, but, since different mechanical tests were performed on the right and left necks, it was deemed appropriate to scan both bone sites and keep the data separate to look for differences in the loading condition that could be explained by the respective densitometric data.

Each graph, displaying the difference from baseline values along the y-axis, is also labeled with the age of the animals along the x-axis, the blue line represents the results of the aging control animals (AC), and the red lines represent the results from the different HU treatments and recovery periods. For consistency and clarity, each point on the graphs is referred to in the text by group, age, and then recovery period length. For instance, BL6 is a reference to the baseline starting point at 6 months of age. AC7 refers to the aging control point (along the blue line) just after the BL point at 7 months of age, while 1HU7 is the first HU (along the red line) that occurs at the same 7 month time slot. 1HU7+R1, 1HU7+R2, and 1HU7+R3 refer to the recovery points, one every month for three months, after the first HU. The 1HU10 and 2HU10 lines diverge from the AC group at month 9 and 1HU7+R2 point respectively and all HU periods are highlighted in yellow. The final HU recovery points are referred to as 1HU10+R2 and 2HU10+R2 because there is a full two month time period from the end of the HU treatment to the final day of the recovery period.

Femoral Neck Densitometric Properties

The densitometric (BMC and vBMD) properties of the right femoral neck are presented via absolute values in Table 1 and percentages with respect to BL shown graphically in Figs. 20 – 25. BMC is lower after HU treatments at month 7 (1HU7) and month 10 (1HU10, 2HU10) across all of the bone compartments: total, cortical, and trabecular. However, total BMC and cortical BMC (Figs. 20-21) increase during the recovery periods, while trabecular (Fig. 22) BMC does not and continues to decrease over the 12 month testing period.

The aging cage control group exhibits some fluctuations in BMC relative to BL rats likely due to the aging of the animals particularly at 8, 10, and/or 12 months of age. As stated previously, recovery can be defined with respect to baseline, cage control, and to a significant increase after HU. 1HU7 and 1HU7+R1 values are significantly different from cage control for both total and cortical BMC but not from baseline. Recovery with respect to cage control and increase from HU occurs by the second recovery point (1HU7+R2) with the final recovery point nearly matching the cage control value at the same time. 1HU10 and 2HU10 also show significant decrements compared to cage control but not to baseline. The 2HU10 value is significantly lower than the 1HU+R3 value showing a large decrease in BMC compared to the recovery point. Both HU treatments at 10 months show recovery with respect to baseline and to cage control values after two recovery periods but not with respect to their HU values at 10 months. Trabecular BMC trends negatively overall for each group with final values at 12 months of age being significantly different from baseline but not cage control or any previous HU value.

Volumetric BMD has similarities and differences compared to the BMC. For instance, the values for the total bone show similar trends to the total bone values for BMC, with reductions at each HU point followed by increases during the recovery period (Fig. 23).

However, the trabecular vBMD (Fig. 24) follows more closely with the trends seen for the total bone vBMD and the cortical vBMD (Fig. 25) shows an increasing trend over time. The total and trabecular bone compartments lose significant vBMD during the HU at 7 months from both baseline and matching cage control values and do not recover with respect to BL or AC until the second recovery point (1HU7+R2). Values after HU at 9-10 months of age (1HU10, 2HU10) are significantly lower compared to BL and AC, but total vBMD does not exhibit reductions due to the increasing cortical vBMD at the same time point. The final data points (1HU10+R2, 2HU10+R2) at month 12 show recovery with respect to cage control but not baseline for the trabecular bone and full recovery for the total bone. Cortical vBMD values increase overall for each group, with the final values at 12 months of age being significantly different from baseline but not cage control. Also, the final values show significant increases compared to the HU values at 10 months of age.

Table 1: Mineral Properties for Total (integral), Cancellous, and Cortical Bone Right Femoral Neck

	Total BMC (mg/mm)	Total vBMD (mg/cm^3)	Cancellous BMC (mg/mm)	Cancellous vBMD (mg/cm^3)	Cortical BMC (mg/mm)	Cortical vBMD (mg/cm^3)
6 Months Old						
BL6	4.80 (0.13)	1130.8 (12.7)	1.49 (0.08)	762.3 (9.57)	3.31 (0.10)	1431.1 (4.62)
7 Months Old						
AC7	5.01 (0.12)	1149.9 (13.1)	1.53 (0.10)	778.1 (14.4)	3.49 (0.08)	1442.8 (5.88)
1HU7	4.60 (0.10)†	1043.6 (16.1)*†	1.45 (0.07)	645.0 (12.3)*†	3.15 (0.06)†	1441.3 (6.00)
8 Months Old						
AC8	5.18 (0.12)*	1130.1 (16.3)	1.67 (0.10)	766.5 (15.2)	3.52 (0.06)	1447.5 (6.61)*
1HU7+R1	4.71 (0.12)†	1074.5 (15.7)*†	1.52 (0.10)	692.3 (14.2)*†◊	3.19 (0.07)†	1437.4 (6.00)
9 Months Old						
AC9	5.01 (0.14)	1148.7 (16.9)	1.47 (0.12)	742.0 (15.7)	3.54 (0.06)	1461.3 (8.86)*
1HU7+R2	4.90 (0.11)	1177.6 (14.7)*◊	1.24 (0.10)	726.8 (16.3)◊	3.66 (0.05)*◊	1469.0 (6.63)*◊
10 Months Old						
AC10	5.50 (0.15)*	1133.9 (16.6)	1.67 (0.12)	747.8 (16.5)	3.82 (0.08)*	1449.1 (9.56)
1HU7+R3	5.34 (0.17)*	1157.6 (16.4)◊	1.41 (0.11)	720.5 (21.0)◊	3.93 (0.10)*◊	1463.4 (8.92)*◊
1HU10	4.81 (0.08)†#	1105.0 (17.6)	1.28 (0.07)†	650.3 (16.8)*†#	3.53 (0.06)†	1458.7 (5.20)*
2HU10	4.62 (0.12)†#‡	1157.0 (14.1)	1.13 (0.08)*†‡	682.8 (13.2)*†#	3.49 (0.06)†#‡	1474.6 (5.11)*†◊
12 Months Old						
AC12	5.09 (0.12)	1210.2 (14.0)*	1.15 (0.10)*	720.4 (18.4)*	3.93 (0.07)*	1495.0 (5.92)*
1HU10+R2	4.93 (0.09)	1169.1 (14.7)◊	1.18 (0.07)*	691.6 (13.0)*	3.75 (0.05)*†◊	1480.7 (4.59)*◊
2HU10+R2	4.90 (0.12)	1232.5 (13.8)◊	1.02 (0.08)*	723.0 (23.6)	3.88 (0.08)*◊	1497.6 (3.82)*◊

Values are presented as mean ± SE

*** Indicates significant difference from baseline value, $p < 0.05$**

† Indicates significant difference from age-matched control value at same time point, $p<0.05$

 # Indicates significant difference from month 9 pre-HU value within same group (i.e. 1HU10(+R2) or 2HU10 + (R2)), $p <0.05$

◊ Indicates significant difference from immediate preceding post-HU value within same group, $p<0.05$

‡ Indicates significant difference between 1HU7+R3 and 2HU10, $p<0.05$

¤ Indicates significant difference between 1HU10 and 2HU10 at the same time point, $p<0.05$

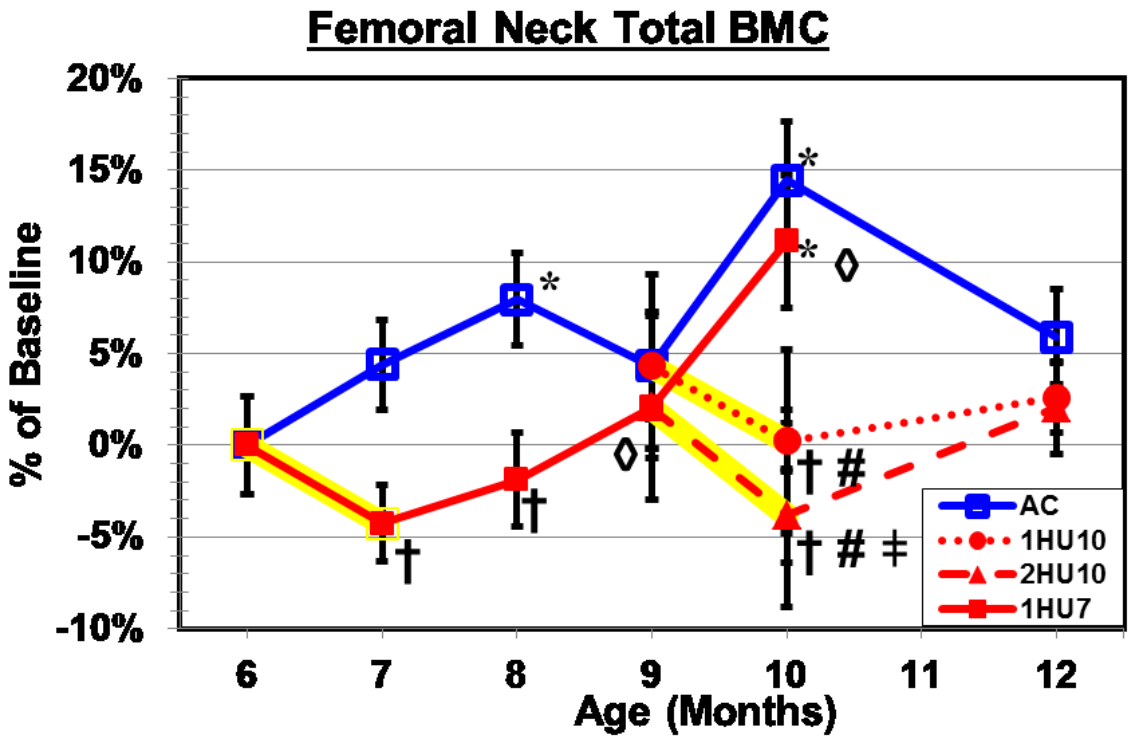

Fig. 20. Total (integral) BMC at multiple time points during unloading and subsequent recovery of the right femoral neck. Numerical values are presented in Table 1 and yellow highlighting indicates HU treatment. AC shows initial increases in BMC with fluctuations at later months likely due to the aging of the animals. 1HU7 shows a decrease (-4.25%) from baseline (BL) with a significant difference from AC. Recovery with respect to CC requires 2 recovery periods and then closely trends with the control. 1HU10 is slightly higher than BL (0.24%) due to the increase of BMC as the animals age and 2HU10 is lower than BL (-3.82%) due to the recovery from the 1HU7 treatment back to AC values. All groups return to approximately baseline values by month 12 and recover with respect to AC. However, the final HU recovery points are not significantly different from the 10 month HU treatments (1HU10, 2HU10).

Values are presented as mean ± SE

*** Indicates significant difference from baseline value; $p<0.05$**

† Indicates significant difference from age-matched cage control value at same time point; $p<0.05$

 # Indicates significant difference from month 9 pre-HU value within same group; $p<0.05$

ǂ Indicates significant difference between 1HU7+R3 and 2HU10; $p<0.05$

¤ Indicates significant difference between 1HU10 and 2HU10 at the same time point; $p<0.05$

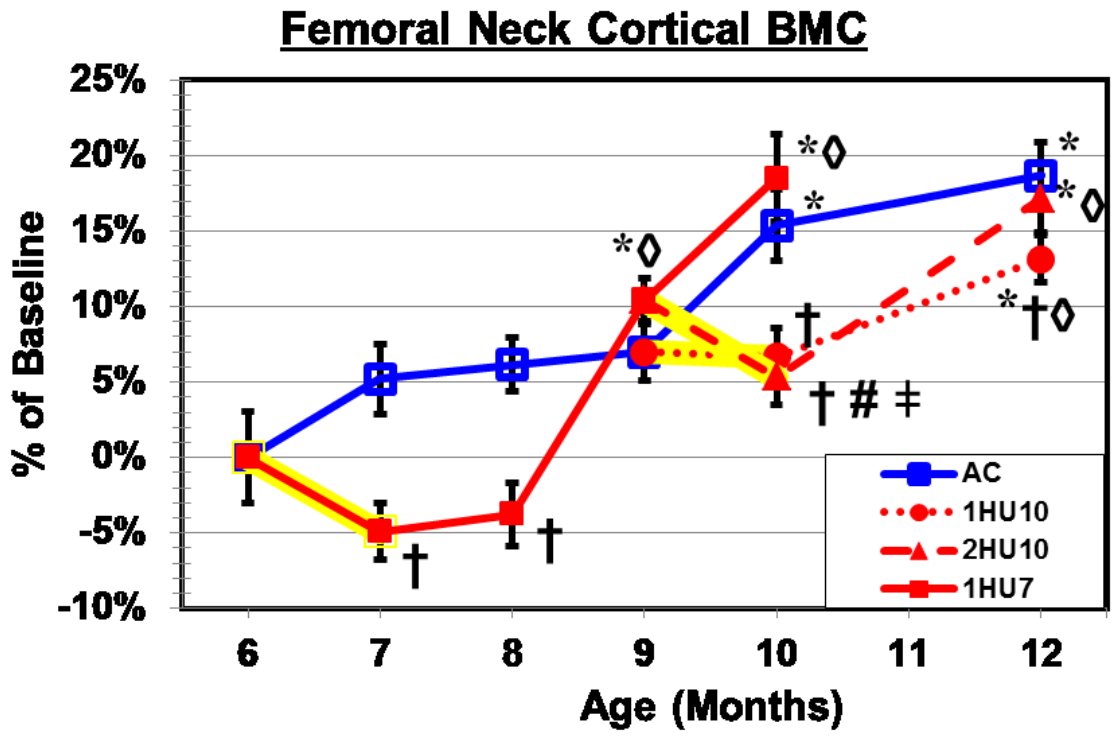

Fig. 21. Cortical BMC at multiple time points during unloading and subsequent recovery of the right femoral neck. Numerical values are presented in Table 1 and yellow highlighting indicates HU treatment. AC shows increases throughout the experiment and is significantly higher (18.69%) than BL by the end of month 12. 1HU7 shows a non-significant drop from BL (-4.91%) with a significant difference from matching AC with only a slight recovery, which is still significantly different from AC, by the end of month 8. A large recovery takes place between months 8 and 9 bringing the initial HU group back to AC values with significant differences from BL and 1HU7+R1. The recovery trend continues and matches AC, finishing at a much higher value than BL (18.52%). 1HU10 and 2HU10 show significant differences from AC without being significantly different than BL, and 2HU10 shows a significant drop from 1HU7+R2 and a significant difference from 1HU7+R3. All groups (HUs and AC) were significantly higher than BL at the end of month 12; however, 1HU10+R2 was significantly lower than AC. Both 1HU10+R2 and 2HU10+R2 recovered significantly higher than 1HU10 and 2HU10 respectively.

Values are presented as mean ± SE

*** Indicates significant difference from baseline value; p<0.05**

† Indicates significant difference from age-matched cage control value at same time point; p<0.05

 # Indicates significant difference from month 9 pre-HU value within same group; p<0.05

ǂ Indicates significant difference between 1HU7+R3 and 2HU10; p<0.05

¤ Indicates significant difference between 1HU10 and 2HU10 at the same time point; p<0.05

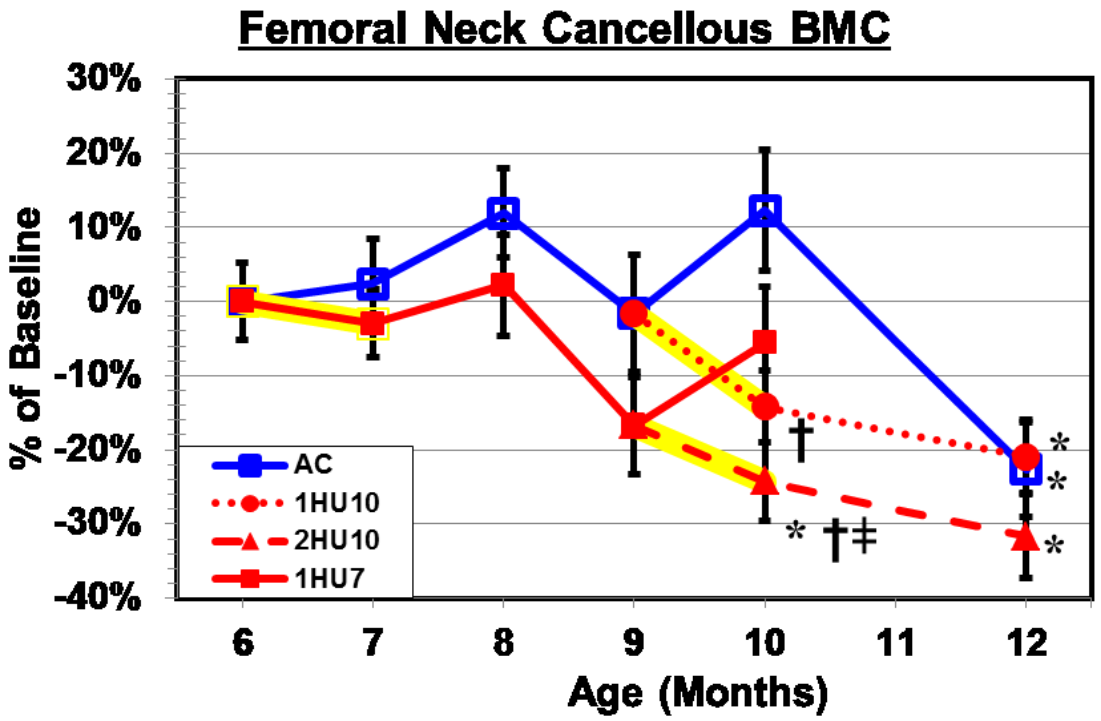

Fig. 22. Cancellous BMC at multiple time points during unloading and subsequent recovery of the right femoral neck. Numerical values are presented in Table 1 and yellow highlighting indicates HU treatment. Trabecular BMC fluctuates for all groups for the first 9 months due to the aging of the animals. 1HU7 shows little change from both BL and from matching AC; however, 1HU10 shows a significant difference from AC and 2HU10 shows a significant decrease from BL (-24.26%) as well as a significant difference from AC and from 1HU7+R3. The final HU recovery groups (1HU10+R2, 2HU10+R2) do not show recovery back to baseline or recovery from 1HU10 and 2HU10 respectively, but are also not significantly different from matching AC.

Values are presented as mean ± SE

*** Indicates significant difference from baseline value; p<0.05**

† Indicates significant difference from age-matched cage control value at same time point; p<0.05

 # Indicates significant difference from month 9 pre-HU value within same group; p<0.05

ǂ Indicates significant difference between 1HU7+R3 and 2HU10; p<0.05

¤ Indicates significant difference between 1HU10 and 2HU10 at the same time point; p<0.05

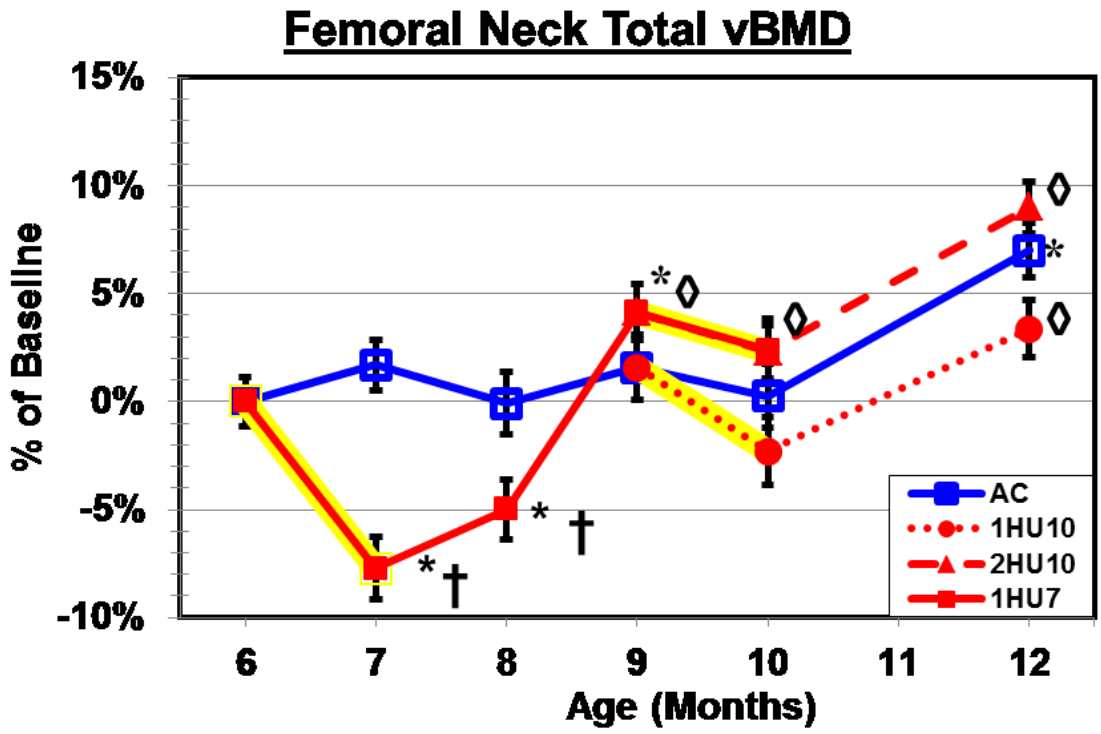

Fig. 23. Total (integral) vBMD at multiple time points during unloading and subsequent recovery of the right femoral neck. Numerical values are presented in Table 1 and yellow highlighting indicates HU treatment. AC shows typical fluctuations due to age, similar to the results seen for BMC. 1HU7 shows a significant decrease from BL (-7.71%) and a significant difference from AC at 7 months that does not recover after one month. By 9 months vBMD has recovered to AC values and is significantly higher than BL and the 2HU10 point shows a non-significant decrease from the 1HU7+R3 point. The 1HU10 point also shows a non-significant decrease from AC and both 1HU10+R2 and 2HU10+R2 show increases which match the aging increases of the AC.
Values are presented as mean ± SE
*** Indicates significant difference from baseline value; p<0.05**
† Indicates significant difference from age-matched cage control value at same time point; p<0.05
 # Indicates significant difference from month 9 pre-HU value within same group; p<0.05
ǂ Indicates significant difference between 1HU7+R3 and 2HU10; p<0.05
¤ Indicates significant difference between 1HU10 and 2HU10 at the same time point; p<0.05

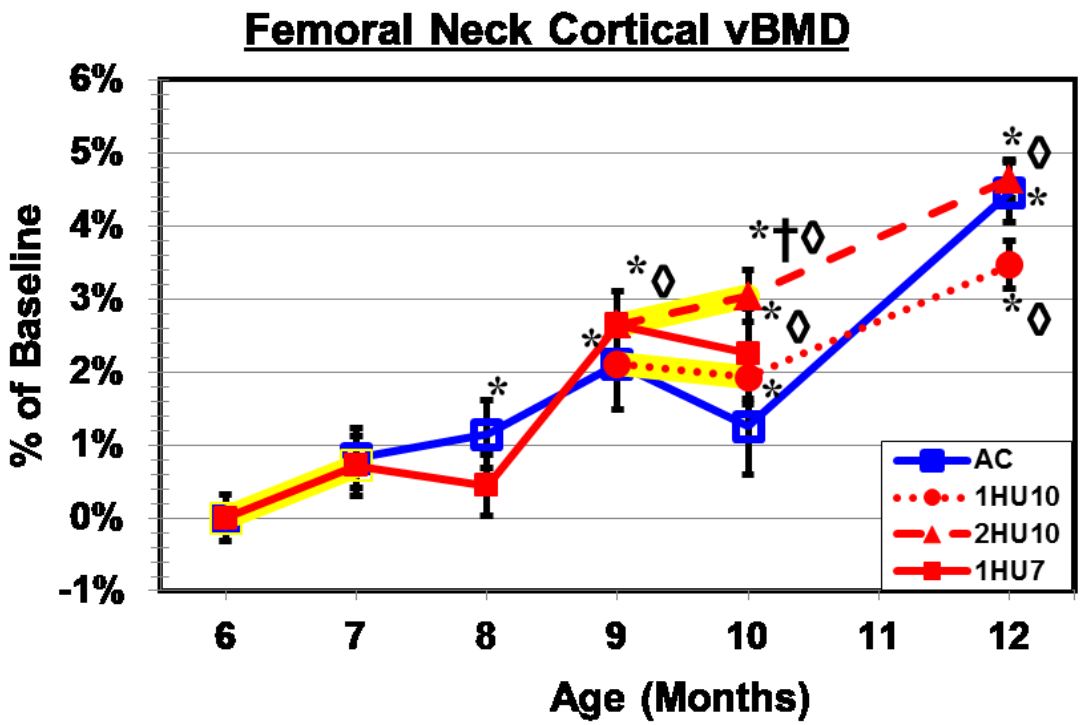

Fig. 24. Cortical vBMD at multiple time points during unloading and subsequent recovery of the right femoral neck.. Numerical values are presented in Table 1 and yellow highlighting indicates HU treatment. Cortical vBMD results show a generally increasing trend for all groups with slight variation likely due to age. There is little difference between the AC group and all of the HU groups, but all groups are significantly higher than baseline by the end of the study.

Values are presented as mean ± SE

*** Indicates significant difference from baseline value; p<0.05**

† Indicates significant difference from age-matched cage control value at same time point; p<0.05

 # Indicates significant difference from month 9 pre-HU value within same group; p<0.05

ǂ Indicates significant difference between 1HU7+R3 and 2HU10; p<0.05

¤ Indicates significant difference between 1HU10 and 2HU10 at the same time point; p<0.05

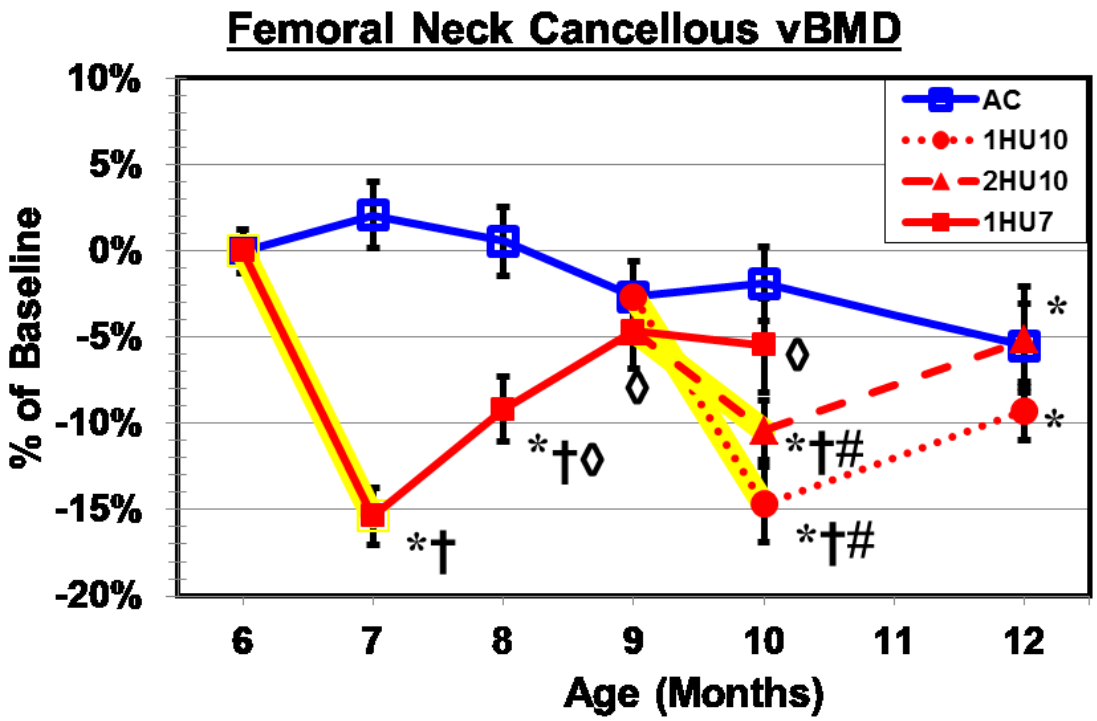

Fig. 25. Cancellous vBMD at multiple time points during unloading and subsequent recovery of the right femoral neck. Numerical values are presented in Table 1 and yellow highlighting indicates HU treatment. The AC group shows a slow decrease in vBMD with only the AC12 point being significantly different from BL. However, 1HU7 shows a large decrease from BL and a significant difference from AC which shows partial recovery, with respect to HU, by 1HU7+R1. By month 9, recovery to BL and AC values occurs, but 1HU10 and 2HU10 show significant decreases from BL and significant differences from AC values. All HU groups recover to AC by the end of the study but are still significantly lower than the original BL value.

Values are presented as mean ± SE

*** Indicates significant difference from baseline value; p<0.05**

† Indicates significant difference from age-matched cage control value at same time point; p<0.05

 # Indicates significant difference from month 9 pre-HU value within same group; p<0.05

ǂ Indicates significant difference between 1HU7+R3 and 2HU10; p<0.05

¤ Indicates significant difference between 1HU10 and 2HU10 at the same time point; p<0.05

Femoral Neck Geometric Properties

Geometric properties (Table 2) were also acquired from the pQCT analyses and included total area, cortical shell area, endocortical area (area inside the cortical shell), and polar moment of inertia. The cortical thickness, maximum moment of inertia, and minimum moment of inertia were calculated from the geometric parameters determined by the scanner software.

Total femoral neck area (Fig. 26) fluctuates for all groups, but only the 2HU10 data point shows significant differences from BL, AC, and 1HU7+R3. The greatest differences between the groups occur at month 10 with all groups converging to similar values by month 12. Cortical area (Fig. 27) differs significantly from BL values during months 9-12, but does not for the earlier months even though non-significant decreases can be seen. Overall cortical area continues to increase for all groups and each group is significantly greater than BL by month 12. The endocortical area (Fig. 28) inside the cortical shell fluctuates much more than the cortical area, with significant decreases versus BL and/or AC rats' values at 10 and 12 months in the 2Hu10 rats. Only the 2HU10 unloading point shows a significant decrease from BL, along with 2HU10+R2 and AC12. Cortical thickness (Fig. 29) follows a similar pattern to cortical area, with particularly large increases from BL for months 9-12 for all groups.

As expected, the moments of inertia (maximum (Fig. 30), minimum (Fig. 31), and polar (Fig. 32)) have similar patterns and only show significant differences from the BL values at month 10 where the greatest variability between all the groups is seen.

Table 2: Geometric Properties for Cortical, Cancellous, and Total (integral) Right Femoral Neck

	Total Area (mm^2)	Endocortical Area (mm^2)	Cortical Area (mm^2)	Cortical Thickness (μm)	I_{max} (mm^4)	I_{min} (mm^4)	I_p (mm^4)
6 Months Old							
BL6	4.27 (0.13)	1.95 (0.10)	2.31 (0.07)	0.38 (0.01)	2.37 (0.14)	1.34 (0.08)	3.71 (0.21)
7 Months Old							
AC7	4.38 (0.14)	1.96 (0.11)	2.42 (0.05)	0.39 (0.01)	2.59 (0.15)	1.38 (0.06)	4.00 (0.20)
1HU7	4.42 (0.12)	2.24 (0.11)	2.19 (0.04)†	0.34 (0.01)*†	2.32 (0.07)	1.37 (0.05)	3.69 (0.11)
8 Months Old							
AC8	4.62 (0.15)	2.18 (0.13)	2.43 (0.05)	0.38 (0.01)	2.69 (0.13)	1.53 (0.07)	4.22 (0.19)
1HU7+R1	4.41 (0.16)	2.19 (0.14)	2.22 (0.05)†	0.35 (0.01)†	2.41 (0.13)	1.32 (0.06)†	3.73 (0.17)
9 Months Old							
AC9	4.39 (0.17)	1.96 (0.15)	2.43 (0.04)	0.40 (0.01)	2.52 (0.17)	1.49 (0.07)	4.01 (0.24)
1HU7+R2	4.19 (0.13)	1.69 (0.12)◊	2.49 (0.04)*◊	0.42 (0.01)*†◊	2.45 (0.10)	1.40 (0.08)	3.85 (0.15)
10 Months Old							
AC10	4.89 (0.21)*	2.25 (0.17)	2.64 (0.05)*	0.41 (0.01)	3.16 (0.26)*	1.69 (0.08)*	4.85 (0.31)*
1HU7+R3	4.64 (0.19)	1.95 (0.14)	2.69 (0.07)*◊	0.43 (0.01)*†◊	2.98 (0.17)*◊	1.62 (0.12)*	4.60 (0.26)◊
1HU10	4.39 (0.13)†	1.97 (0.12)	2.42 (0.04)†	0.39 (0.01)	2.56 (0.15)†	1.45 (0.05)†	4.02 (0.19)†
2HU10	4.02 (0.14)†#‡	1.65 (0.11)*†	2.37 (0.04)†#‡	0.41 (0.01)*	2.28 (0.13)†‡	1.31 (0.07)†‡	3.59 (0.19)†‡
12 Months Old							
AC12	4.22 (0.13)	1.59 (0.11)*	2.63 (0.05)*	0.45 (0.01)*	2.62 (0.13)	1.47 (0.06)	4.09 (0.19)
1HU10+R2	4.25 (0.13)	1.71 (0.11)	2.53 (0.04)*◊	0.43 (0.01)*◊	2.54 (0.15)	1.45 (0.05)	3.99 (0.19)
2HU10+R2	4.00 (0.12)	1.40 (0.10)*	2.60 (0.05)*◊	0.46 (0.01)*◊	2.38 (0.11)	1.36 (0.06)	3.73 (0.18)

Values are presented as mean ± SE

*** Indicates significant difference from baseline value, $p < 0.05$**

† Indicates significant difference from age-matched control value at same time point, $p<0.05$

 # Indicates significant difference from month 9 pre-HU value within same group (i.e. 1HU10(+R2) or 2HU10 + (R2)), $p <0.05$

◊ Indicates significant difference from immediate preceding post-HU value within same group, $p<0.05$

‡ Indicates significant difference between 1HU7+R3 and 2HU10, $p<0.05$

¤ Indicates significant difference between 1HU10 and 2HU10 at the same time point, $p<0.05$

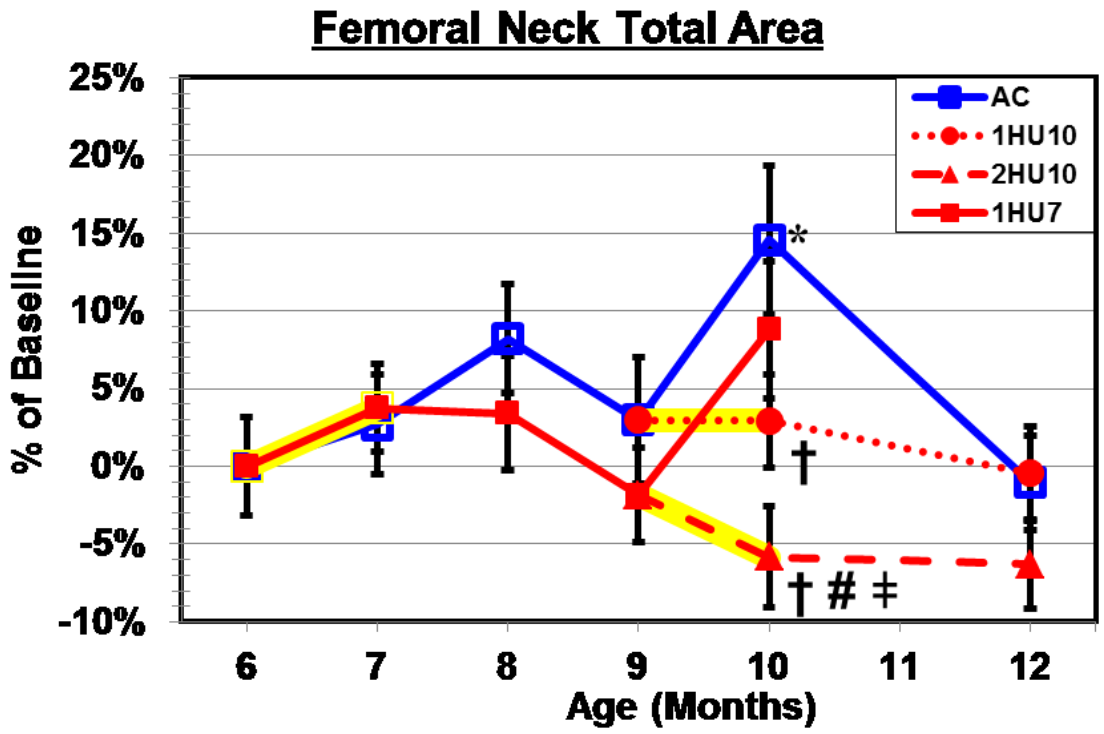

Fig. 26. Total (integral) Area at multiple time points during unloading and subsequent recovery of the right femoral neck. Numerical values are presented in Table 2 and yellow highlighting indicates HU treatment. No significant changes from BL or AC occur until month 10. AC10 shows a sharp jump to 14.56% greater than BL and 1HU10 and 2HU10 are both significantly different from AC10. All groups however recover with respect to BL and AC by the end of month 12.

Values are presented as mean ± SE

*** Indicates significant difference from baseline value; $p<0.05$**

† Indicates significant difference from age-matched cage control value at same time point; $p<0.05$

 # Indicates significant difference from month 9 pre-HU value within same group; $p<0.05$

ǂ Indicates significant difference between 1HU7+R3 and 2HU10; $p<0.05$

¤ Indicates significant difference between 1HU10 and 2HU10 at the same time point; $p<0.05$

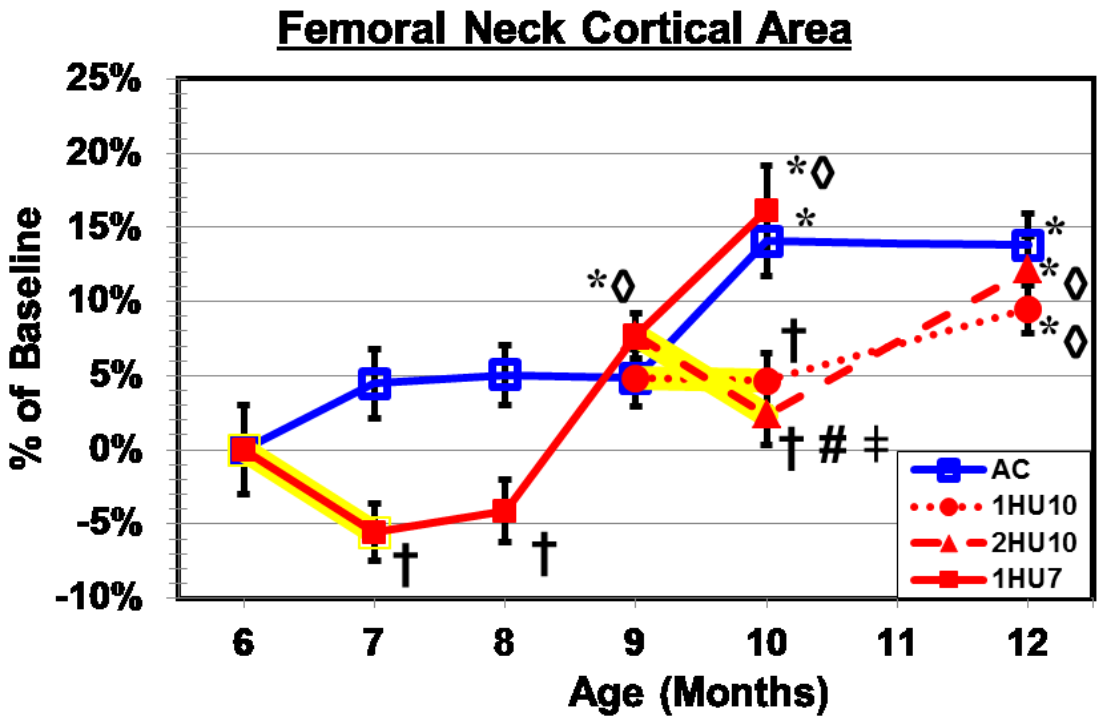

Fig. 27. Cortical area at multiple time points during unloading and subsequent recovery of the right femoral neck. Numerical values are presented in Table 2 and yellow highlighting indicates HU treatment. Cortical area trends are similar to those seen in BMC and vBMD with an initial decrease from BL for the 1HU7 point which is significantly different than AC. 1HU7+R1 is still significantly different than AC but recovers to higher than BL at 9 months and 10 months. 1HU10 and 2HU10 are both significantly lower than AC due in large part to an increase in AC area between months 9 and 10. All groups are recovered with respect to BL and significantly different than the respective HU points for month 12, but all groups are still significantly higher than BL.

Values are presented as mean ± SE

*** Indicates significant difference from baseline value; p<0.05**

† Indicates significant difference from age-matched cage control value at same time point; p<0.05

 # Indicates significant difference from month 9 pre-HU value within same group; p<0.05

ǂ Indicates significant difference between 1HU7+R3 and 2HU10; p<0.05

¤ Indicates significant difference between 1HU10 and 2HU10 at the same time point; p<0.05

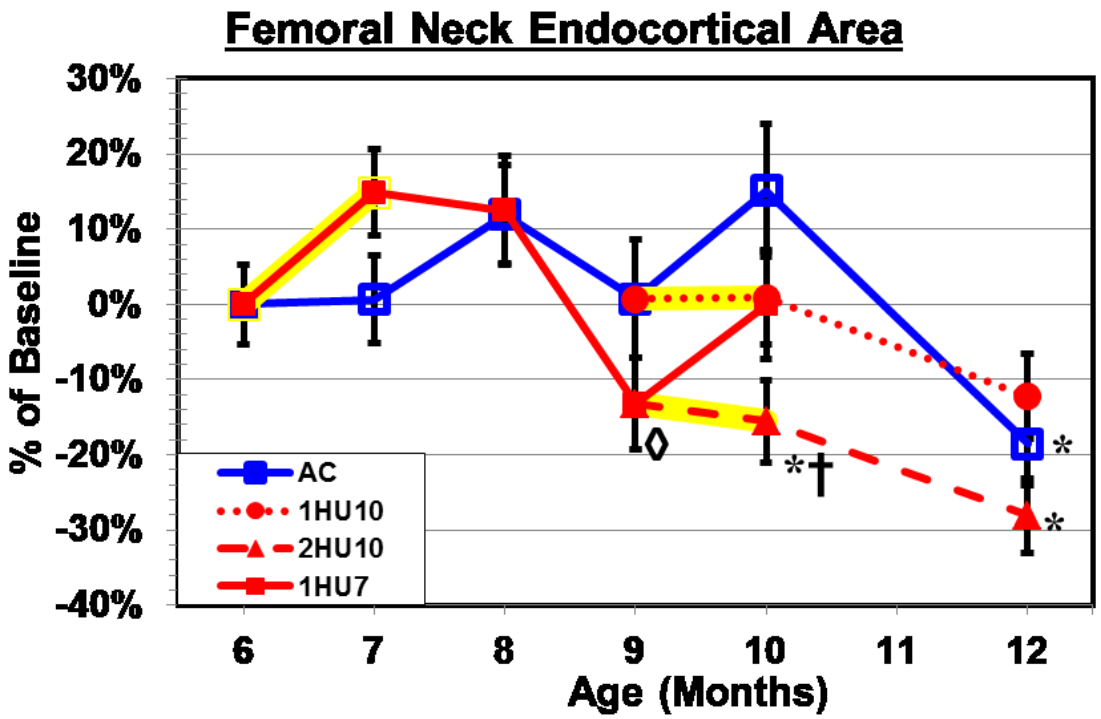

Fig. 28. Endocortical area at multiple time points during unloading and subsequent recovery of the right femoral neck. Numerical values are presented in Table 2 and yellow highlighting indicates HU treatment. Endocortical area fluctuates with few significant differences over the 6 month study period. Non-significant increases during 1HU7 correspond with decreases in cortical area during the same time period. Also, final values during month 12 show significant differences between 2HU10+R2 and AC from BL which corresponds with the increases in cortical area during the final months of the study.

Values are presented as mean ± SE

*** Indicates significant difference from baseline value; $p<0.05$**

† Indicates significant difference from age-matched cage control value at same time point; $p<0.05$

 # Indicates significant difference from month 9 pre-HU value within same group; $p<0.05$

ǂ Indicates significant difference between 1HU7+R3 and 2HU10; $p<0.05$

¤ Indicates significant difference between 1HU10 and 2HU10 at the same time point; $p<0.05$

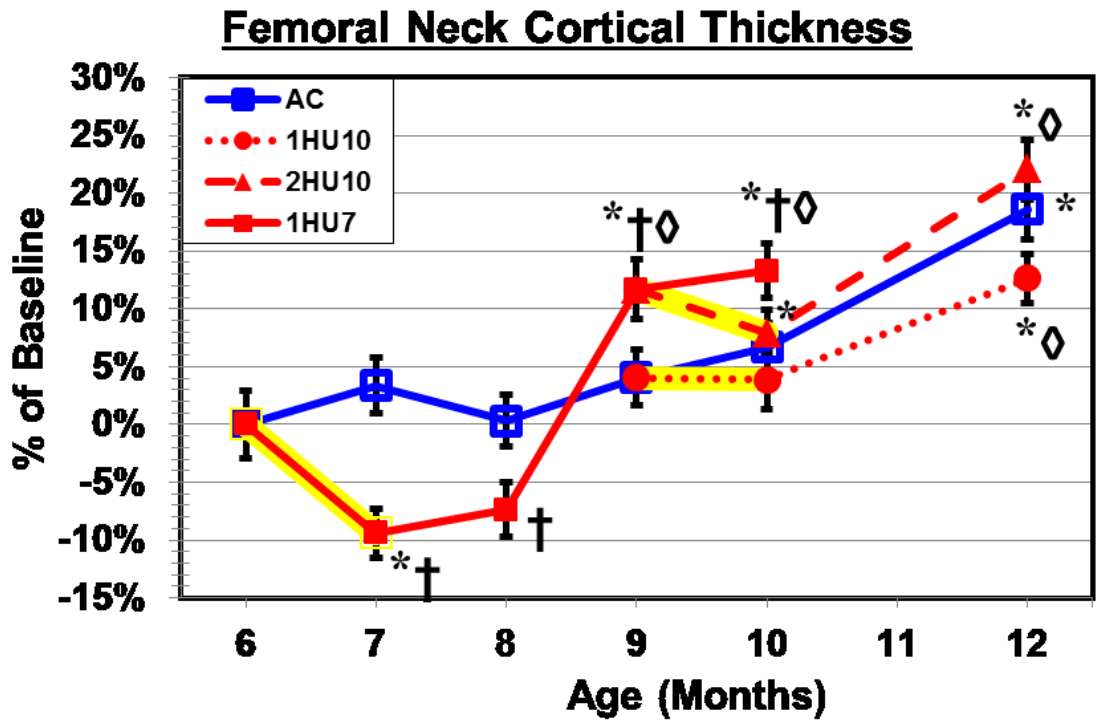

Fig. 29. Cortical thickness at multiple time points during unloading and subsequent recovery of the right femoral neck. Numerical values are presented in Table 2 and yellow highlighting indicates HU treatment. Cortical thickness trends are similar to cortical area naturally. A significant drop due to 1HU7 occurs, which is significantly different from BL and AC, and does not recover to AC after one recovery period but does after the second. A general increase in thickness occurs with all points at month 12 being significantly greater than BL and 1HU10+R2 and 2HU10+R2 also being significantly greater than their respective HU treatments.

Values are presented as mean ± SE

*** Indicates significant difference from baseline value; p<0.05**

† Indicates significant difference from age-matched cage control value at same time point; p<0.05

 # Indicates significant difference from month 9 pre-HU value within same group; p<0.05

ǂ Indicates significant difference between 1HU7+R3 and 2HU10; p<0.05

¤ Indicates significant difference between 1HU10 and 2HU10 at the same time point; p<0.05

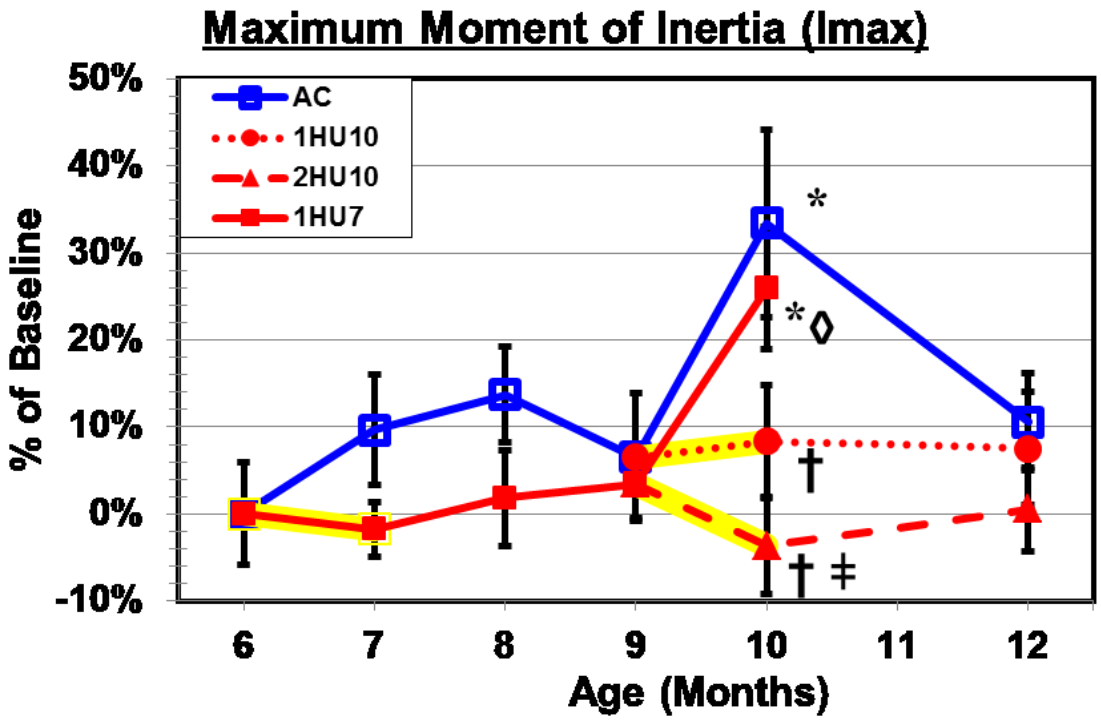

Fig. 30. Maximum moment of inertia at multiple time points during unloading and subsequent recovery of the right femoral neck. Numerical values are presented in Table 2 and yellow highlighting indicates HU treatment. AC shows typical age fluctuation with a sharp increase at AC10 which is significantly greater than BL. 1HU7 has no significant effect but causes the group to be slightly less than matching AC values. 1HU7+R3 shows a dramatic rise similar to its matched AC which is significantly greater than BL and the previous 1HU7+R2. 1HU10 and 2HU10 are both significantly smaller than AC10 due to the large increase of the control point. The final values at month 12 are not significantly different from BL or AC.

Values are presented as mean ± SE

*** Indicates significant difference from baseline value; p<0.05**

† Indicates significant difference from age-matched cage control value at same time point; p<0.05

 # Indicates significant difference from month 9 pre-HU value within same group; p<0.05

ǂ Indicates significant difference between 1HU7+R3 and 2HU10; p<0.05

¤ Indicates significant difference between 1HU10 and 2HU10 at the same time point; p<0.05

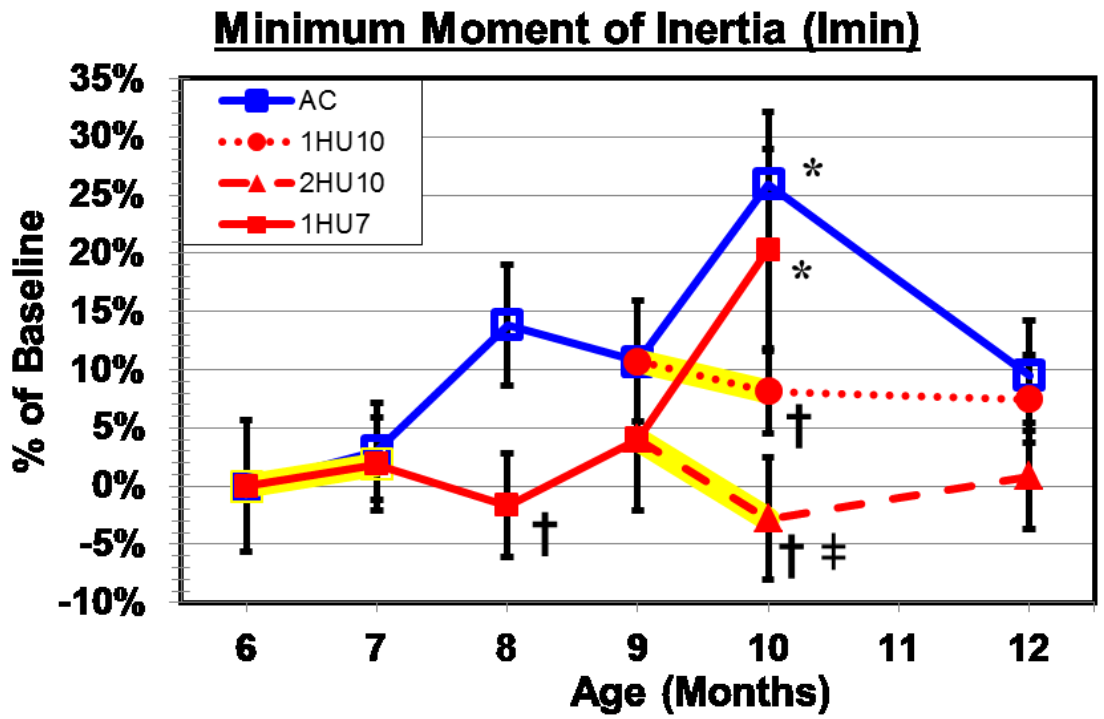

Fig. 31. Minimum moment of inertia at multiple time points during unloading and subsequent recovery of the right femoral neck. Numerical values are presented in Table 2 and yellow highlighting indicates HU treatment. Trends for the minimum moment of inertia for each group are similar to the maximum moment of inertia shown previously. AC again shows typical age fluctuation with a sharp increase at AC10 which is significantly greater than BL. 1HU7 tracks nearly exactly with AC but 1HU7+R1 decreases slightly causing a significant difference between it and AC8. 1HU7+R3 shows a dramatic rise again similar to its matched AC and is significantly greater than BL. 1HU10 and 2HU10 are both significantly smaller than AC10 again due to the large increase of the control point. The final values at month 12 are not significantly different from BL or AC.

Values are presented as mean ± SE

*** Indicates significant difference from baseline value; $p<0.05$**

† Indicates significant difference from age-matched cage control value at same time point; $p<0.05$

 # Indicates significant difference from month 9 pre-HU value within same group; $p<0.05$

ǂ Indicates significant difference between 1HU7+R3 and 2HU10; $p<0.05$

¤ Indicates significant difference between 1HU10 and 2HU10 at the same time point; $p<0.05$

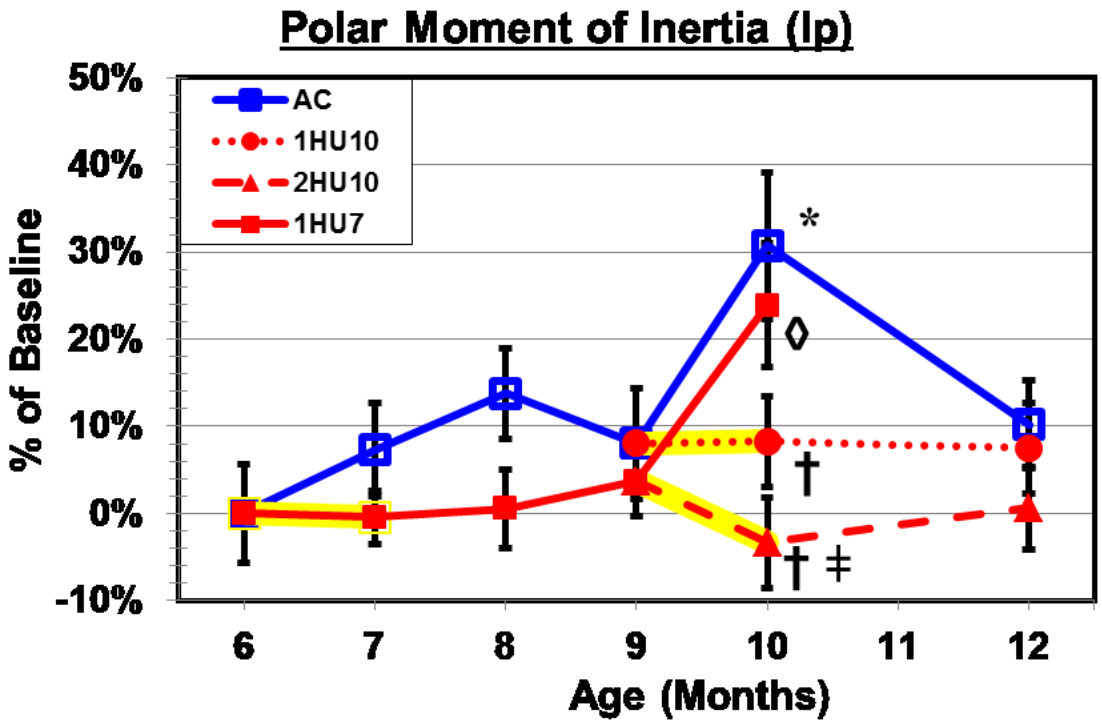

Fig. 32. Polar moment of inertia at multiple time points during unloading and subsequent recovery of the right femoral neck. Numerical values are presented in Table 2 and yellow highlighting indicates HU treatment. Polar moment of inertia is more similar to the maximum moment of inertia shown previously. AC shows the age fluctuations and has a sharp increase at AC10 which is significantly greater than BL. Again, 1HU7 has no significant effect but causes the group to be slightly less than matching AC values. 1HU7+R3 shows a large increase similar to its matched AC but is not significantly greater than BL. However, 1HU7+R3 is significantly greater than 1HU7+R2. 1HU10 and 2HU10 are both significantly smaller than AC10 due to the large increase of the control point again. The final values at month 12 are not significantly different from BL or AC.
Values are presented as mean ± SE
*** Indicates significant difference from baseline value; $p<0.05$**
† Indicates significant difference from age-matched cage control value at same time point; $p<0.05$
 # Indicates significant difference from month 9 pre-HU value within same group; $p<0.05$
ǂ Indicates significant difference between 1HU7+R3 and 2HU10; $p<0.05$
¤ Indicates significant difference between 1HU10 and 2HU10 at the same time point; $p<0.05$

Midshaft Densitometric and Geometric Properties

The femoral midshaft is compromised exclusively of a cortical shell and it is unnecessary to acquire and report total and trabecular bone parameters. Only the cortical mineral properties (cortical BMC, cortical vBMD) and the geometric properties (cortical area, cortical thickness, moments of inertia) will be reported. Generally, all midshaft properties increase in magnitude as the animals age, with less noticeable effect from the HU treatments than those seen for the femoral neck.

The aging control cortical BMC (Fig. 33) increases significantly versus BL values by AC7 and continues to increase through AC12. 1HU7 also shows a significant increase from BL, but to a lesser extent than AC7, with continual increases through 1HU7+R3. 1HU10 and 2HU10 show slight decreases which are still significantly higher than BL values and immediately resume increasing in magnitude after 10 months.

Volumetric BMD (Fig. 34) for all groups increases steadily for the full 12 months. AC7 and 1HU7 track almost exactly together and are significantly greater than BL. All points continue to trend together and are significantly larger than BL until month 10, when slight variations between the groups occur. 1HU10 is significantly different from AC10 and remains lower at month 12, with both 1HU10+R2 and 2HU10+R2 being significantly lower than AC12 values.

Femur cortical area (Fig. 35) also exhibits very similar trends to those of BMC, with 1HU7 experiencing a blunting of the initial rise in area that is seen by AC7. All data points are significantly larger than BL, but the older HU treatments (1HU10, 2HU10) show non-significant decreases, which quickly resume increasing once the recovery period begins. Cortical thickness (Fig. 36) trends are very similar to those seen in the area data with early, significant increases for both control and treated group values from BL; a decline occurs after 10 month HU treatments, with subsequent quick recovery.

Moments of inertia (Figs. 37-39) are very similar to one another and show large increases (30-50 % by the end of the study) as the animals age and as the area increases. 1HU10 decreases non-significantly for each moment of inertia and all points are significantly greater than BL.

Table 3: Mineral and Geometric Properties for Femoral Midshaft

	Cortical BMC (mg/mm)	Cortical vBMD (mg/cm^3)	Cortical Area (mm^2)	Cortical Thickness (μm)	I_{max} (mm^4)	I_{min} (mm^4)	I_p (mm^4)
6 Months Old							
BL6	11.5 (0.21)	1423.4 (2.19)	8.09 (0.14)	0.82 (0.01)	13.2 (0.46)	8.94 (0.28)	22.2 (0.72)
7 Months Old							
AC7	13.0 (0.22)*	1432.6 (3.01)*	9.05 (0.15)*	0.89 (0.01)*	15.8 (0.59)*	10.9 (0.33)*	26.8 (0.91)*
1HU7	12.2 (0.23)*†	1430.8 (2.37)*	8.54 (0.15)*†	0.84 (0.01)†	14.5 (0.48)	10.3 (0.31)*	24.8 (0.77)*
8 Months Old							
AC8	13.1 (0.17)*	1442.2 (2.11)*	9.10 (0.13)*	0.87 (0.01)*	16.3 (0.48)*	11.5 (0.33)*	27.8 (0.79)*
1HU7+R1	12.6 (0.24)*	1443.8 (2.37)*◊	8.72 (0.16)*	0.85 (0.01)*	14.9 (0.61)*	10.7 (0.34)*	25.6 (0.94)*
9 Months Old							
AC9	13.5 (0.31)*	1446.1 (1.68)*	9.34 (0.21)*	0.89 (0.01)*	16.8 (0.79)*	12.2 (0.59)*	29.0 (1.35)*
1HU7+R2	13.1 (0.14)*◊	1447.2 (2.56)*◊	9.07 (0.09)*◊	0.88 (0.01)*◊	16.0 (0.52)*	11.1 (0.22)*◊	27.0 (0.70)*◊
10 Months Old							
AC10	13.7 (0.35)*	1456.1 (1.99)*	9.42 (0.24)*	0.91 (0.02)*	16.2 (0.70)*	12.2 (0.59)*	28.4 (1.27)*
1HU7+R3	14.1 (0.38)*◊	1460.8 (2.84)*◊	9.66 (0.26)*◊	0.92 (0.02)*◊	17.5 (0.80)*◊	12.7 (0.52)*◊	30.2 (1.31)*◊
1HU10	13.3 (0.21)*	1458.3 (1.63)*†	9.10 (0.15)*	0.87 (0.01)*†	16.4 (0.51)*	11.5 (0.40)*	27.9 (0.89)*
2HU10	12.9 (0.22)*‡	1453.9 (1.86)*#‡	8.86 (0.15)*‡	0.85 (0.01)*#‡	15.9 (0.54)*	11.3 (0.41)*‡	27.2 (0.94)*
12 Months Old							
AC12	14.6 (0.27)*	1472.5 (2.07)*	9.91 (0.18)*	0.92 (0.01)*	18.4 (0.53)*	13.6 (0.54)*	32.0 (1.05)*
1HU10+R2	14.0 (0.28)*◊	1458.0 (2.17)*†	9.59 (0.18)*◊	0.89 (0.01)*◊	18.1 (0.63)*◊	13.0 (0.45)*◊	31.0 (1.05)*◊
2HU10+R2	14.1 (0.38)*◊	1465.3 (1.66)*†◊	9.65 (0.26)*◊	0.91 (0.02)*◊	17.5 (0.77)*	13.0 (0.60)*◊	30.6 (1.34)*◊

Values are presented as mean ± SE

*** Indicates significant difference from baseline value, $p < 0.05$**

† Indicates significant difference from age-matched control value at same time point, $p<0.05$

 # Indicates significant difference from month 9 pre-HU value within same group (i.e. 1HU10(+R2) or 2HU10 + (R2)), $p <0.05$

◊ Indicates significant difference from immediate preceding post-HU value within same group, $p<0.05$

‡ Indicates significant difference between 1HU7+R3 and 2HU10, $p<0.05$

¤ Indicates significant difference between 1HU10 and 2HU10 at the same time point, $p<0.05$

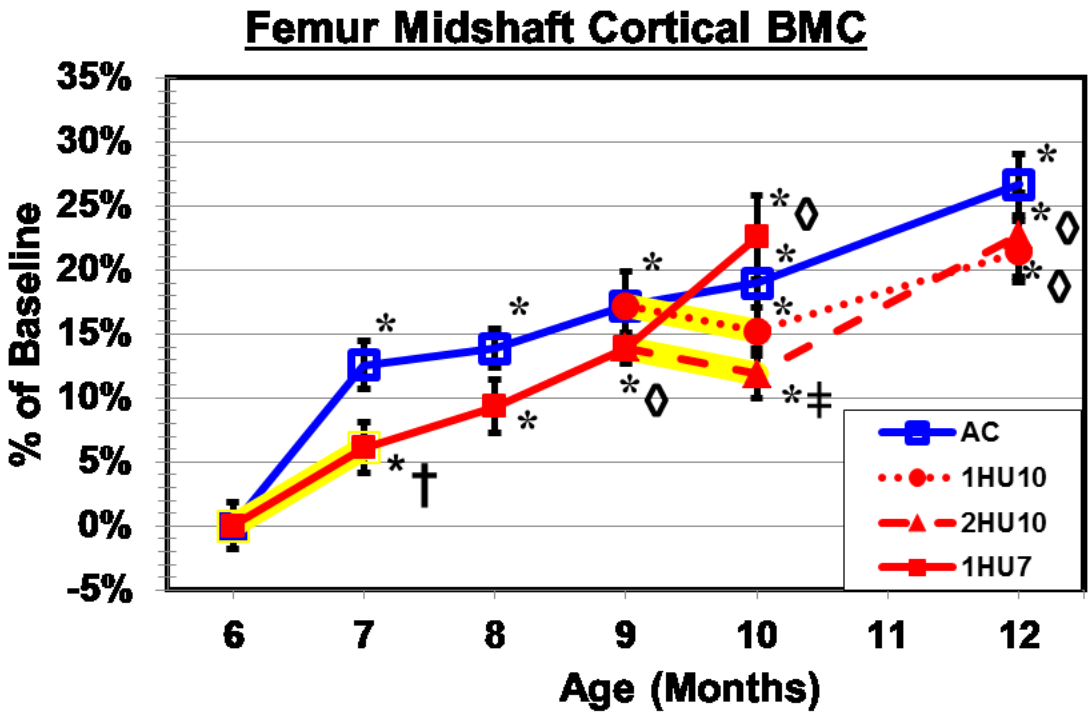

Fig. 33. Cortical BMC at multiple time points during unloading and subsequent recovery of the femoral midshaft. Numerical values are presented in Table 3 and yellow highlighting indicates HU treatment. AC7 shows a sudden, significant rise in BMC from the BL value. 1HU7 also shows a significant increase from BL but to a significantly smaller degree from AC7 suggesting HU causes a blunting effect on normal BMC growth. Recovery occurs quickly, by 1HU7+R1 with respect to AC and by 1HU7+R2 with respect to 1HU7, and all points during recovery are still significantly higher than BL. 1HU10 and 2HU10 show non-significant decreases from AC with 2HU10 being significantly smaller than the matching 1HU7+R3 time point. Both 1HU10 and 2HU10 are recovered with respect to AC and previous HU by month 12, but are still significantly larger than BL.

Values are presented as mean ± SE

*** Indicates significant difference from baseline value; p<0.05**

† Indicates significant difference from age-matched cage control value at same time point; p<0.05

 # Indicates significant difference from month 9 pre-HU value within same group; p<0.05

ǂ Indicates significant difference between 1HU7+R3 and 2HU10; p<0.05

¤ Indicates significant difference between 1HU10 and 2HU10 at the same time point; p<0.05

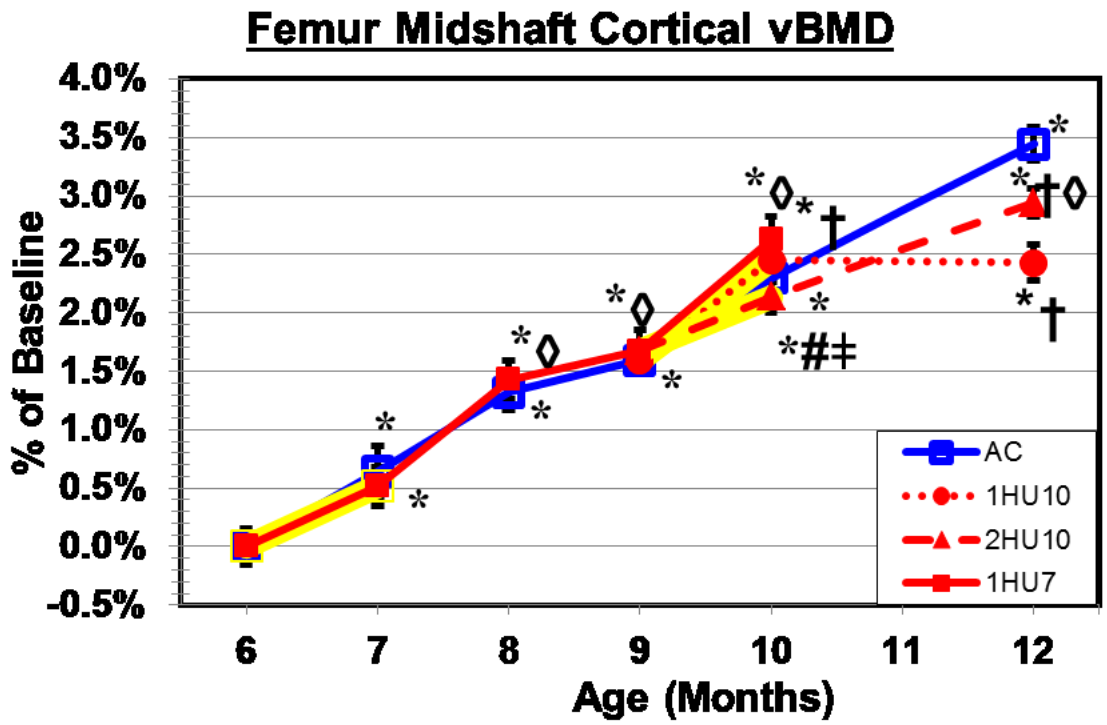

Fig. 34. Cortical vBMD at multiple time points during unloading and subsequent recovery of the femoral midshaft. Numerical values are presented in Table 3 and yellow highlighting indicates HU treatment. Control and HU groups are clustered tightly together and increase to significantly greater than BL rapidly. 1HU7 appears to have no effect on vBMD as it tracks extremely closely with AC7 and this trend continues until month 10. Slightly greater variability between data points is seen at the 10 month time period with 1HU10 being significantly greater than BL. The final recovery points at month 12 show even greater variability with 1HU10+R2 and 2HU10+R2 ending significantly lower than the AC12 value.

Values are presented as mean ± SE

*** Indicates significant difference from baseline value; p<0.05**

† Indicates significant difference from age-matched cage control value at same time point; p<0.05

 # Indicates significant difference from month 9 pre-HU value within same group; p<0.05

ǂ Indicates significant difference between 1HU7+R3 and 2HU10; p<0.05

¤ Indicates significant difference between 1HU10 and 2HU10 at the same time point; p<0.05

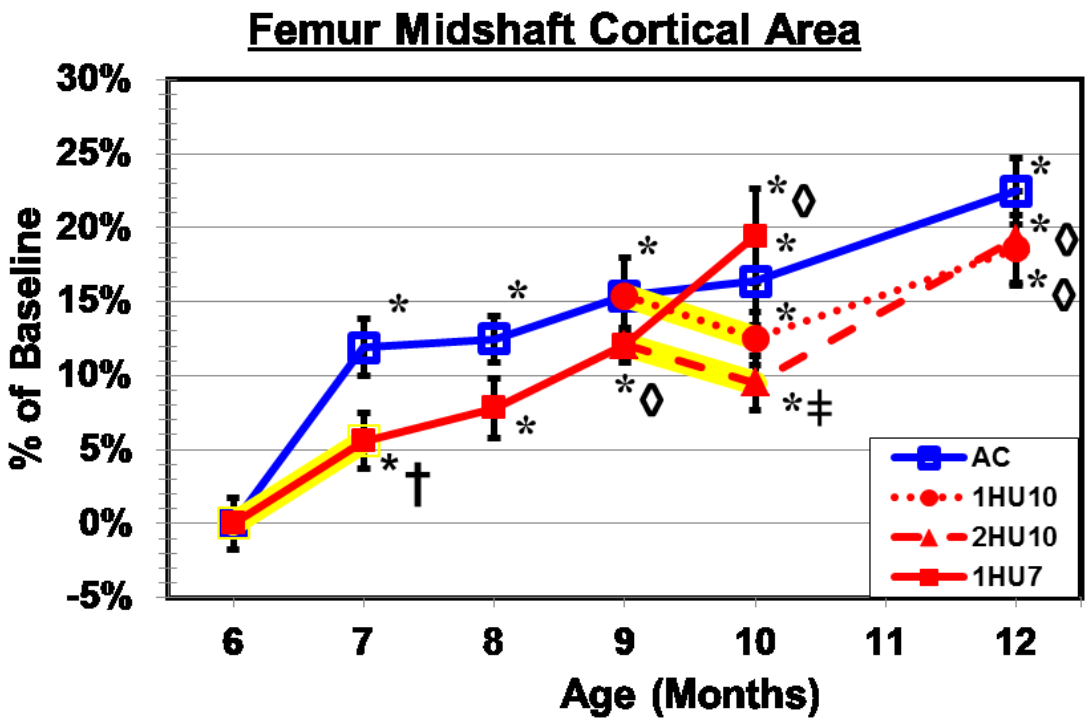

Fig. 35. Cortical area at multiple time points during unloading and subsequent recovery of the femoral midshaft. Numerical values are presented in Table 3 and yellow highlighting indicates HU treatment. Similar to BMC, area also increases significantly from BL for both AC7 and 1HU7. However, 1HU7 seems to blunt the increase in area because it is significantly smaller than the matching AC7 value. 1HU10 and 2HU10 show non-significant decreases again with large increases during recovery.

Values are presented as mean ± SE

*** Indicates significant difference from baseline value; p<0.05**

† Indicates significant difference from age-matched cage control value at same time point; p<0.05

 # Indicates significant difference from month 9 pre-HU value within same group; p<0.05

ǂ Indicates significant difference between 1HU7+R3 and 2HU10; p<0.05

¤ Indicates significant difference between 1HU10 and 2HU10 at the same time point; p<0.05

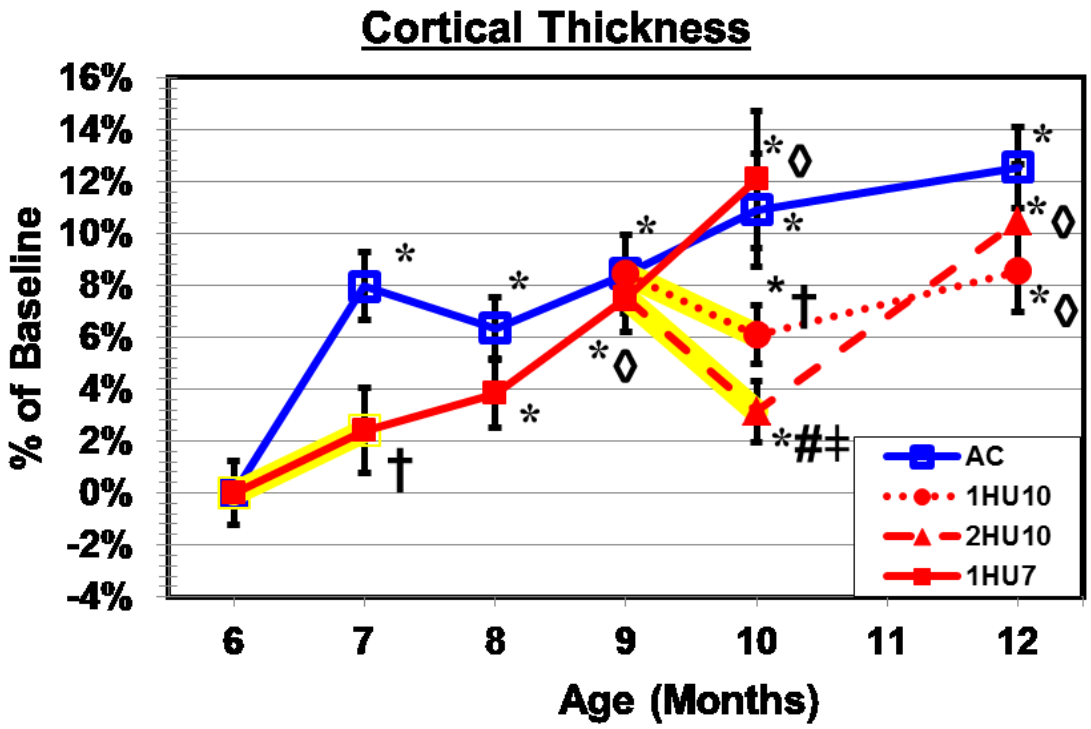

Fig. 36. Cortical thickness at multiple time points during unloading and subsequent recovery of the femoral midshaft. Numerical values are presented in Table 3 and yellow highlighting indicates HU treatment. Similar to BMC and area, cortical thickness increases significantly from BL for AC7 and increases non-significantly from BL for 1HU7. 1HU7 again seems to blunt the increase in thickness because it is significantly smaller than the matching AC7 value. However, 1HU10 and 2HU10 show significant decreases from AC but are still significantly larger than BL. Large increases are seen again during recovery with the final values showing full recovery with respect to AC and previous HU but remaining significantly higher than BL.

Values are presented as mean ± SE

*** Indicates significant difference from baseline value; p<0.05**

† Indicates significant difference from age-matched cage control value at same time point; p<0.05

 # Indicates significant difference from month 9 pre-HU value within same group; p<0.05

ǂ Indicates significant difference between 1HU7+R3 and 2HU10; p<0.05

¤ Indicates significant difference between 1HU10 and 2HU10 at the same time point; p<0.05

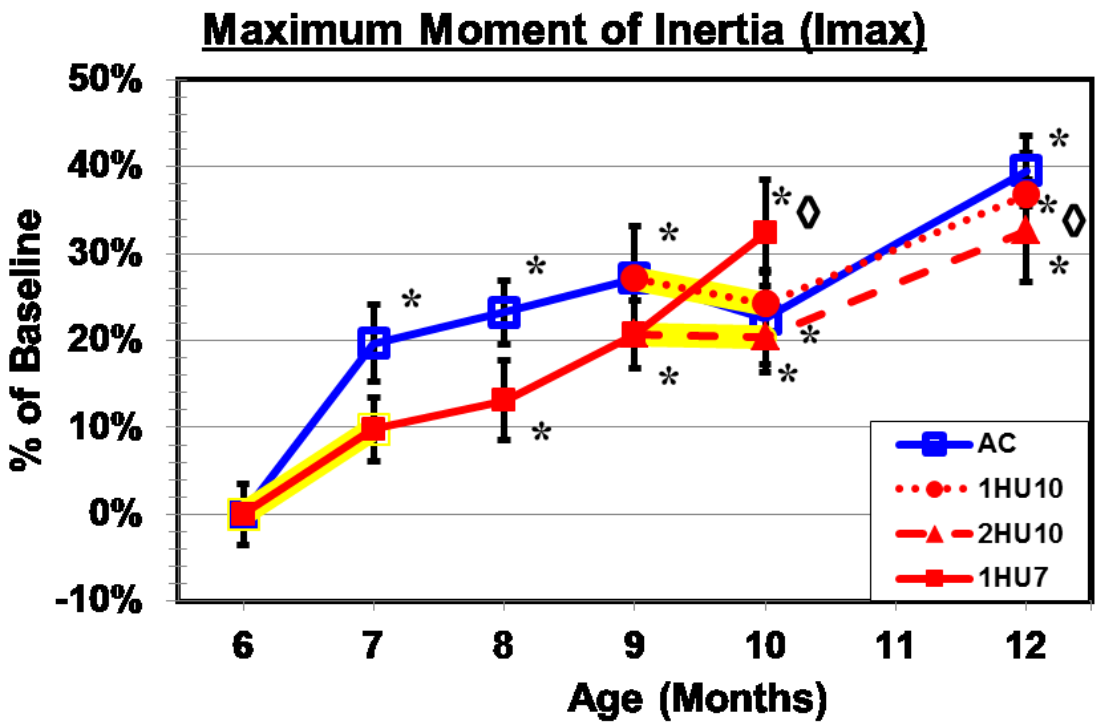

Fig. 37. Maximum moment of inertia at multiple time points during unloading and subsequent recovery of the femoral midshaft. Numerical values are presented in Table 3 and yellow highlighting indicates HU treatment. Maximum moment of inertia results naturally follow cortical area and thickness results. Initial increases are seen with a significant increase from BL for AC7 and a non-significant increase for 1HU7. Inertial increases occur throughout the study except for slight decreases during month 10 for AC10, 1HU10, and 2HU10 which show only significant increases from BL.

Values are presented as mean ± SE

*** Indicates significant difference from baseline value; p<0.05**

† Indicates significant difference from age-matched cage control value at same time point; p<0.05

 # Indicates significant difference from month 9 pre-HU value within same group; p<0.05

ǂ Indicates significant difference between 1HU7+R3 and 2HU10; p<0.05

¤ Indicates significant difference between 1HU10 and 2HU10 at the same time point; p<0.05

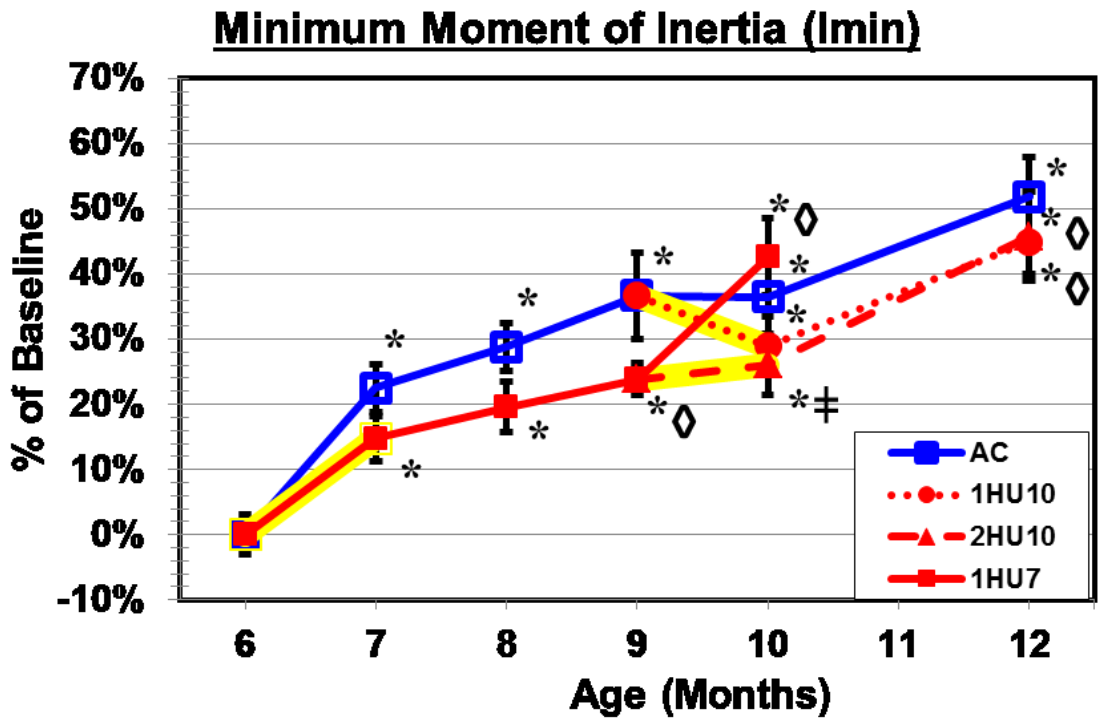

Fig. 38. Minimum moment of inertia at multiple time points during unloading and subsequent recovery of the femoral midshaft. Numerical values are presented in Table 3 and yellow highlighting indicates HU treatment. Minimum moment of inertia trends are very similar to maximum moment of inertia. The initial increase at month 7 is significantly higher than BL for both AC7 and 1HU7. 1HU10 shows a slight decrease which is still significantly higher than BL and all values for AC and HU groups are closely grouped at month 12.

Values are presented as mean ± SE

*** Indicates significant difference from baseline value; p<0.05**

† Indicates significant difference from age-matched cage control value at same time point; p<0.05

 # Indicates significant difference from month 9 pre-HU value within same group; p<0.05

ǂ Indicates significant difference between 1HU7+R3 and 2HU10; p<0.05

¤ Indicates significant difference between 1HU10 and 2HU10 at the same time point; p<0.05

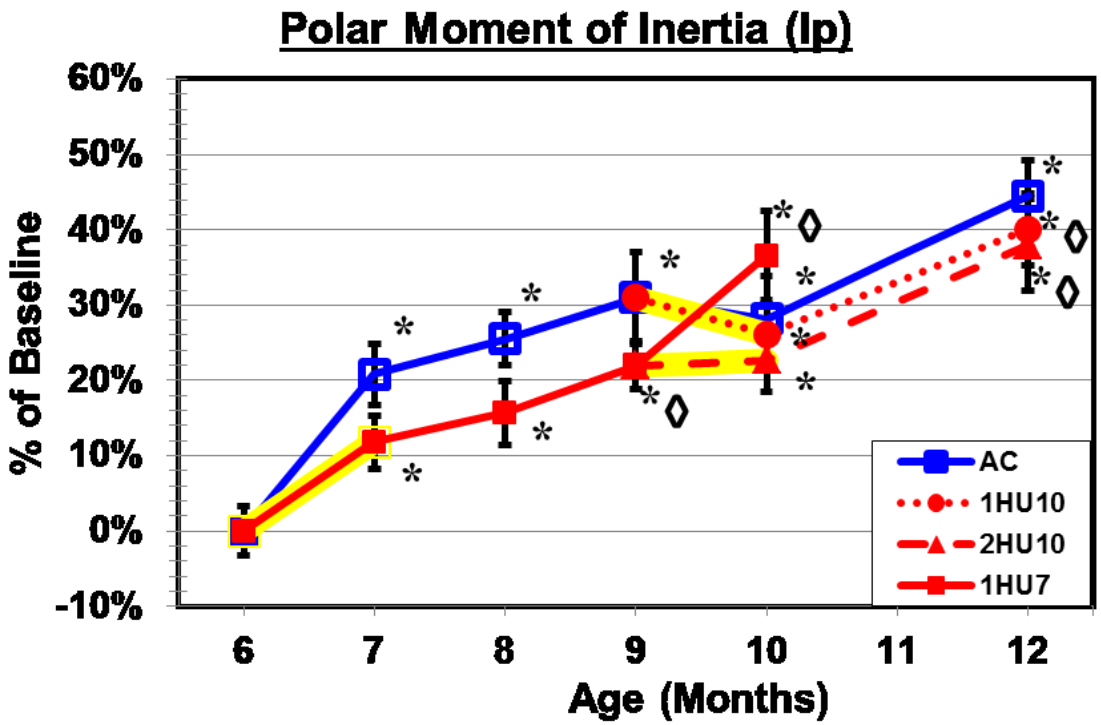

Fig. 39. Polar moment of inertia at multiple time points during unloading and subsequent recovery of the femoral midshaft. Numerical values are presented in Table 3 and yellow highlighting indicates HU treatment. Polar moment is almost exactly the same as the maximum moment of inertia results seen previously. A sudden rise in inertia at month 7 with both AC7 and 1HU7 showing significant increases from BL. 1HU10 and AC10 show slight, non-significant decreases. Otherwise, all points continue to increase significantly from the original BL value.

Values are presented as mean ± SE

*** Indicates significant difference from baseline value; p<0.05**

† Indicates significant difference from age-matched cage control value at same time point; p<0.05

 # Indicates significant difference from month 9 pre-HU value within same group; p<0.05

ǂ Indicates significant difference between 1HU7+R3 and 2HU10; p<0.05

¤ Indicates significant difference between 1HU10 and 2HU10 at the same time point; p<0.05

Mechanical Testing Results

Axial (Figs. 40-41) and lateral (Figs. 42-43) compression tests were done on the right and left femoral necks respectively, and 3-point bending (Figs. 44-45) was performed on the femur midshafts to acquire mechanical properties. However, due to the unique shape of the proximal femur a large number of loading conditions are present during the test including compression, shear, and bending. This makes the calculation of intrinsic properties extremely difficult; therefore only maximum force and stiffness are reported for the axial and lateral tests. Beam theory can be applied to the three point bending tests at the midshaft though and intrinsic properties can be estimated. Therefore, stress, strain, and energies will be reported in addition to force and stiffness for the femoral midshaft.

Since each bone has a slightly different shape, properties, and different responses to HU, the force displacement curves acquired from the Instron testing machine are different for each bone. The linear region of the curve and the final breaking force were left up to the author's judgment and interpretation of the force displacement curve. However, the Instron software displayed the maximum force reading for each test. As previously, the absolute values are presented in Table 4 while the percentages with respect to baseline are shown graphically afterwards.

Both the axial (Fig. 40) and lateral (Fig. 42) force/displacement curves show similar patterns of change but different magnitudes of effect due to the HU treatments. A significant reduction from BL occurs for the 1HU7 point in both tests. The axial force is reduced by nearly 20 percent from its respective BL value, while lateral force is reduced approximately 10 percent from its respective BL value. The lateral force recovers by the first recovery point but not as sharply as for axial results and both axial and lateral forces recover to values greater than BL. The 1HU10 and 2HU10 points again show significant decreases due to HU treatment for both axial and lateral but the lateral 2HU10 decrease is much larger than the axial. However, the 1HU10 points show approximately the same

reductions. Similar to the 1HU7 treatment, both 1HU10 and 2HU10 treatments for axial and lateral tests show quick recoveries. Also, AC values remain fairly steady and show only slight fluctuations due to age, except for an increase at AC10 for the axial test which matches the densitometric results.

Max force values for the 3-point bending results (Fig. 44) change differently over time compared with the femoral neck test results since the force values generally increase as the animals age. The AC7 and 1HU7 points both increase significantly from BL and the increasing trend continues until month 10. The 1HU10 treatment decreases slightly, but remains significantly higher than BL, and quickly continues to increase during the two month recovery period. The control animals show a large increase from BL at month 7 followed by less sudden increases until the end of the study at month 12.

The stiffness trends area also different between the three mechanical tests. The axial femoral neck stiffness (Fig. 41) values track relatively closely between AC and the HU groups except for month 12, where AC12 and 2HU10+R2 increase dramatically while 1HU10+R2 only increases slightly. Lateral femoral neck stiffness (Fig. 43) trends look closer to those seen in the lateral max force graph except for 1HU7 which shows an increase with respect to BL. 1HU10 and 2HU10 results in large decreases with quick recoveries as seen in Fig. 43. The stiffness values calculated for the midshaft 3-point bending test (Fig. 45) for AC and HU groups track closely together, similar to the axial femoral neck test results, and show the typical increases over the course of the study that have been associated with midshaft properties.

Table 4: Mechanical Testing Results for Axial and Lateral Femoral Neck Tests and 3pt Bending of the Femoral Midshaft

	Axial Maximum Force (N)	Axial Stiffness (N/mm)	Lateral Maximum Force (N)	Lateral Stiffness (N/mm)	3pt Bending Maximum Force (N)	3pt Bending Stiffness (N/mm)
Months Old						
BL6	93.96 (3.94)	135.31 (7.46)	90.44 (2.51)	55.26 (2.52)	222.35 (5.12)	683.65 (25.45)
Months Old						
AC7	97.55 (2.82)	135.09 (9.61)	97.00 (2.62)	62.12 (2.23)	263.87 (5.71)*	722.97 (44.29)
1HU7	78.69 (2.18)*†	138.12 (10.26)	83.12 (1.73)*†	56.99 (1.75)	247.76 (7.28)*	816.95 (50.03)*
Months Old						
AC8	99.34 (2.24)	149.77 (9.87)	94.86 (2.75)	63.29 (3.10)	264.37 (3.90)*	857.71 (94.00)
1HU7+R1	95.53 (3.60)◊	165.81 (8.51)*◊	84.69 (3.79)†	58.92 (2.86)	257.05 (7.32)*	865.96 (70.72)*
Months Old						
AC9	97.45 (3.20)	169.81 (5.75)*	93.94 (3.97)	65.45 (2.96)*	269.43 (10.34)*	897.93 (75.62)*
1HU7+R2	102.74 (3.20)◊	178.93 (8.26)*◊	89.2 (2.17)◊	63.41 (3.01)*	266.18 (5.48)*	851.58 (74.81)*
Months Old						
AC10	111.08 (4.93)*	165.29 (9.24)*	96.67 (2.28)	64.75 (2.55)*	280.87 (12.33)*	918.77 (97.40)*
1HU7+R3	114.85 (3.58)*◊	162.82 (10.85)*	105.56 (6.05)*◊	69.70 (3.79)*◊	288.53 (11.88)*◊	883.96 (53.83)*
1HU10	84.40 (3.89)†#	156.92 (9.05)*	83.72 (2.71)†#	55.72 (3.09)†#	259.96 (8.12)*	934.41 (108.41)*
2HU10	86.43 (3.63)†#‡	162.64 (8.50)*	72.33 (5.69)*†#‡	52.77 (3.82)†#‡	268.42 (6.82)*	967.56 (121.74)*
Months Old						
AC12	97.2 (4.37)	224.62 (30.57)*	92.94 (3.86)	66.53 (2.92)*	295.45 (10.70)*	1010.26(107.23)*
1HU10+R2	102.01 (2.16)	164.17 (7.94)*	86.24 (3.34)	57.09 (2.78)†	290.70 (8.32)*◊	1154.82 (89.54)*
2HU10+R2	98.28 (3.76)	235.39 (31.36)*	93.26 (4.60)◊	67.22 (4.44)*◊	292.00 (11.94)*	1142.84 (73.01)*

Values are presented as mean ± SE

*** Indicates significant difference from baseline value, $p < 0.05$**

† Indicates significant difference from age-matched control value at same time point, $p<0.05$

 # Indicates significant difference from month 9 pre-HU value within same group (i.e. 1HU10(+R2) or 2HU10 + (R2)), $p <0.05$

◊ Indicates significant difference from immediate preceding post-HU value within same group, $p<0.05$

‡ Indicates significant difference between 1HU7+R3 and 2HU10, $p<0.05$

¤ Indicates significant difference between 1HU10 and 2HU10 at the same time point, $p<0.05$

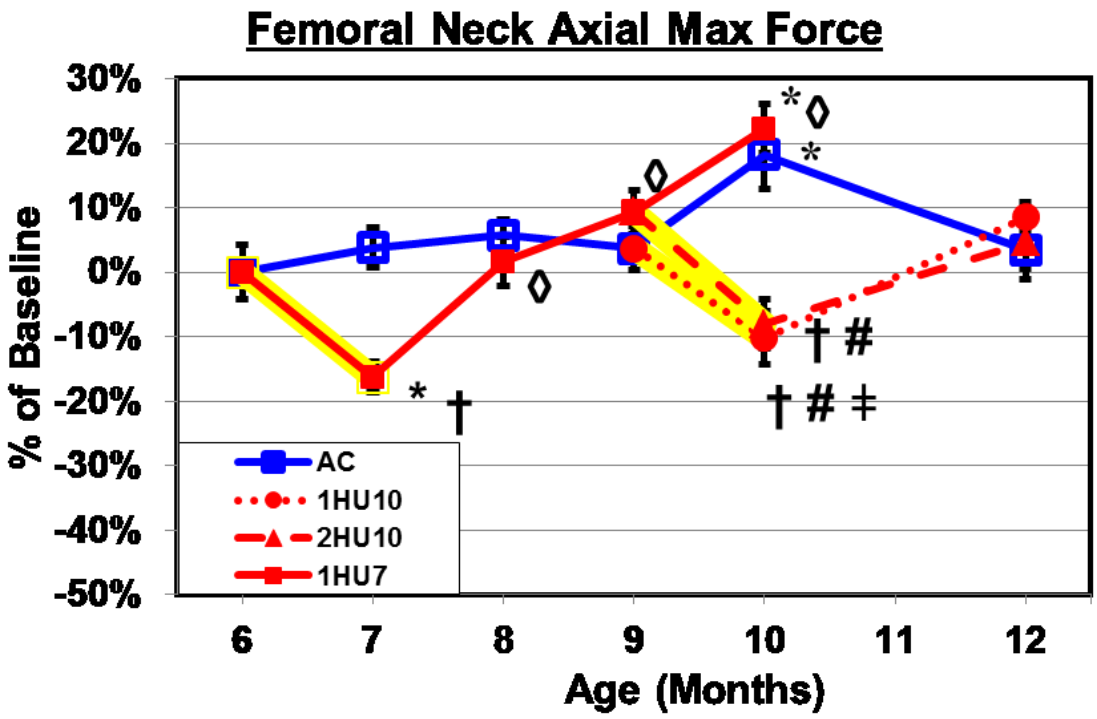

Fig. 40. Axial mechanical testing maximum force at multiple time points during unloading and subsequent recovery of the right femoral neck. Numerical values are presented in Table 4 and yellow highlighting indicates HU treatment. AC values remain relatively stable throughout the experiment except at AC10 which shows a sudden significant increase with respect to BL. By AC12 the control max force decreases back to close to the original BL value. 1HU7 has a significant decrease from BL and from AC7 but recovers back to within BL, AC, and a significant increase from HU within one recovery period. By 1HU7+R3 the max force value has increased to significantly greater than BL. 1HU10 and 2HU10 both show significant decreases from AC10 but not from BL and both recover with respect to BL and AC by month 12. However, neither 1HU10+R2 and 2HU10+R2 increased significantly from their respective HU treatments.
Values are presented as mean ± SE
*** Indicates significant difference from baseline value; p<0.05**
† Indicates significant difference from age-matched cage control value at same time point; p<0.05
 # Indicates significant difference from month 9 pre-HU value within same group; p<0.05
ǂ Indicates significant difference between 1HU7+R3 and 2HU10; p<0.05
¤ Indicates significant difference between 1HU10 and 2HU10 at the same time point; p<0.05

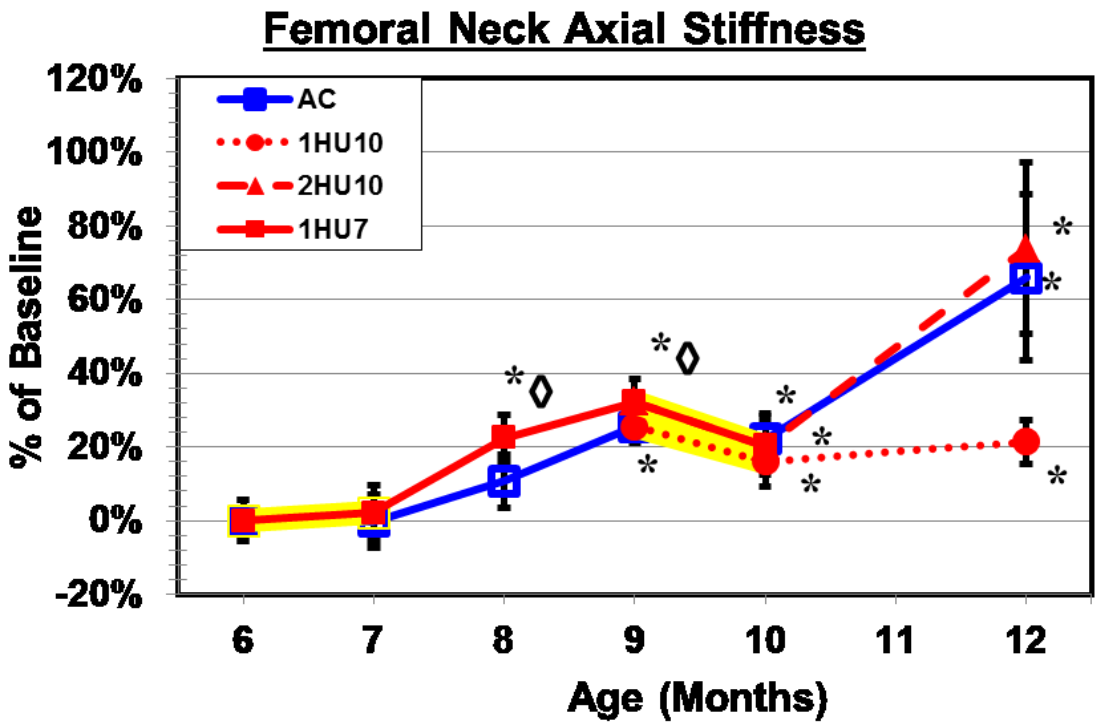

Fig. 41. Axial mechanical testing stiffness at multiple time points during unloading and subsequent recovery of the right femoral neck. Numerical values are presented in Table 4 and yellow highlighting indicates HU treatment. AC values generally increase as the animals age and are significantly greater than BL by month 9. There is a slight increase at 1HU7 but the HU group tracks with the AC group except that all HU points are significantly larger than BL by month 8. 1HU10 and 2HU10 decrease slightly but still appear to track along with AC10. AC12 and 2HU10+R2 increase together to over 60% larger than BL. However, 1HU10+R2 shows little recovery increase but remains significantly higher than BL.

Values are presented as mean ± SE

*** Indicates significant difference from baseline value; p<0.05**

† Indicates significant difference from age-matched cage control value at same time point; p<0.05

 # Indicates significant difference from month 9 pre-HU value within same group; p<0.05

ǂ Indicates significant difference between 1HU7+R3 and 2HU10; p<0.05

¤ Indicates significant difference between 1HU10 and 2HU10 at the same time point; p<0.05

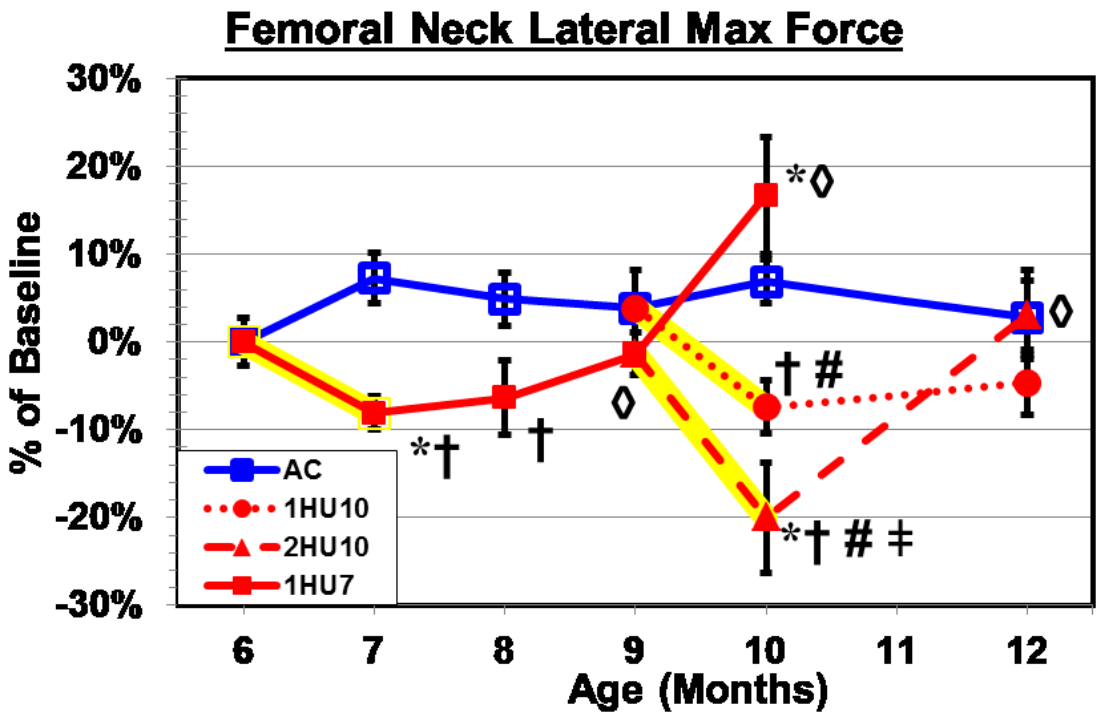

Fig. 42. Lateral mechanical testing maximum force at multiple time points during unloading and subsequent recovery of the left femoral neck. Numerical values are presented in Table 4 and yellow highlighting indicates HU treatment. Similar to the axial test, AC values remain relatively stable throughout the experiment with only slight fluctuations which are likely due to aging. 1HU7 has a significant decrease from BL and AC7 but recovers back to BL by the end of the first recovery period. Recovery with respect to AC and a significant increase from HU occurs by the second recovery period, 1HU7+R2. By 1HU7+R3 the max force value has increased to significantly greater than BL. 1HU10 and 2HU10 both show significant decreases from AC10 but only 2HU10 shows a significant decrease from BL.2HU10 recovers with respect to BL and both 1HU10 and 2HU10 recover with respect to AC by month 12, but 2HU10 shows a significant increase from the HU treatment.

Values are presented as mean ± SE
*** Indicates significant difference from baseline value; p<0.05**
† Indicates significant difference from age-matched cage control value at same time point; p<0.05
 # Indicates significant difference from month 9 pre-HU value within same group; p<0.05
ǂ Indicates significant difference between 1HU7+R3 and 2HU10; p<0.05
¤ Indicates significant difference between 1HU10 and 2HU10 at the same time point; p<0.05

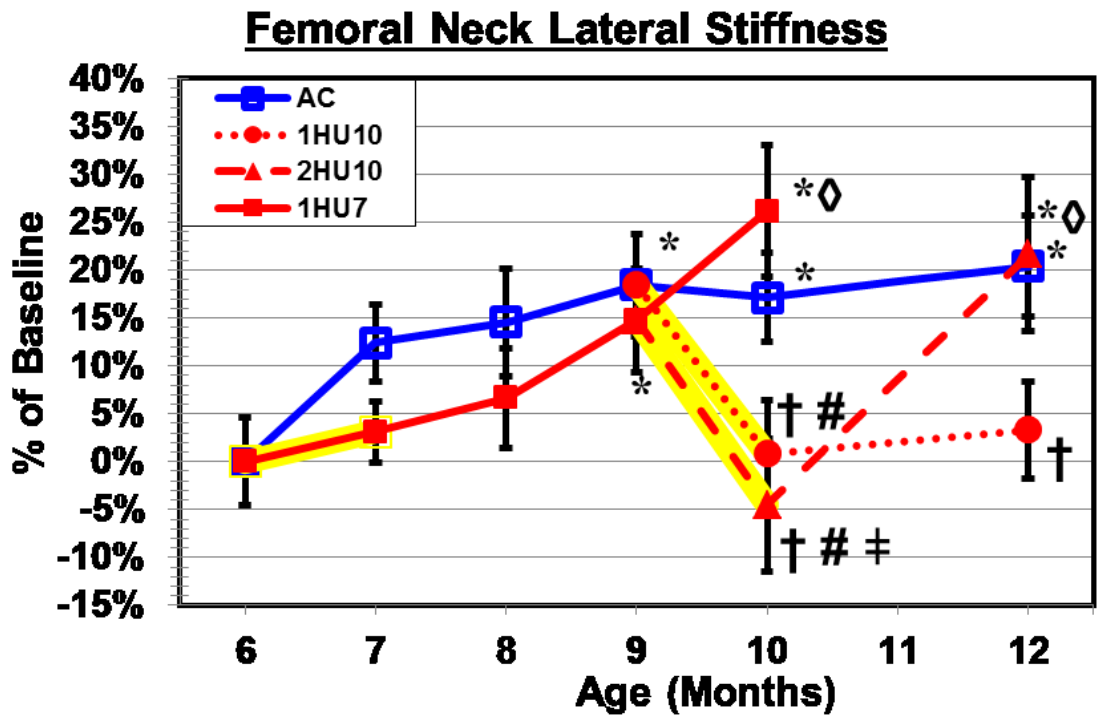

Fig. 43. Lateral mechanical testing maximum force at multiple time points during unloading and subsequent recovery of the left femoral neck. Numerical values are presented in Table 4 and yellow highlighting indicates HU treatment. Trends for lateral testing stiffness are closer to the trends seen in the previous force graphs as well as some of the densitometric data. AC values increase slightly throughout the experiment with only slight fluctuations which are likely due to aging. The 1HU7 point increases with respect to BL but not significantly and it is also not significantly lower than AC7. Like the axial stiffness, the HU group continues to increase so that by 1HU7+R3 the value has increased to significantly greater than BL. 1HU10 and 2HU10 both show significant decreases from AC10 but not BL. 2HU10+R2 increases to the matching AC12 point which is significantly higher than BL, but 1HU10+R2 barely increases remaining significantly different from AC12 but not from BL.

Values are presented as mean ± SE

*** Indicates significant difference from baseline value; p<0.05**

† Indicates significant difference from age-matched cage control value at same time point; p<0.05

 # Indicates significant difference from month 9 pre-HU value within same group; p<0.05

ǂ Indicates significant difference between 1HU7+R3 and 2HU10; p<0.05

¤ Indicates significant difference between 1HU10 and 2HU10 at the same time point; p<0.05

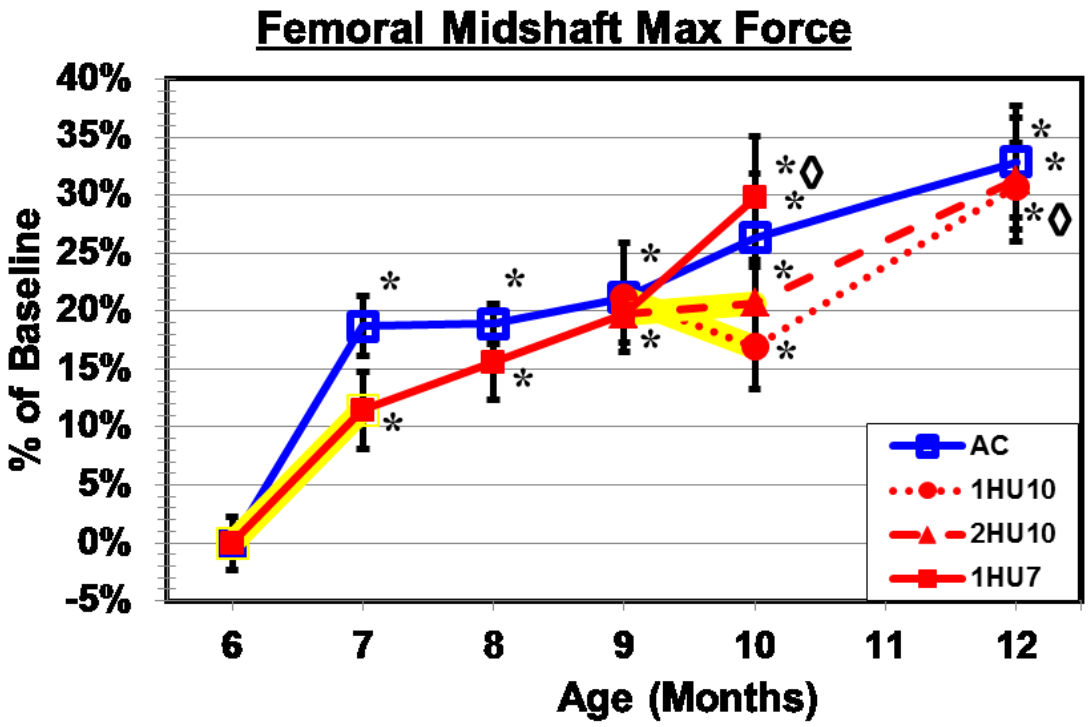

Fig. 44. Three-point bending mechanical testing maximum force at multiple time points during unloading and subsequent recovery of the femoral midshaft. Numerical values are presented in Table 4 and yellow highlighting indicates HU treatment. Both AC and HU lines track together and are not significantly different from each other. At month 7 both 1HU7 and AC7 significantly increase with respect to BL. This trend generally continues until the end of the study at month 12. 1HU10 shows a small, non-significant decrease which quickly resumes increasing until 1HU10+R2 is nearly the same value as AC12 and 2HU10+R2.

Values are presented as mean ± SE

*** Indicates significant difference from baseline value; $p<0.05$**

† Indicates significant difference from age-matched cage control value at same time point; $p<0.05$

 # Indicates significant difference from month 9 pre-HU value within same group; $p<0.05$

ǂ Indicates significant difference between 1HU7+R3 and 2HU10; $p<0.05$

¤ Indicates significant difference between 1HU10 and 2HU10 at the same time point; $p<0.05$

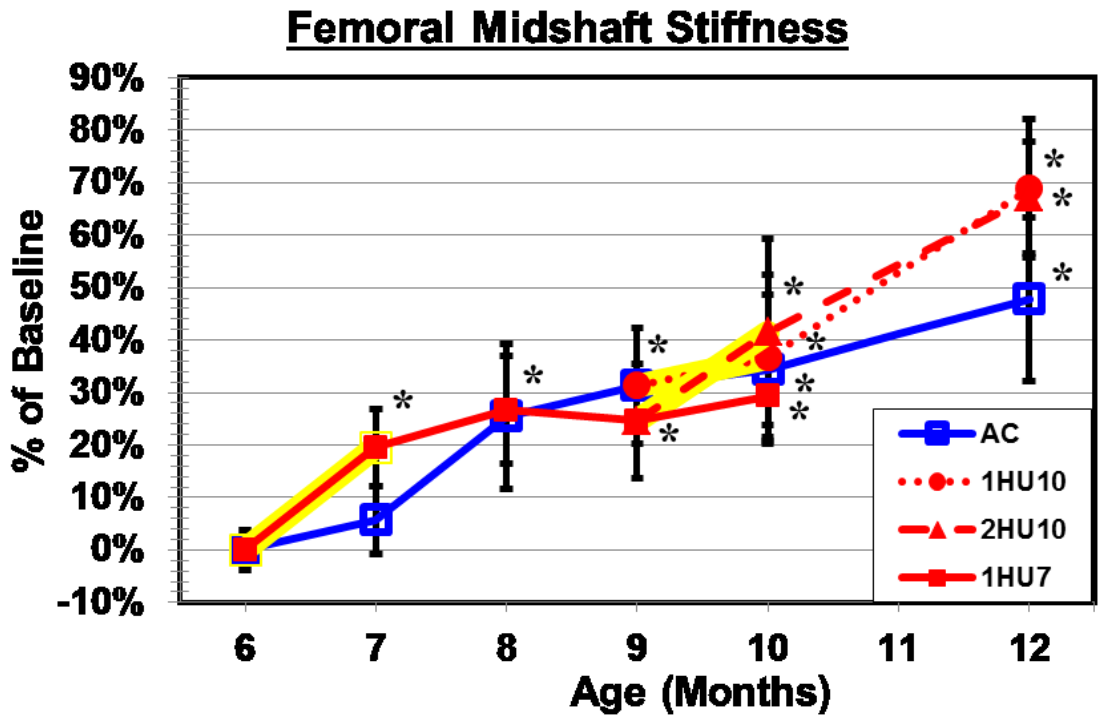

Fig. 45. Three-point bending mechanical testing stiffness at multiple time points during unloading and subsequent recovery of the femoral midshaft. Numerical values are presented in Table 4 and yellow highlighting indicates HU treatment. Similar to the 3pt bending max force graph, stiffness trends increase throughout the study for both AC and HU groups. 1HU7 and 1HU7+R1 increase to significantly higher than BL while AC7 and AC8 do not. By month 9, both AC and HU groups are significantly higher than BL and continue to increase regardless of HU treatment until the end of study at month 12. However, AC12 has a lower average stiffness than both 1HU10+R2 and 2HU10+R2 which have a very similar stiffness value.

Values are presented as mean ± SE

*** Indicates significant difference from baseline value; $p<0.05$**

† Indicates significant difference from age-matched cage control value at same time point; $p<0.05$

 # Indicates significant difference from month 9 pre-HU value within same group; $p<0.05$

ǂ Indicates significant difference between 1HU7+R3 and 2HU10; $p<0.05$

¤ Indicates significant difference between 1HU10 and 2HU10 at the same time point; $p<0.05$

Cortical Bone Material Properties from Three-Point Bending Tests

After three-point bending testing was performed on the left femoral midshaft, the force displacement data was analyzed as described in the Methods section, classical beam theory equations and analysis were used by the DatMet software to calculate estimate values for extrinsic properties including: elastic modulus, energies, yield stress, and ultimate stress. Pre-yield toughness was calculated separately using an equation developed by Turner and Burr et. al. (32). As mentioned previously, these values are most appropriate for pre-yield values of the force/displacement curves, but can be used as reasonable estimates for post yield parameters.

Changes in elastic modulus (Fig. 46) trends are different compared to those seen previously. The HU groups increase after treatment while the AC values remain lower; 1HU7 mean elastic modulus increases non-significantly with respect to that of BL as does 1HU10 and 2HU10, but AC7 actually decreases with respect to BL. Only 1HU10+R2 and 2HU10+R2 are significantly higher than BL, but the large error bars prevent significant differences from being seen. However, elastic modulus weighted bending strength index (EM BSI) (Fig. 47) shows steady, significant increases with respect to BL and does not appear to be affected by HU. AC and HU groups are not significantly different from each other for EM BSI and all groups end the study with mean values over 25% greater than BL.

Pre-yield toughness (Fig. 48) trends return to those seen for HU previously, with decreases during treatments and increases during recoveries. All HU groups decrease but 1HU7 has a larger decrease with respect to BL, while the decrease in pre-yield toughness in 1HU10 and 2HU10 are smaller. 1HU7+R1 continues to increase but then rapidly increases during 1HU7+R2 while 1HU10+R2 and 2HU10+R2 still show decreases, with 2HU10+R2 decreasing to significantly smaller than BL. AC values fluctuate but also decrease over time. Only the 1HU7 mean is significantly different from that of AC7 and

the 2HU10+R2 mean shows a significant difference from BL; the large error bars again likely prevent statistically significant differences from being seen.

Energy absorbed to yield (Fig. 49) and energy absorbed to fracture (Fig. 50) show very different trends. The energy to yield has a similar trend as has been seen previously for HU treatments, including pre-yield toughness. Mean values in HU groups show decreases with respect to BL, but the recovery period for 1HU7 decreases until 1HU7+R2. 1HU10+R2 increases slightly after its matching HU treatment but 2HU10+R2 decreases rapidly from 2HU10. Few significant differences are seen between data points, though, likely due to the large error bars. Energy to fracture shows all groups fluctuating wildly with no clear patterns. 1HU7 and 1HU10 mean values increase sharply, while 2HU10 mean decreases and AC has large increases from BL to AC8, a sharp decrease at AC9, and another large increase to AC12. Similarly, yield stress (Fig. 51) and ultimate stress (Fig. 52) mean values also fluctuate, though less noticeably than those for energy to fracture, while not showing the typical patterns seen previously for HU treatments.

Table 5: Estimated 3pt Bending Mechanical Properties at the Femoral Midshaft

	Elastic Modulus	EM BSI	Pre-Yield Toughness	Energy to Yield	Energy to Fracture	Yield Stress	Ultimate Stress
6 Months Old							
BL6	4.34 (0.19)	2.89 (0.11)	1.85 (0.25)	29.7 (3.89)	116.8 (8.77)	109.1 (5.90)	139.9 (4.43)
7 Months Old							
AC7	3.87 (0.27)	3.17 (0.08)*	1.97 (0.16)	35.9 (3.79)	133.1 (7.71)	112.0 (3.23)	144.1 (3.29)
1HU7	4.68 (0.29)	2.97 (0.11)*	1.52 (0.13)†	25.5 (2.24)†	137.1 (8.22)	106.1 (3.95)	144.9 (4.21)
8 Months Old							
AC8	4.41 (0.49)	3.42 (0.09)*	1.75 (0.16)	32.1 (3.24)	144.3 (8.22)*	105.3 (3.04)	140.2 (3.00)
1HU7+R1	4.71 (0.27)	3.17 (0.09)*	1.44 (0.13)	24.2 (1.96)†	122.4 (6.98)	107.5 (5.16)	146.0 (2.91)
9 Months Old							
AC9	4.35 (0.28)	3.47 (0.13)*	1.73 (0.25)	32.2 (4.88)	94.6 (12.9)	107.7 (6.38)	137.9 (4.76)
1HU7+R2	4.44 (0.40)	3.30 (0.07)*◊	1.72 (0.32)	31.4 (5.42)	129.9 (6.49)†	107.2 (7.37)	141.1 (4.67)
10 Months Old							
AC10	4.57 (0.45)	3.44 (0.11)*	1.76 (0.22)	32.6 (4.19)	120.5 (10.4)	111.5 (6.25)	145.7 (5.73)
1HU7+R3	4.09 (0.30)	3.66 (0.11)*◊	1.69 (0.25)	33.1 (5.06)	140.7 (15.8)	103.3 (6.39)	139.6 (4.21)
1HU10	4.77 (0.52)	3.45 (0.08)*	1.54 (0.26)	29.2 (4.71)	130.2 (10.5)#	106.7 (6.11)	135.0 (5.05)
2HU10	5.05 (0.62)	3.39 (0.10)*	1.58 (0.31)	28.8 (5.61)	116.0 (8.97)	106.4 (4.29)	143.5 (3.23)
12 Months Old							
AC12	4.50 (0.50)	3.88 (0.11)*	1.35 (0.16)	26.4 (3.02)	141.4 (13.6)	104.2 (3.31)	140.1 (5.28)
1HU10+R2	5.41 (0.50)*	3.75 (0.10)*◊	1.49 (0.37)	29.8 (8.40)	131.3 (10.4)	96.6 (6.17)	141.3 (2.95)
2HU10+R2	5.44 (0.47)*	3.70 (0.12)*	1.09 (0.09)*	20.7 (1.99)◊	141.4 (12.7)	102.9 (3.66)	145.2 (3.99)

Values are presented as mean ± SE

*** Indicates significant difference from baseline value, p < 0.05**

† Indicates significant difference from age-matched control value at same time point, p<0.05

 # Indicates significant difference from month 9 pre-HU value within same group (i.e. 1HU10(+R2) or 2HU10 + (R2)), p <0.05

◊ Indicates significant difference from immediate preceding post-HU value within same group, p<0.05

‡ Indicates significant difference between 1HU7+R3 and 2HU10, p<0.05

¤ Indicates significant difference between 1HU10 and 2HU10 at the same time point, p<0.05

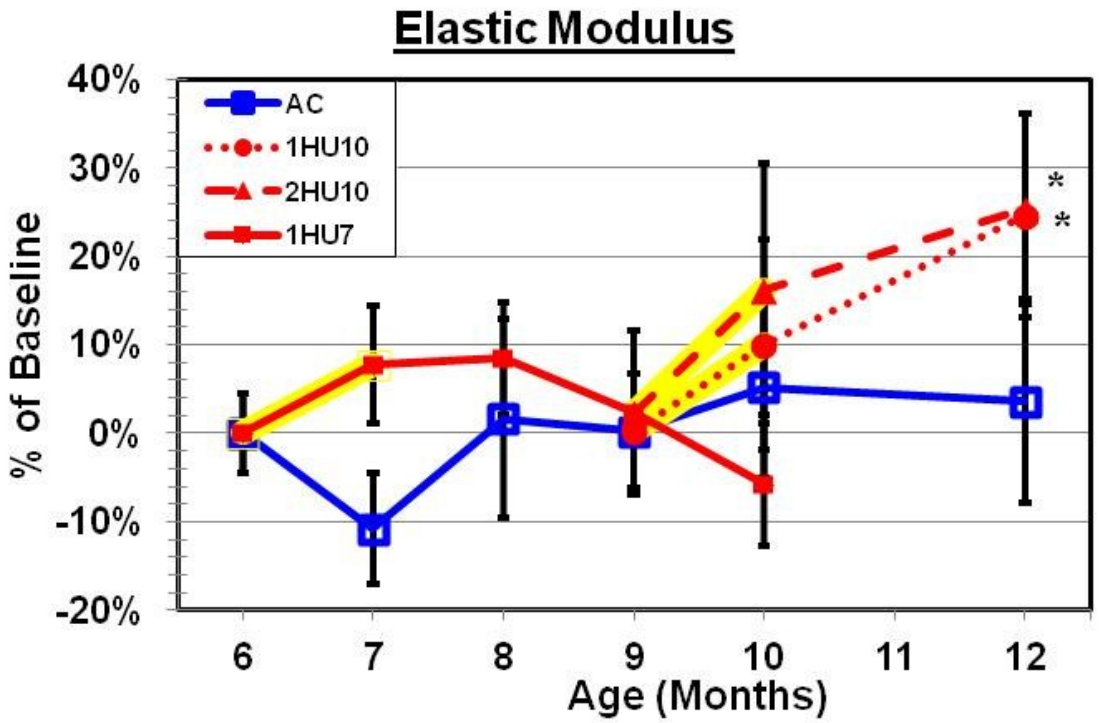

Fig. 46. Three-point bending mechanical testing elastic modulus at multiple time points during unloading and subsequent recovery of the femoral midshaft. Numerical values are presented in Table 5 and yellow highlighting indicates HU treatment. Calculated elastic modulus values show different trends compared to previous results. AC still fluctuates throughout the life of the animals, but HU treatments appear to increase the elastic modulus. 1HU7, 1HU10, and 2HU10 show non-significant increases with respect to BL and show increase during the first week of recovery. 1HU10 and 2HU10 recoveries continue to increase through the second month while the 1HU7+R2 and 1HU7+R3 begin to decrease. Only 1HU10+R2 and 2HU10+R2 show a significant increase with respect to BL but the large standard error bars contribute to the lack of significance.
Values are presented as mean ± SE
*** Indicates significant difference from baseline value; $p<0.05$**
† Indicates significant difference from age-matched cage control value at same time point; $p<0.05$
 # Indicates significant difference from month 9 pre-HU value within same group; $p<0.05$
ǂ Indicates significant difference between 1HU7+R3 and 2HU10; $p<0.05$
¤ Indicates significant difference between 1HU10 and 2HU10 at the same time point; $p<0.05$

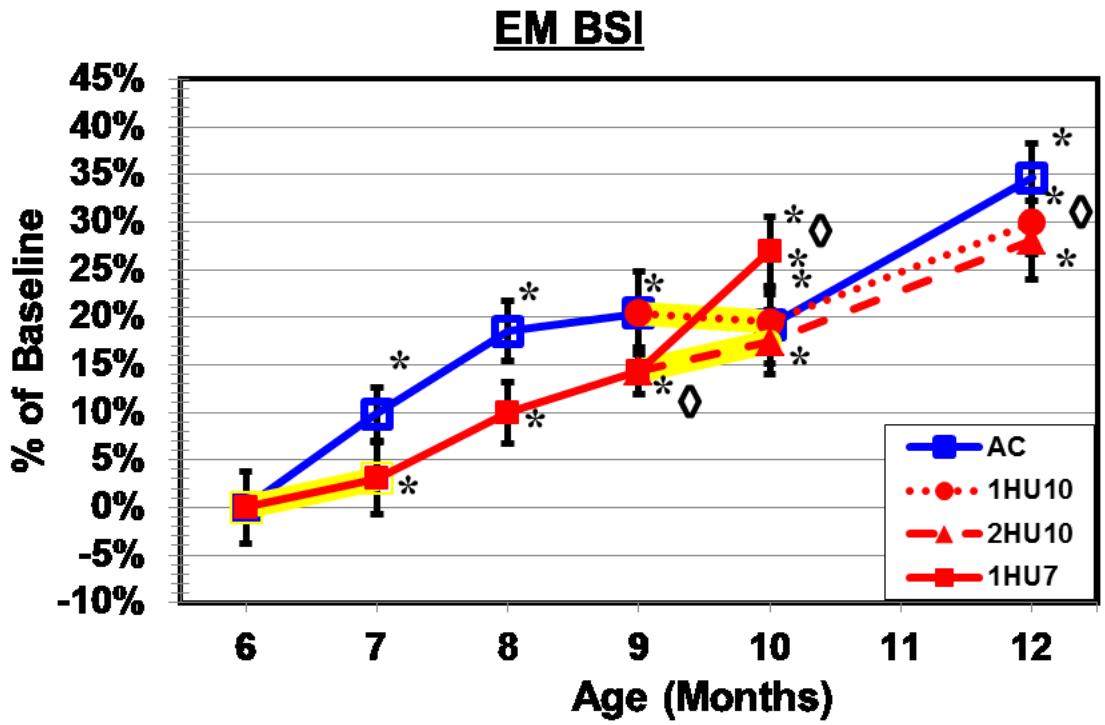

Fig. 47. Three-point bending elastic modulus weighted bending strength index calculated from pQCT parameters at multiple time points during unloading and subsequent recovery of the femoral midshaft. Numerical values are presented in Table 5 and yellow highlighting indicates HU treatment. EM BSI appears to be unaffected by HU and shows continual increases throughout the study. AC and HU groups are significantly different from BL starting at month 7 and continuing through month 12. AC and HU groups do not show any significant differences from each other.
Values are presented as mean ± SE
*** Indicates significant difference from baseline value; $p<0.05$**
† Indicates significant difference from age-matched cage control value at same time point; $p<0.05$
 # Indicates significant difference from month 9 pre-HU value within same group; $p<0.05$
ǂ Indicates significant difference between 1HU7+R3 and 2HU10; $p<0.05$
¤ Indicates significant difference between 1HU10 and 2HU10 at the same time point; $p<0.05$

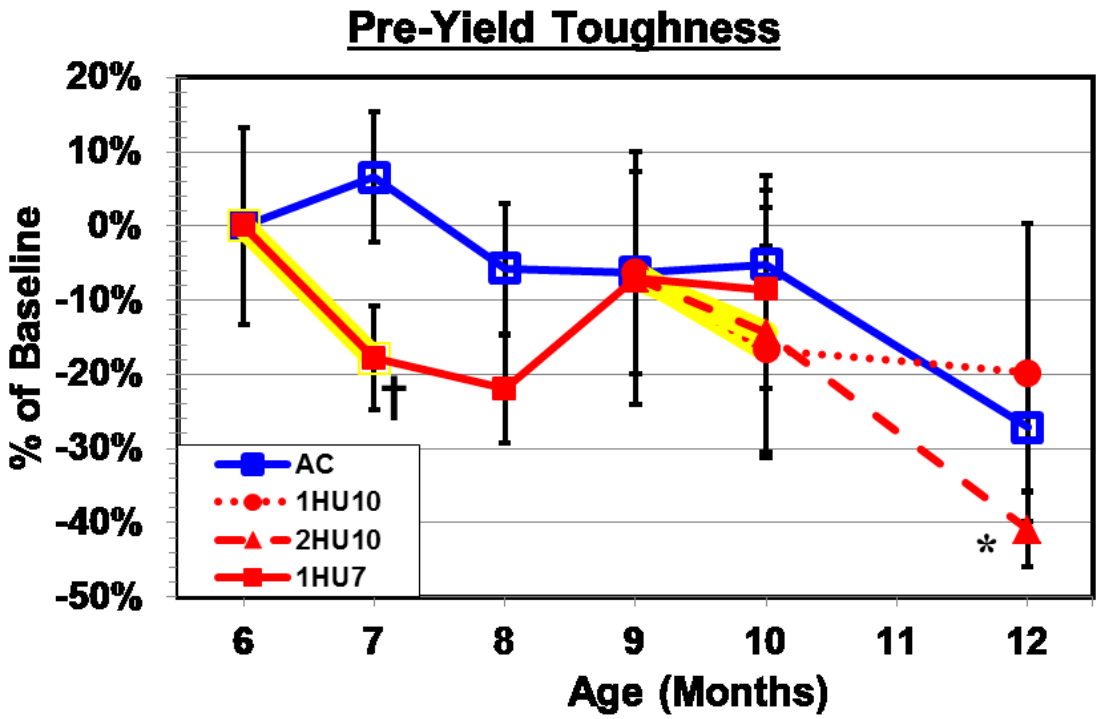

Fig. 48. Pre-yield toughness at multiple time points during unloading and subsequent recovery of the femoral midshaft. Numerical values are presented in Table 5 and yellow highlighting indicates HU treatment. Pre-yield toughness values trend more closely with previous results and show decreases during all HU treatments. There is a generally negative trend across all the groups with AC fluctuating and decreasing for each time interval. 1HU7 is significantly smaller than AC7 and recovers with respect to AC by 1HU7+R1 even though it is still decreasing. 1HU7+R2 shows a sharp increase back to the AC9 value. 1HU10 and 2HU10 show small, non-significant decreases which continue to decrease during the recovery period. 2HU10+R2 is significantly smaller than BL but, similar to elastic modulus values, the large error bars prevent any significant changes from being seen.

Values are presented as mean ± SE

*** Indicates significant difference from baseline value; $p<0.05$**

† Indicates significant difference from age-matched cage control value at same time point; $p<0.05$

 # Indicates significant difference from month 9 pre-HU value within same group; $p<0.05$

ǂ Indicates significant difference between 1HU7+R3 and 2HU10; $p<0.05$

¤ Indicates significant difference between 1HU10 and 2HU10 at the same time point; $p<0.05$

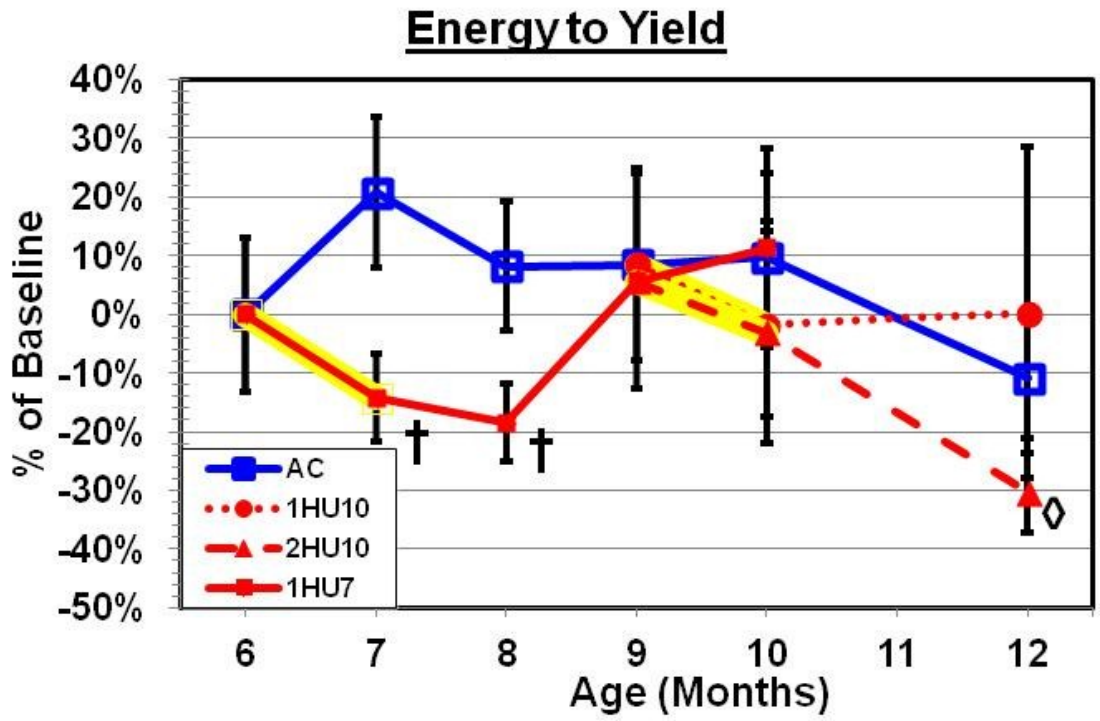

Fig. 49. Energy to yield at multiple time points during unloading and subsequent recovery of the femoral midshaft. Numerical values are presented in Table 5 and yellow highlighting indicates HU treatment. The energy absorbed up to yielding of the bone has very similar trends to the pre-yield toughness shown previously. AC values fluctuate and decrease slightly over the course of the study. All HU treatments appear to cause decreases with 1HU7 being significantly smaller than AC7. 1HU7+R1 continues to decrease until the sharp rise during 1HU7+R2. 1HU10 and 2HU10 decrease slightly and non-significantly and the 2HU10+R2 value shows a significant decrease from its previous HU value. 1HU10+R2 increases slightly but non-significantly.

Values are presented as mean ± SE

*** Indicates significant difference from baseline value; $p<0.05$**

† Indicates significant difference from age-matched cage control value at same time point; $p<0.05$

 # Indicates significant difference from month 9 pre-HU value within same group; $p<0.05$

ǂ Indicates significant difference between 1HU7+R3 and 2HU10; $p<0.05$

¤ Indicates significant difference between 1HU10 and 2HU10 at the same time point; $p<0.05$

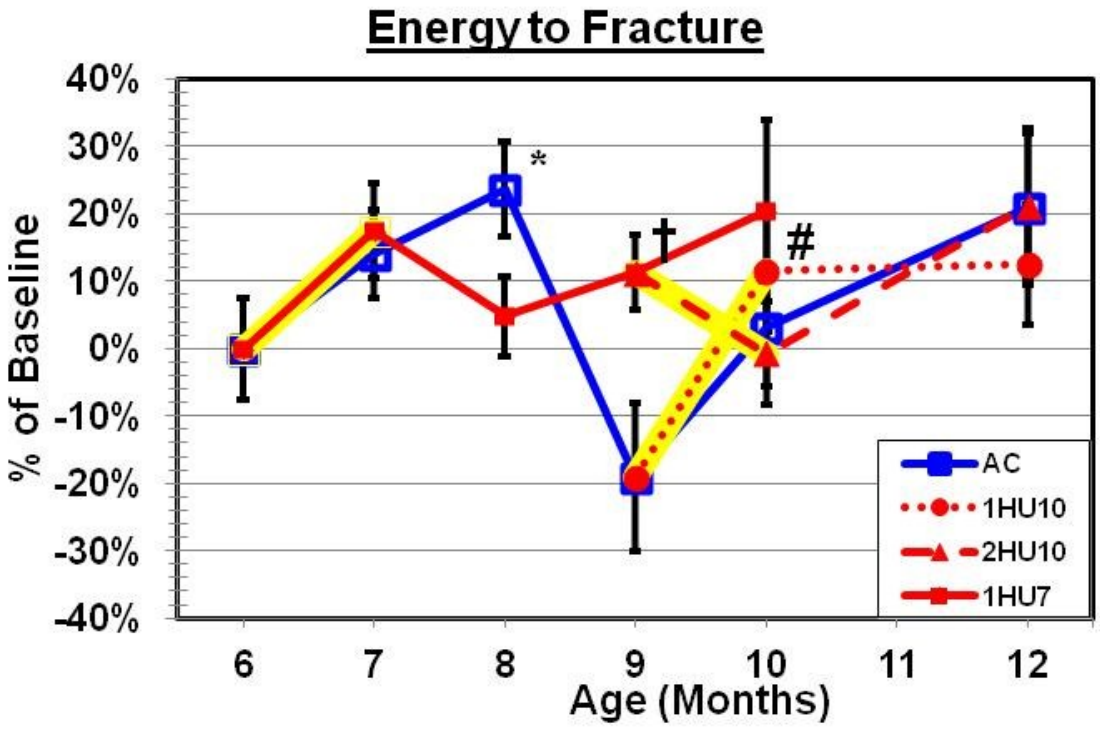

Fig. 50. Energy to fracture at multiple time points during unloading and subsequent recovery of the femoral midshaft. Numerical values are presented in Table 5 and yellow highlighting indicates HU treatment. The energy absorbed till the bone fractures shows large fluctuations that seem unassociated with HU treatment. These values are only an estimate because the calculations are most valid in the pre-yield region of the force/displacement curve.

Values are presented as mean ± SE

*** Indicates significant difference from baseline value; $p<0.05$**

† Indicates significant difference from age-matched cage control value at same time point; $p<0.05$

 # Indicates significant difference from month 9 pre-HU value within same group; $p<0.05$

ǂ Indicates significant difference between 1HU7+R3 and 2HU10; $p<0.05$

¤ Indicates significant difference between 1HU10 and 2HU10 at the same time point; $p<0.05$

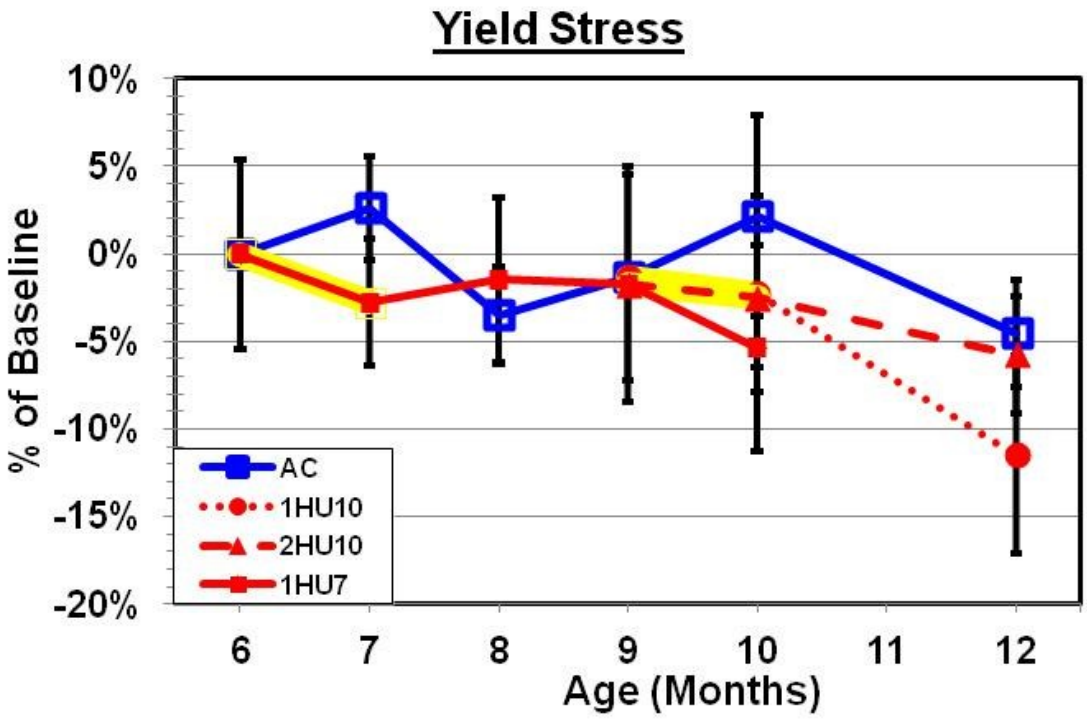

Fig. 51. Yield stress at multiple time points during unloading and subsequent recovery of the femoral midshaft. Numerical values are presented in Table 5 and yellow highlighting indicates HU treatment. Yield stress shows small fluctuations across all of the groups. No significant differences were calculated and the HU and AC values stay fairly close together except for the 1HU10+R2 point which decreases more noticeably than AC12 or 2HU10+R2.

Values are presented as mean ± SE

*** Indicates significant difference from baseline value; $p<0.05$**

† Indicates significant difference from age-matched cage control value at same time point; $p<0.05$

 # Indicates significant difference from month 9 pre-HU value within same group; $p<0.05$

ǂ Indicates significant difference between 1HU7+R3 and 2HU10; $p<0.05$

¤ Indicates significant difference between 1HU10 and 2HU10 at the same time point; $p<0.05$

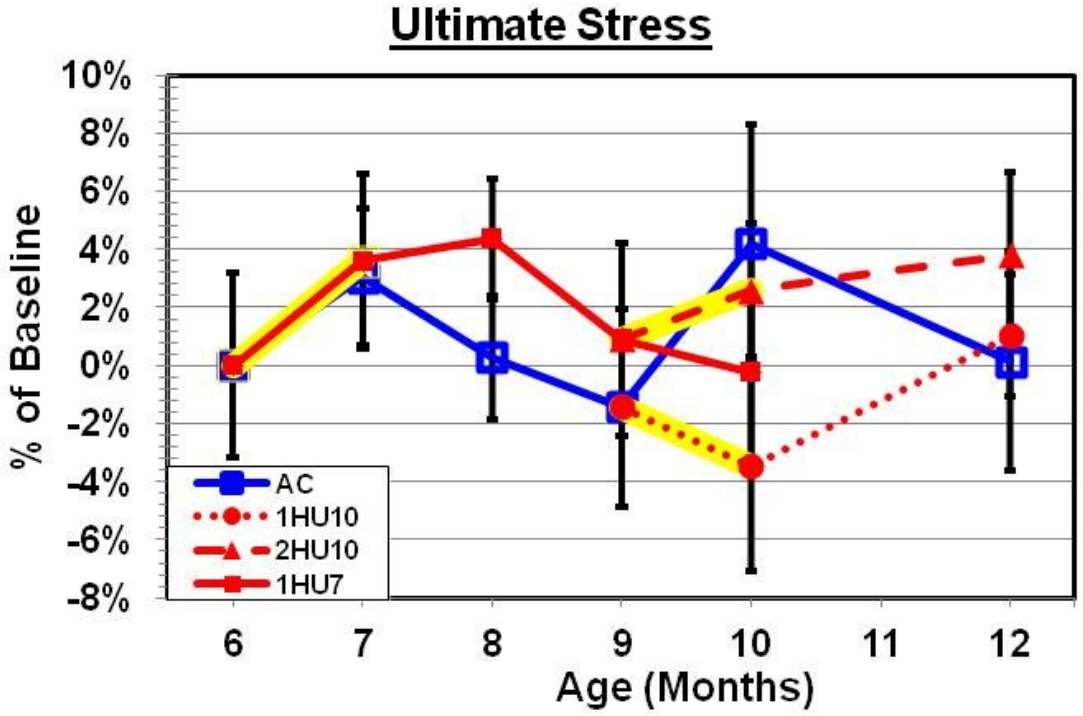

Fig. 52. Ultimate stress at multiple time points during unloading and subsequent recovery of the femoral midshaft. Numerical values are presented in Table 5 and yellow highlighting indicates HU treatment. Ultimate stress values also fluctuate with no significant differences present. The various groups remain fairly close together and the large error bars prevent any significant differences from being seen.

Values are presented as mean ± SE

*** Indicates significant difference from baseline value; $p<0.05$**

† Indicates significant difference from age-matched cage control value at same time point; $p<0.05$

 # Indicates significant difference from month 9 pre-HU value within same group; $p<0.05$

ǂ Indicates significant difference between 1HU7+R3 and 2HU10; $p<0.05$

¤ Indicates significant difference between 1HU10 and 2HU10 at the same time point; $p<0.05$

Calculated Strengths for the Femoral Neck

Calculated changes in femoral neck strength for axial testing are similar to those in lateral testing but the magnitudes of change are different. This suggests that there is a difference between the loading conditions which primarily affects the strength magnitudes; therefore, both right and left calculated strengths will provide similar insight into how unloading affects mechanical strength. Right femoral neck structural strength index (SSI) (Figs. 53-54) is taken directly from the pQCT scanner and is weighted by bone density. There are few differences that are significant with respect to BL. At month 10, AC increases to significantly higher than BL and this increase in AC10 properties is also seen in the pQCT scanning results. HU data points vary for each group but none show a significant difference from BL.

Compressive strength index (CSI) (Figs. 55-56) is calculated from total density values provided by the pQCT scanner; therefore, the trends seen graphically closely resemble those seen previously for total density. AC values increase significantly with respect to BL by 8 months for both the right and left femoral necks. 1HU7 values are significantly smaller than BL for both, but the right femoral neck seems to recover slightly faster and, while both right and left recover with respect to AC values, right femoral neck CSI increases to 15% above BL values while left only increases to 10% greater. 1HU10 and 2HU10 decreases for both right and left femoral neck and 2HU10+R2 and AC12 show a significant increase from BL, but 1HU10+R2 does not.

Bending strength indices (BSI) (Figs. 57-58) are calculated from geometric properties, polar moment of inertia and bone width, and are usually density weighted. AC values for both right and left femoral neck increase by 10 months and, similar to SSI and pQCT parameters, show a large increase for AC10 with respect to BL. Right BSI decreases slightly for the 1HU7 point while left BSI increases slightly, but both right and left 1HU7 treatment groups increase during the recovery period to greater than BL. The right

1HU10 group continues to increase through the recovery period while the right 2HU10 group decreases during HU and increases during recovery. Neither group shows any differences with respect to BL. However, left BSI shows decreases for both 1HU10 and 2HU10 and increases during the recovery period. 1HU10+R2 increases to significantly greater than BL, but all groups finish the study at approximately the same value based upon significance.

A second BSI was calculated for the right femoral neck (MNCS EM BSI) in which the strength index was weighted by elastic modulus for the minimum cross sectional area of each femoral neck specimen instead of by density (Fig. 59). The results showed a significant decrease at 1HU7+R1 with respect to BL, but no other significant differences between data points. 1HU7 and 1HU10 both show non-significant increases while 2HU10 shows a non-significant decrease. All groups show non-significant fluctuations throughout the course of the study, which remain close to the original BL value except at 1HU7+R1.

Table 6: Calculated Strengths from pQCT Parameters for Right and Left Femoral Neck Bone

	Right FN SSI	Right FN CSI	Right FN BSI	Right FN EM BSI	Left FN SSI	Left FN CSI	Left FN BSI
6 Months Old							
BL6	2.07 (0.09)	5.43 (0.14)	1.58 (0.06)	0.53 (0.03)	2.23 (0.09)	5.50 (0.13)	1.68 (0.05)
7 Months Old							
AC7	2.16 (0.10)	5.75 (0.11)	1.68 (0.06)	0.57 (0.03)	2.43 (0.10)	5.96 (0.09)*	1.80 (0.04)
1HU7	2.21 (0.09)	4.80 (0.13)*†	1.55 (0.03)	0.54 (0.02)	2.43 (0.07)	4.99 (0.09)*†	1.68 (0.03)†
8 Months Old							
AC8	2.37 (0.12)	5.85 (0.11)*	1.73 (0.05)	0.52 (0.04)	2.45 (0.12)	5.77 (0.11)	1.83 (0.06)
1HU7+R1	2.22 (0.14)	5.06 (0.12)†	1.57 (0.05)†	0.43 (0.05)*	2.29 (0.11)	5.06 (0.14)*†	1.67 (0.06)
9 Months Old							
AC9	2.25 (0.14)	5.74 (0.13)	1.68 (0.06)	0.53 (0.04)	2.31 (0.16)	5.84 (0.12)	1.74 (0.08)
1HU7+R2	2.05 (0.12)	5.77 (0.11)◊	1.66 (0.04)◊	0.56 (0.03)	2.24 (0.14)	5.89 (0.16)◊	1.73 (0.06)
10 Months Old							
AC10	2.57 (0.17)*	6.21 (0.12)*	1.93 (0.08)*	0.57 (0.05)	2.54 (0.14)*	6.04 (0.11)*	1.87 (0.05)*
1HU7+R3	2.40 (0.16)	6.17 (0.18)*◊	1.88 (0.07)*◊	0.60 (0.08)	2.48 (0.13)	6.07 (0.17)*◊	1.89 (0.06)*◊
1HU10	2.18 (0.09)†	5.31 (0.08)†#	1.69 (0.06)†	0.58 (0.05)	2.17 (0.09)†	5.30 (0.10)†#	1.71 (0.05)†
2HU10	1.95 (0.10)†#	5.34 (0.12)†#‡	1.58 (0.06)†‡	0.51 (0.04)	1.99 (0.09)†‡	5.45 (0.10)†#‡	1.61 (0.06)†‡
12 Months Old							
AC12	2.06 (0.09)	6.16 (0.14)*	1.76 (0.06)	0.55 (0.02)	2.23 (0.13)	6.10 (0.13)*	1.78 (0.07)
1HU10+R2	2.12 (0.09)	5.75 (0.06)†◊	1.71 (0.06)	0.56 (0.03)	2.32 (0.11)	5.87 (0.21)◊	1.84 (0.05)*
2HU10+R2	1.91 (0.08)	6.04 (0.14)*◊	1.65 (0.06)	0.51 (0.02)	2.17 (0.13)	6.30 (0.22)*◊	1.75 (0.08)

Values are presented as mean ± SE

*** Indicates significant difference from baseline value, p < 0.05**

† Indicates significant difference from age-matched control value at same time point, p<0.05

 # Indicates significant difference from month 9 pre-HU value within same group (i.e. 1HU10(+R2) or 2HU10 + (R2)), p <0.05

◊ Indicates significant difference from immediate preceding post-HU value within same group, p<0.05

‡ Indicates significant difference between 1HU7+R3 and 2HU10, p<0.05

¤ Indicates significant difference between 1HU10 and 2HU10 at the same time point, p<0.05

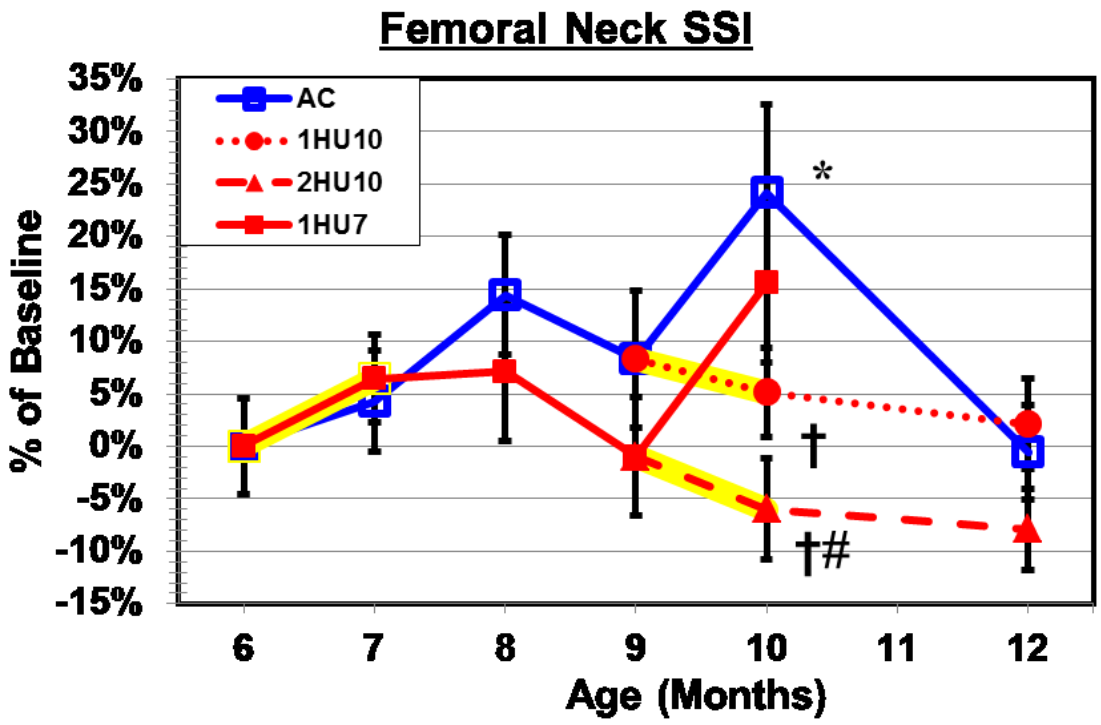

Fig. 53. Structural strength index from pQCT scanning at multiple time points during unloading and subsequent recovery of the right femoral neck. Numerical values are presented in Table 6 and yellow highlighting indicates HU treatment. AC SSI values show large fluctuations starting at month 8 with AC10 showing a significant increase from BL. 1HU7 increases along with AC7 but does not increase as much during the first month of recovery (1HU7+R1) even though it trends similar to AC. 1HU10 and 2HU10 both show slight decreases with respect to BL and are significantly smaller than AC10. 1HU10+R2 and 2HU10+R2 do not recover but instead decrease slightly till the end of month 12.

Values are presented as mean ± SE

*** Indicates significant difference from baseline value; p<0.05**

† Indicates significant difference from age-matched cage control value at same time point; p<0.05

 # Indicates significant difference from month 9 pre-HU value within same group; p<0.05

ǂ Indicates significant difference between 1HU7+R3 and 2HU10; p<0.05

¤ Indicates significant difference between 1HU10 and 2HU10 at the same time point; p<0.05

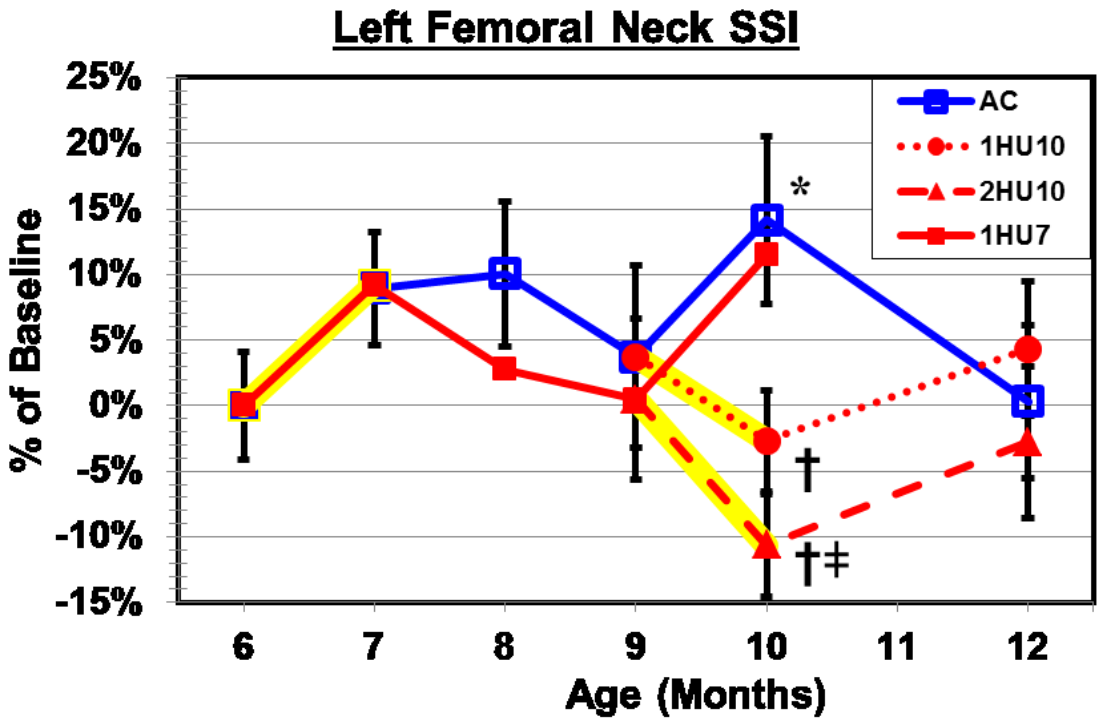

Fig. 54. Structural strength index from pQCT scanning at multiple time points during unloading and subsequent recovery of the left femoral neck. Numerical values are presented in Table 6 and yellow highlighting indicates HU treatment. SSI associated with lateral testing is very similar to the axial SSI. AC fluctuates throughout the life of the animals, an initial increase at 1HU7 with decreases during recovery, and decreases at 1HU10 and 2HU10 are all similar trends to the axial. Only the sharp increase in SSI at AC10 shows a significant difference from BL and this sharp increase paired with the decreases at 1HU10 and 2HU10 means both HU treatments are significantly smaller than AC10. 2HU10 is also significantly smaller than 1HU7+R3.
Values are presented as mean ± SE
*** Indicates significant difference from baseline value; p<0.05**
† Indicates significant difference from age-matched cage control value at same time point; p<0.05
 # Indicates significant difference from month 9 pre-HU value within same group; p<0.05
ǂ Indicates significant difference between 1HU7+R3 and 2HU10; p<0.05
¤ Indicates significant difference between 1HU10 and 2HU10 at the same time point; p<0.05

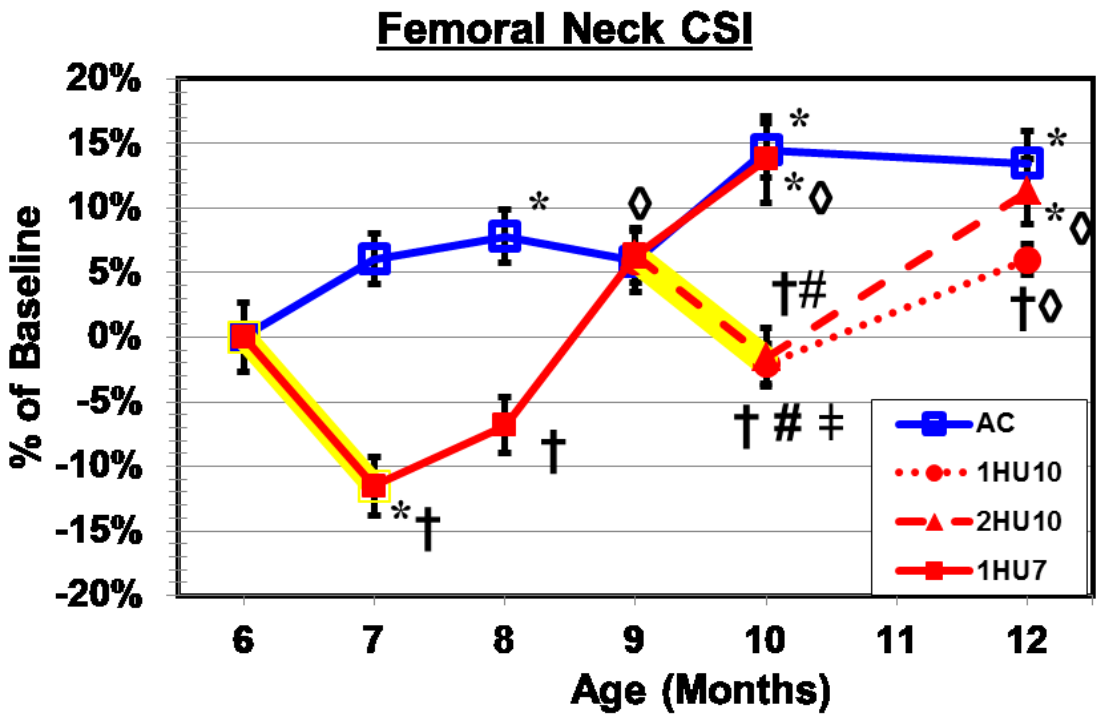

Fig. 55. Compressive strength index from pQCT scanning at multiple time points during unloading and subsequent recovery of the right femoral neck. Numerical values are presented in Table 6 and yellow highlighting indicates HU treatment. AC values show initial small increases until month 8 and then begin to fluctuate through the rest of the study. AC8, AC10, and AC12 all show significant increases with respect to BL. The HU trends are similar to those seen previously with 1HU7 having a large decrease with respect to BL and being significantly smaller than AC7. By 1HU7+R1, the HU group has recovered with respect to BL but not with respect to AC8. Final recovery with respect to BL

Values are presented as mean ± SE

*** Indicates significant difference from baseline value; p<0.05**

† Indicates significant difference from age-matched cage control value at same time point; p<0.05

 # Indicates significant difference from month 9 pre-HU value within same group; p<0.05

ǂ Indicates significant difference between 1HU7+R3 and 2HU10; p<0.05

¤ Indicates significant difference between 1HU10 and 2HU10 at the same time point; p<0.05

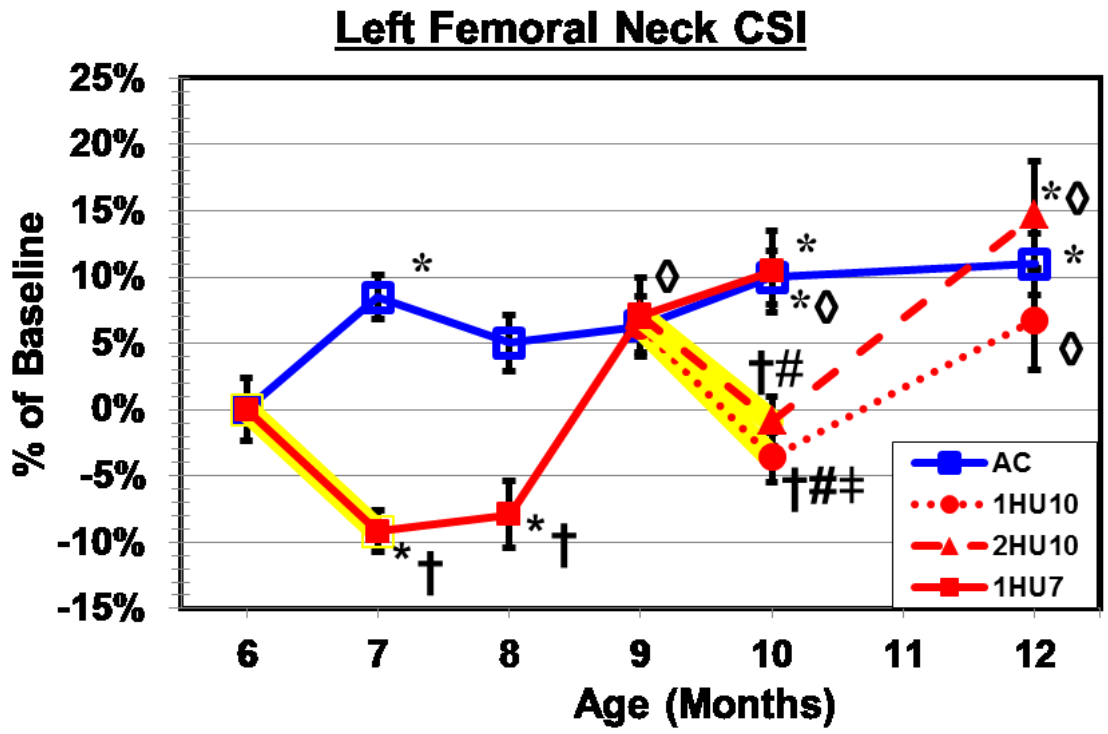

Fig. 56. Compressive strength index from pQCT scanning at multiple time points during unloading and subsequent recovery of the left femoral neck. Numerical values are presented in Table 6 and yellow highlighting indicates HU treatment. Lateral CSI, like lateral SSI, is very similar to the axial CSI except that axial shows slightly greater increases. 1HU7 shows a sharp, significant decrease from BL with little recovery at 1HU7+R1 but large recovery at 1HU7+R2 which continues into 1HU7+R3. 1HU10 and 2HU10 both decrease and are significantly smaller than AC10 with recoveries during 1HU10+R2 and 2HU10+R2 that are significantly larger than BL and significantly larger than their respective HU treatments. AC values fluctuate very little over the study but finish significantly larger than the original BL value.

Values are presented as mean ± SE

*** Indicates significant difference from baseline value; $p<0.05$**

† Indicates significant difference from age-matched cage control value at same time point; $p<0.05$

 # Indicates significant difference from month 9 pre-HU value within same group; $p<0.05$

ǂ Indicates significant difference between 1HU7+R3 and 2HU10; $p<0.05$

¤ Indicates significant difference between 1HU10 and 2HU10 at the same time point; $p<0.05$

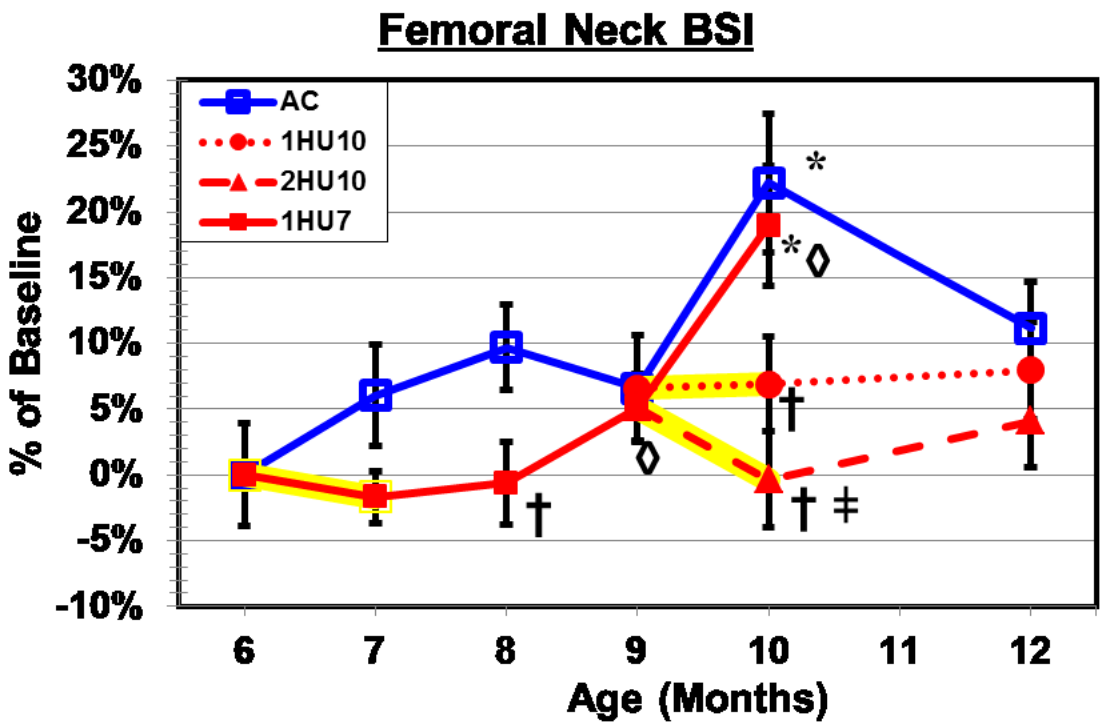

Fig. 57. Bending strength index from pQCT scanning at multiple time points during unloading and subsequent recovery of the right femoral neck.. Numerical values are presented in Table 6 and yellow highlighting indicates HU treatment. Density weighted BSI AC values generally increase with an especially sharp rise at month 10, but decrease from AC10 to AC12. 1HU7 decreases slightly and non-significantly with respect to BL and continues to increase during the recovery period up to nearly matching the AC10 value at month 10. 1HU10 continues to increase very slightly and continues this trend through the recovery. 2HU10 though, decreases but not to significantly less than BL and then increases during the recovery to within the 1HU10+R2 and AC12 values.
Values are presented as mean ± SE
*** Indicates significant difference from baseline value; p<0.05**
† Indicates significant difference from age-matched cage control value at same time point; p<0.05
 # Indicates significant difference from month 9 pre-HU value within same group; p<0.05
ǂ Indicates significant difference between 1HU7+R3 and 2HU10; p<0.05
¤ Indicates significant difference between 1HU10 and 2HU10 at the same time point; p<0.05

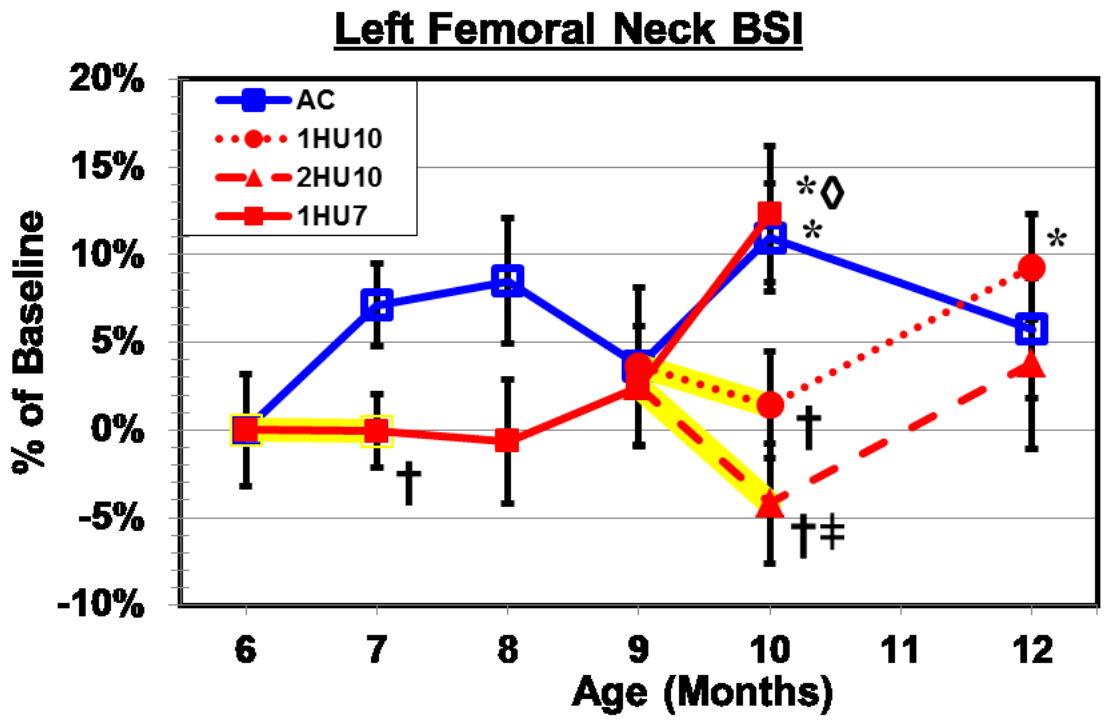

Fig. 58. Bending strength index from pQCT scanning at multiple time points during unloading and subsequent recovery of the left femoral neck. Numerical values are presented in Table 6 and yellow highlighting indicates HU treatment. Similar to the SSI graphs and the CSI graphs, the lateral density weighted BSI is similar to the previous axial BSI graph. AC values show initial increases until month 8 and then fluctuates for the rest of the study. AC10 is significantly larger than BL but decreases back to approximately the original BL value at AC12. 1HU7 shows a very slight, non-significant decrease with respect to BL which continues to decrease for 1HU7+R1. 1HU7+R2 increases and 1HU7+R3 continues this trend and ends significantly higher than BL and with respect to HU treatment. 1HU 10 shows a small, non-significant decrease which recovers to significantly higher than BL at the 1HU10+R2 point. 2HU10 also shows a non-significant decrease with respect to BL and AC10, and then increases to approximately AC12 value.

Values are presented as mean ± SE

*** Indicates significant difference from baseline value; p<0.05**

† Indicates significant difference from age-matched cage control value at same time point; p<0.05

 # Indicates significant difference from month 9 pre-HU value within same group; p<0.05

ǂ Indicates significant difference between 1HU7+R3 and 2HU10; p<0.05

¤ Indicates significant difference between 1HU10 and 2HU10 at the same time point; p<0.05

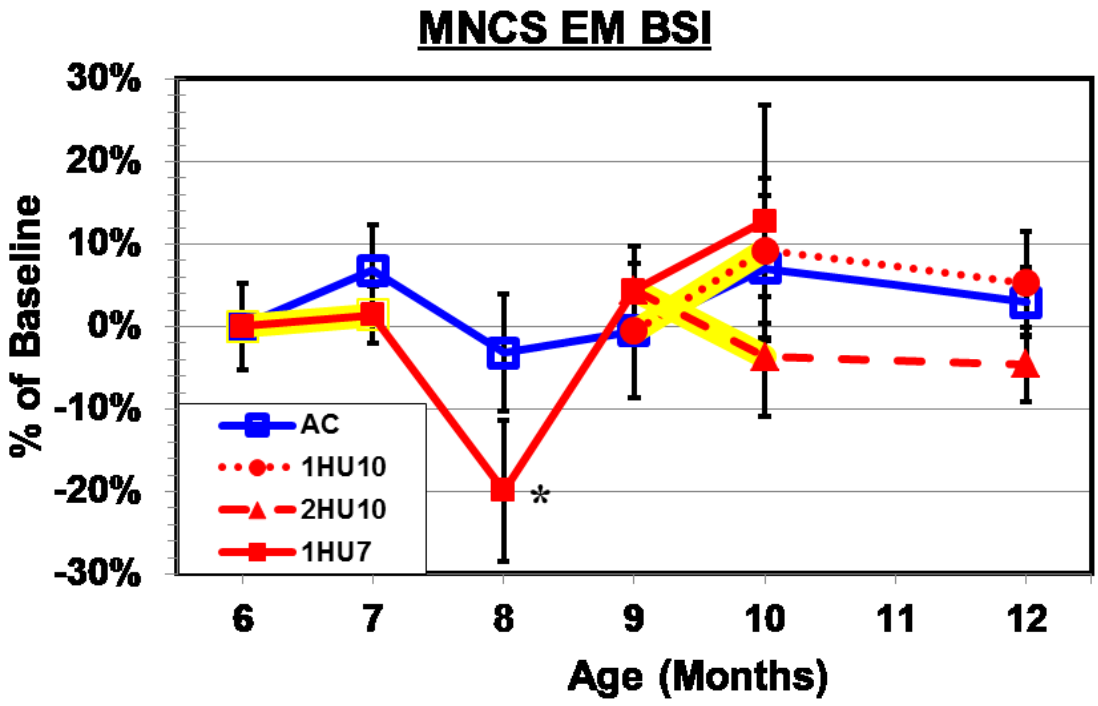

Fig. 59. Elastic modulus weighted bending strength index calculated from pQCT parameters at multiple time points during unloading and subsequent recovery of the right femoral neck. Numerical values are presented in Table 6 and yellow highlighting indicates HU treatment. The elastic modulus weighted (EM) BSI was calculated for the minimum cross sectional area of each femoral neck. The results show only 1HU7+R1 being significantly different from BL with no other significant differences seen. Both AC7 and 1HU7 increase slightly with respect to BL and both groups decrease at month 8 with 1HU7+R1 showing a sharp, significant decrease. 1HU7+R2 recovers back to within AC and BL values followed by increases for 1HU7+R3, 1HU10, and AC10. However, 2HU10 decreases non-significantly and 1HU10+R2 and 2HU10+R2 show little change along with AC12.

Values are presented as mean ± SE

*** Indicates significant difference from baseline value; $p<0.05$**

† Indicates significant difference from age-matched cage control value at same time point; $p<0.05$

 # Indicates significant difference from month 9 pre-HU value within same group; $p<0.05$

ǂ Indicates significant difference between 1HU7+R3 and 2HU10; $p<0.05$

¤ Indicates significant difference between 1HU10 and 2HU10 at the same time point; $p<0.05$

DISCUSSION

The discussion of the results will be split up into three sections in this chapter. First, the major trends and overall characteristics in the results will be overviewed and summarized. Next, the hypotheses will be evaluated for the major outcome variables including: total BMC, total vBMD, trabecular vBMD, cortical area, endocortical area, cortical thickness, and maximum force. Finally, the results will be compared to relevant literature while discussing broader implications.

Aging Control

Femoral Neck

Rat bone properties fluctuate and change somewhat due to age which was an important reason to include an aging control (AC) group as a reference during this study. The AC values may actually be the most appropriate indicator of recovery for this study since they serve as a reference for the values that normal (unaffected by HU) rat bone properties would have. Femoral neck cortical BMC appears to increase while trabecular BMC fluctuates and decreases over the 6 months of study time. When paired, the total for AC BMC increases steadily during the first three months of the study and then begins to fluctuate. Cortical vBMD also increases and fluctuates slightly especially after month 9, but trabecular vBMD generally decreases throughout the study causing the total vBMD to stay relatively steady around BL except for an increase at month 12. Even with the natural fluctuations occurring due to the aging of the animals, cortical BMC and vBMD increase throughout the study to values significantly greater than BL while trabecular BMC and vBMD values decrease to significantly less than BL. These dynamics imply that age causes the densitometric properties at the femoral neck to change for adult male rats from ages 6 to 12 months.

Cortical and trabecular area at the femoral neck for AC animals also fluctuate during the study but generally remained approximately the same as the original BL value except at month 10. Cortical thickness also remains relatively stable near BL values, as do the moments of inertia (maximum, minimum, and polar). Therefore, geometric properties of the femoral neck cross-section appear to change very little due to aging effects when the animals are unaffected by environmental stimuli such as unloading. The noticeable difference of the AC10 point compared to the other AC values may possibly be due to the different batches of animals used, but this is not known.

Femur Diaphysis

Femoral diaphysis densitometric properties continually increase over the course of the study for BMC and vBMD and are significantly higher than BL by month 7. Cross-sectional geometry properties increase in the same way as the densitometric properties, with all geometric properties (area, cortical area, and moments of inertia) continually increasing through the study.

Cortical bone in rats appears to always increase with age since both femoral neck cortical properties and midshaft properties showed fairly steady increases through the life of the animals. However, since the midshaft is composed of only cortical bone, the "total" bone for the midshaft is unaffected by trabecular bone effects unlike the femoral neck.

Effects Due to Hindlimb Unloading

Single, Younger HU (1HU7)

Femoral Neck

HU effects on densitometric properties typically cause decreases at the femoral neck. Cortical BMC shows a larger decrease from BL (~4%) than trabecular, which decreases only slightly (~1%) during HU. This causes an overall, total decrease in BMC of approximately 4% from BL. Cortical vBMD uncharacteristically increases during 1HU7 but trabecular vBMD shows a sharp reduction of more than 15%. Total vBMD still shows a significant decrease, even with the small increase of cortical vBMD, due to the large, significant decrease in trabecular density. The cortical density results indicate that pure cortical bone may not be greatly affected by unloading treatments while trabecular bone still seems to be the area most affected.

Femoral neck geometric properties largely increase during 1HU7, unlike densitometric properties, except for cortical area and thickness. The increases seen in endocortical area suggest endocortical resorption of the cortical bone with periosteal expansion on the outer surface of the cortical shell, which causes the total area to increase. Moments of inertia remain relatively unchanged during 1HU7 for the femoral neck, even though the geometries are increaseing. The stability of the moments of inertia provides more evidence that geometry-based adaptive changes are taking place to resist the detrimental effects of the HU.

Femur Diaphysis

Femur diaphysis densitometric and geometric properties at the femoral midshaft show increases at 1HU7 similar to what is seen for the AC group, but to a slightly lesser degree. This seems to suggest that unloading has a slight, non-significant retarding effect on normal, age-related bone growth.

Single, Older HU (1HU10)

Femoral Neck

When unloading occurs at an older age for the animals, a different pattern of changes occurs. Femoral neck total BMC decreases approximately 5%, similar to the younger unloading effect, but cortical BMC remains stable at 1HU10. Trabecular BMC shows a large, significant decrease (-12.55%) that causes the drop in total BMC. vBMD follows a similar pattern with trabecular bone showing a large, significant decrease at month 10, which causes a drop in total vBMD at the same time point. Cortical vBMD again remains stable and appears to be unaffected by the unloading while the trabecular vBMD is greatly affected by the unloading and causes changes to the total bone. Unlike the younger HU, geometric properties remain mostly unchanged. Total area, cortical area, endocortical area, and cortical thickness show almost no change during the unloading period between month 9 and 10. Maximum moment of inertia increases slightly and non-significantly with respect to BL while minimum decreases and polar stays nearly the same. Unloading at 9 months of age vs. 6 months of age appears to have no effect on the geometry of the bone itself, but significant, detrimental effects on its trabecular mineral content and density.

Femur Diaphysis

At the midshaft however, both BMC and all geometric properties show slight, non-significant decreases during the older HU. Density shows very little difference from AC and continues to increase significantly from BL. Content and the cortical areas of the midshaft may be affected by unloading since their relative increases are noticeable, but they are not significant with respect to AC and remain significantly higher than BL.

Second, Older HU (2HU10)

Femoral Neck

The second unloading treatment shows similar magnitudes and rates of decrease for femoral neck total BMC as for the younger unloading. Femoral neck total BMC decreases approximately 6% due to decreases in both cortical BMC and trabecular BMC; however, only trabecular BMC decreases significantly from BL at 2HU10. Femoral neck total vBMD shows a small, non-significant decrease during the second HU due to a large decrease in trabecular vBMD which is offset by an increase in cortical vBMD. The 2HU10 trabecular vBMD decrease is smaller than the first, while the 2HU10 cortical vBMD increase is approximately the same, which prevents the total decrease from having the same magnitude and rate as the initial HU. The similar rate of increase for the cortical bone along with the smaller decrease in trabecular density may imply a reduction of the effect of HU for a second unloading. However, femoral neck total area shows a decrease for 2HU10 unlike the first HU, which had an increase for matching AC. The femoral neck cortical area shows a decrease of approximately 5%, which is similar in rate and magnitude to 1HU7 while trabecular area shows a slight decrease. Trabecular area for 1HU7 increased noticeably, but not significantly, from BL which is very different from the 2HU10 decrease. Cortical thickness at 2HU10 is still significantly higher than BL but shows a small decrease as do the moments of inertia, which may show that femoral neck total area and geometric parameters are more affected by a second bout of unloading compared to a single treatment.

Femur Diaphysis

The midshaft may be affected by a second treatment of unloading since BMC, cortical thickness, and the area show slight, but non-significant, changes that were not seen for 1HU7. Cortical vBMD and moments of inertia show similar increases for 2HU10 that were seen for the first HU, which seems to suggest that BMC and area are more affected

by unloading and external stimuli. However, the decreases for BMC, thickness, and area are non-significant compared to AC and still significantly higher than BL so further study is needed to clearly determine whether a second bout of HU affects the bone properties at the femoral midshaft. Also, the 2HU10 decreases are similar to the 1HU10 so the changes may be age-induced instead of treatment-induced.

Recovery Dynamics

Femoral Neck

Recovery periods allow the different groups to recover from the respective HU exposures. For instance, femoral neck total BMC decreases during 1HU7 but the increases for 1HU7+R1 and 1HU7+R2 return the HU values back to AC by month 9. 1HU7+R3 increases at a similar rate as AC10 and is approximately the same value, while the recoveries of both 1HU10 and 2HU10 also bring their respective HU groups back to approximately the same as AC by month 12. Cortical BMC shows strong recoveries particularly during the second months of 1HU7+R2, 1HU10+R2, and 2HU10+R2. Unloading seems to slightly stunt the initial increase seen in the AC trabecular BMC. Femoral neck cortical and trabecular vBMD confirm this. Cortical vBMD shows no noticeable effect from HU and the recovery points are approximately the same as the matching AC values. Trabecular vBMD; however, decreases significantly for all HU treatments, and recovers with respect to AC by two months of recovery. This causes the total bone vBMD for 1HU7 to decrease significantly but to recover by the second month and to show slight, non-significant decreases for the month 10 HU treatments.

Geometric parameters for the femoral neck show consistent patterns during unloading and recovery for cortical and trabecular bone area as well as cortical thickness. Cortical geometry (area and thickness) decreases during HU and increases at varying rates during recovery for all HU groups. At the same time, trabecular area increases during HU and

generally decreases during recovery which causes total bone to fluctuate greatly during the study. When observing bone geometries, particularly for a mixed site, the current results indicate that it may be more appropriate to look at each type of bone separately, observing how one type affects the other instead, of looking at the total bone as a whole. Also, the recovery values for the moments of inertia change very little except for 1HU7+R3, which can be attributed to the simultaneous increase of cortical and trabecular area during this time period.

Femur Diaphysis

Recovery for the midshaft still shows little difference from the matching AC values. The recovery points continue to increase and are usually approximately the same as the matching AC values except for midshaft vBMD at 1HU10+R2 and 2HU10+R2. These final recovery values are significantly smaller than AC which may suggest that unloading at an older age does in fact cause a significant effect on cortical density. Also, the 1HU10+R2 value is smaller (non-significantly) than the 2HU10+R2 value which suggests that multiple exposures to HU may actually help maintain density as age increases.

Mechanical Testing Observations

Axial and Lateral Femoral Neck

The maximum mechanical loads for the right and left femoral neck follow trends that are similar to the results seen for total vBMD and total BMC. For the axial maximum loads, AC values remain relatively stable until month 10 when a sudden increase occurs which returns to approximately the BL value by month 12. The increase at month 10 was also seen for the previous densitometric results. HU causes a significant decrease at 1HU7 but recovers rapidly by the end of the first recovery month and the same occurs for the older HU groups. Lateral max force values are very similar to the axial, but do not show the large increase for AC10 that was seen previously. All HU groups show significant

decreases again, but 1HU7 takes 2 recovery periods to fully recover instead of only one. Mechanical strength is clearly affected by the unloading which causes significant decreases; however, recovery occurs rapidly for each type of mechanical test and for each HU group. Also, 2HU10 decreases nearly 10% more for the lateral mechanical testing than the axial which indicates that there may be some differences between the two testing types even though comparison plots of the axial and lateral testing shown in the appendix reveal how similar their trends are.

Further indications of potential differences between axial and lateral testing are the stiffness results. The axial stiffness differs little between the HU and AC groups except for 1HU10+R2, which has a considerably smaller value than 2HU10+R2 and AC12. 2HU10+R2 and AC12 have a large increase of over 40% from month 10. Also, the 1HU7 group is slightly larger than the AC group during recovery, but the lateral AC stiffness is larger than the 1HU7 stiffness until the third recovery point. 1HU10 and 2HU10 for the lateral stiffness show significant decreases from HU and neither AC12 nor 2HU10+R2 show the large increases seen by the axial stiffness. However, 1HU10+R2 remains relatively flat after the 1HU10 treatment similar to the axial 1HU10+R2 point. These differences could be an indication of differences between the loading conditions and may result from how stiff the bone is in relation to the different loading vectors.

Femoral Midshaft

Extrinsic Mechanical Testing Properties

As expected, the midshaft max force values show different trends from the femoral neck and are similar to the previous densitometric and geometric graphs. The 1HU7 max force shows increases that are approximately the same as the AC but slightly lower until after the 1HU7+R2 recovery point. 2HU10 shows a slowing of the increase while 1HU10 shows a slight decrease for the later HU treatments but all of the month 12

recovery values are approximately the same as AC12. Midshaft stiffness also increases throughout the study for all HU groups and the AC group. In fact, the midshaft stiffness plot appears similar to the axial femoral neck stiffness, but this may only be a coincidence. Hindlimb unloading seems to have little to no effect on the mechanical strength at the femoral midshaft. The slower increases in maximum force for 1HU7 than AC7 and the small decreases at month 10 are non-significant with respect to AC. All groups remain significantly higher than BL and at approximately the same value at month 12 which shows there is not enough evidence to suggest that HU affects cortical bone at the femoral midshaft.

Intrinsic Mechanical Testing Properties

The intrinsic mechanical properties for the three-point bending of the femur midshaft show some unique trends, but the large error bars for the average values prevent the statistical t-tests from showing significant differences. Greater sample sizes for each point in each group are needed to determine whether there are statistically important differences in many of the plots. For instance, elastic modulus shows increases for HU treatments which make the HU values higher than the AC values for the majority of the study. However, none of the differences between HU and AC are significantly different which makes it difficult to decide if the increases during HU are a sign of unloading effects.

Interestingly, Pre-yield Toughness and Energy to Yield follow similar patterns as seen in the femoral neck with large decreases for 1HU7 and noticeable, but smaller, decreases for 1HU10 and 2HU10. However, 2HU10+R2 for both toughness and energy continue to decrease rapidly. Again, the large error bars cloud most of the potential, significant differences but 1HU7 is significantly smaller than AC7 for energy and toughness. These patterns imply that HU causes the bones to lose the ability to absorb energy during mechanical testing but the midshaft maximum loads do not support this since the loads, especially during 1HU7, actually increase. Energy to fracture does not help to illuminate

this issue since the groups fluctuate greatly over the course of the study. This is likely caused because of the difficulty in calculating intrinsic properties after yielding. Ultimate and yield stress plots also reveal very little because of the fluctuations within the groups coupled with the lack of statistical differences due to the large error bars. These issues may be caused due to the aforementioned difficulties in calculating intrinsic properties paired with the difficulty in accurately calculating the stress in the bone due to the irregular and changing shape of the femur along the shaft.

Finally, the elastic modulus weighted bending strength index (EM BSI) appears very similar to the maximum load seen previously. AC and HU groups continue to increase over the course of the study but HU values remain below AC except for 1HU7+R3. HU values are never significantly different from AC and all groups increase significantly higher than BL which implies again that unloading has little to no effect on the mechanical strength. Calculating this form of BSI for the midshaft appears to accurately approximate the actual mechanical testing.

Femoral Neck Calculated Strength Comparisons

The need to find a good calculated strength approximation for true mechanical strength is extremely important for understanding the strength of human bone for individuals who have undergone multiple missions for NASA or individuals with osteoporosis. The SSI provided by the pQCT scanner does not seem to provide a good approximation of the femoral neck mechanical testing strength though. 1HU7 SSI for both right and left femoral neck show increases instead of the decreases seen in the maximum force plots. 1HU10 and 2HU10 for the SSI show decreases but not to the same magnitudes as the actual mechanical testing and SSI recovery does not follow the same patterns as actual testing. CSI appears to be a much better approximation for true mechanical strength since each HU group decreases, just like maximum force, and the magnitudes are much more similar to the true value than the SSI was. However, calculated CSI predicts that recovery will occur rapidly, by the second month, which is not supported in the true

mechanical testing data which takes at least two months to recover. BSI appears to be a slightly better approximation than SSI, but not as accurate an approximation as CSI. The CSI calculations predict that 1HU7 will remain relatively stable and not decrease, which is not accurate, and even though the older HU treatments show decreases their magnitudes are not nearly as large as those seen for the testing strength. The minimum cross sectional area elastic modulus weighted bending strength index (MNCS EM BSI) was expected to be a good approximation, like the midshaft EM BSI, but proved to be the least accurate at calculating the strength. The MNCS EM BSI fluctuates greatly and only shows a significant difference (decrease) at 1HU7+R1. Femoral neck cross sections can vary greatly and the nature of the mixed site means partial volume effects can cause very different properties from voxel to voxel. These problems may prevent a good approximation from being developed at a mixed site, such as the femoral neck, because there is both a large percentage of cortical bone and a large percentage of trabecular bone.

Of the four different calculations performed for an approximation of the true mechanical strength, CSI appears to be the most accurate. The comparisons between actual mechanical force and CSI are close because of the similar trends and magnitudes, including the large AC10 increase seen previously for densitometric properties. SSI fluctuates too greatly to serve as a good approximation as does the MNCS EM BSI. The density weighted BSI calculations may be used to see possible trends for true mechanical strength, but the magnitudes and patterns should only be considered possible approximations.

Hypothesis H1

To evaluate whether the first HU (1HU7) has a negative effect on the second HU exposure (2HU10) the proper test is to compare the response of the second HU (2HU10) to the age-matched single HU (1HU10). A relevant related question is to compare the response to the second HU (2HU10) to that for the first HU (1HU7), which will assess

whether the second is worse (or better) than the first. The way the study was structured and the data collected does not lend itself to a direct statistical test for these comparisons. The hypothesis can nevertheless be evaluated in two ways. For each HU exposure, the post-HU values can be compared to the pre-HU values to determine if there is a statistically significant difference. In addition to this, the extent of the difference can be quantified in terms of the percent change from pre- to post-HU. The possible scenarios are described below. An important qualification is that these descriptions are for the case of HU resulting in a decrease in the variable of interest and the interpretation that lower values are indeed worse (such as BMC or vBMD).

(a) If the pre-post change is significant for 2HU10 but not for 1HU10, then the hypothesis would be true; i.e., the first HU (1HU7) had a negative effect on the second.

(b) If the pre-post change is significant for 1HU10 but not for 2HU10, then the hypothesis would be false; i.e., the first HU (1HU7) had no negative effect on the second.

(c) If the pre-post change is not significant for either 2HU10 or 1HU10, then the hypothesis would be false; i.e., the first HU (1HU7) had no negative effect on the second.

(d) If the pre-post change is significant for both 2HU10 and 1HU10, then the hypothesis could still be tested by comparing the percent changes for each. If the percent change is negative and larger in magnitude for 2HU10 than for 1HU10, then the hypothesis would be considered to be true.

There were significant reductions in femoral neck total BMC for both 2HU10 and 1HU10, which suggests that the first HU did not have a major effect on the second HU. However, the percent reduction for 2HU10 is -5.88% compared to -4.1% for 1HU10,

which suggests a slight negative effect of the first HU on the response for 2HU10. Midshaft BMC did not exhibit significant decreases for either 2HU10 or 1HU10. Femoral neck total vBMD did not decrease significantly for 2HU10 or for 1HU10, which does not suggest that hypothesis 1 is true. However, both 2HU10 and 1HU10 exhibit non-significant decreases from the previous time point. Also, femoral neck cancellous vBMD decreases significantly for both 2HU10 and 1HU10. The percent reduction for 2HU10 is -5.78% compared to -12.03% for 1HU10. Unlike the results presented by Carpenter et al., the cancellous vBMD recovers to AC values within 2 months (37).

Femoral neck cortical area decreases significantly for 2HU10 but not for 1HU10 indicating that hypothesis 1 may be true. Percent reduction for 2HU10 is -5.35% while 1HU10 is only -0.19%. However, femoral neck cancellous area did not decrease significantly for either 2HU10 or 1HU10. Also, midshaft vBMD inecreased significantly for 2HU10 and increased non-significantly for 1HU10. Cortical thickness at the femoral neck did not decrease significantly for either 2HU10 or 1HU10 or for midshaft 1HU10 but did decrease significantly at 2HU10 for the midshaft. Percent reduction was -4.39% for the midshaft 2HU10 mean value.

Maximum mechanical testing force decreased significantly for axial and lateral testing for both 2HU10 and 1HU10. Axial 2HU10 percent reduction was -17.36% while axial 1HU10 percent reduction was -13.89%. Lateral 2HU10 percent reduction -18.65% while lateral 1HU10 percent reduction was -11.3% which strongly indicates hypothesis 1 is true. However, midshaft maximum force values did not significantly decrease for either 2HU10 or 1HU10. Lateral testing does not always have the lowest or highest fracture load unlike the results observed by Keyak and Jamsa (41,40,42,35).

Given these results, a second exposure to HU appears to cause greater negative effects at the femoral neck but not at the midshaft. Therefore, hypothesis 1 is conditionally true

because it is site specific since the femoral neck is more affected by HU exposure. The femoral neck being more affected than the midshaft is expected based upon the results of previous studies. The rat studies which compared various bone sites observed that femoral neck is highly sensitive to change while the midshaft is not (14,57,38,42). Also, human studies have observed significant changes in densitometric properties and finite-element model derived failure loads of astronauts (40,37,13). A second exposure to unloading is more detrimental to bone loss and deterioration.

Hypothesis H2

To evaluate whether age has a greater, negative effect on HU exposure the proper test is to compare the response of the younger, single HU (1HU7) to the older, single HU (1HU10). The way the study was structured and the data collected does not lend itself to a direct statistical test for these comparisons. The hypothesis can nevertheless be evaluated in two ways. For each HU exposure, the post-HU values can be compared to the pre-HU values to determine if there is a statistically significant difference. In addition to this, the extent of the difference can be quantified in terms of the percent change from pre- to post-HU. The possible scenarios are described below. As before, these descriptions are for the case of HU resulting in a decrease in the variable of interest and the interpretation that lower values are indeed worse.

(a) If the pre-post change is significant for 1HU10 but not for 1HU7, then the hypothesis would be true; i.e., the older HU (1HU10) was more negatively affected than the younger (1HU7).

(b) If the pre-post change is significant for 1HU7 but not for 1HU10, then the hypothesis would be false; i.e., the younger HU (1HU7) was more negatively affected than the older (1HU10).

(c) If the pre-post change is significant for both 1HU7 and 1HU10, then the hypothesis

could still be tested by comparing the percent changes for each. If the percent change is negative and larger in magnitude for 1HU10 than for 1HU, then the hypothesis would be considered to be true.

There is a significant reduction (-4.14%) in femoral neck total BMC for 1HU10 but not 1HU7, which suggests that age had an effect on the older exposure. However, Midshaft BMC did not exhibit significant decreases for either 1HU7 or 1HU10. Also, 1HU7 femoral neck vBMD has a significant reduction of -7.71% while 1HU10 does not have a significant decrease. Midshaft vBMD exhibited a significant increase for 1HU10 and a non-significant increase for 1HU7. However, Perrien et al. saw significant reductions in cortical BMD, but this study observed increases in femoral neck cortical BMD at both the older and younger HU (47). Femoral neck cancellous BMC has no significant reductions for either 1HU7 or 1HU10 but femoral neck vBMD has significant reductions for both 1HU7 and 1HU10. Percent reductions for 1HU7 and 1HU10 vBMD are -12.03% and -15.39%, respectively, revealing a slightly greater negative effect on cancellous vBMD at the older age.

Femoral neck cortical area decreases, but not significantly, for 1HU7 and 1HU10. Alternatively, endocortical area increases during HU but the mean values are non-significant for both groups. Also, femoral neck cortical thickness significantly decreases at 1HU7 by -9.39% but does not significantly change at 1HU10. Midshaft area increases significantly for 1HU7 but also decreases non-significantly for 1HU10. Percent increase for midshaft 1HU7 area is 5.59% suggesting a greater negative effect from HU at the older age. Midshaft cortical thickness increases for 1HU7 but decreases for 1HU10; however, both percent changes are non-significant.

Maximum mechanical testing force decreased significantly for axial and lateral testing for both 1HU7 and 1HU10. Axial 1HU7 percent reduction was -16.25% while axial 1HU10 percent reduction was -13.89%. Lateral 1HU7 percent reduction -8.10% while

lateral 1HU10 percent reduction was -11.3%; however, midshaft 1HU7 maximum force increased significantly (11.43%) while the pre-post change at 1HU10 was non-significant.

These data indicate that age may not worsen how bone responds to HU, but the effect depends on the type of bone and the site. Total BMC at the femoral neck is reduced during HU but not significantly; however, cortical BMC changes very little, which causes the total BMC to be significantly reduced at 1HU10. Femoral neck total vBMD and axial maximum force exhibit smaller reductions for the 1HU10 group compared to the 1HU7. However, lateral maximum force is more reduced at 1HU10 when compared to 1HU7, and midshaft pQCT parameters and mechanical testing show non-significant decreases compared to increases for the younger animals. Thomsen et al. reported bone loses for older animals while Perrien et al. reported decreases in cortical BMD with increases in porosity (47,48). Bone appears to be affected by age but it remains unclear if the effects are negative, especially during disuse..

LIMITATIONS

This study assumed that six month old rats were both skeletally mature and can serve as a good approximation for how human bone would react after extended unloading sessions. However, the results reveal that the skeletal properties of AC rat bones change and fluctuate somewhat throughout the life of each animal, so the assumption of skeletal maturity is not true in the strictest sense and constitutes a limitation. Also, the structure of the proximal rat femur is different than the human proximal femur. The rat femoral neck has a larger cortical shell and smaller amount of trabecular bone with a different shape compared to humans who have a thin cortical shell and larger amount of trabecular bone. However, total bone properties and mechanical testing results are indicative of the types of changes that are expected for human bone during unloading. Therefore, the use of rats for this type of study seems appropriate when looking at how bone is affected, but future research should be careful when making comparisons between rat results and how humans would be affected. Also, using older animals may provide for less variation in bone properties over time for the control, but will likely lead to higher attrition rates during HU. Higher attrition rates would require more animals and lead to higher costs to perform the study.

This study also utilized ex-vivo results consisting of end point data. In other words, the bones of the animals were scanned, tested, and analyzed after the animals had been sacrificed. A two-sample t-test was used to look at differences between end points of interest; however, this does not take into account other factors such as interactions between age and HU. Typically, ANOVA tests are used to analyze when multiple factors are involved, but the double-HU study design does not lend itself to a straightforward ANOVA approach. Therefore, t-tests have been used to compare mean values between groups and time points of interests and aging effects are included by comparing to aging controls (AC) . Also, the ex-vivo design of the study means that each data point consists of totally different groups of animals, which may vary slightly in age and biology.

However, animals were placed into groups based upon two variables at baseline: total vBMD at the proximal tibia metaphysis and total body weight. Groups were organized to ensure that there were no statistically significant differences for these two variables at BL. Unfortunately, this approach does not guarantee that all groups will age and/or respond to HU exposures similarly, but biological variation is always a limitation in animal studies. This study used a robust 15 animals per group to help minimize potential negative effects.

CONCLUSIONS

At the beginning of this study a number of hypotheses were generated to answer specific questions on how bone is affected by unloading. For instance, it was important to understand if multiple exposures to HU will cause worse reductions in properties such as vBMD and mechanical strength and if these reductions will recover over time. Also, since many astronauts perform multiple missions in space, knowing the effects of multiple bouts of unloading and how multiple sessions affect the recovery dynamics is very important. Furthermore, some astronauts and individuals with osteoporosis experience bone loss at an older age so this study addressed how unloading at an older age affects the response to HU and recovery. Femoral neck properties do show significant effects from HU treatment and more pronounced effects during the second HU, especially for trabecular bone. However, the detrimental effects of the first and second HU typically recover with respect to matching AC values after two months of recovery time. Also, except for trabecular BMC, densitometric and strength properties for the femoral neck are typically not significantly different from BL or AC after two months of recovery for either a single HU or a double HU treatment. At the midshaft, cortical bone densitometric, geometric, and mechanical properties increase throughout the study and even though there are slight decreases during the older HU treatments, they are not significantly different from AC or BL. The unloading may stunt the normal growth of bone since the values for the HU group are slightly less than the values for the AC group, but these differences were not statistically significant. Also, HU at an older age may have caused the slight decreases seen for midshaft pQCT and mechanical testing parameters but having multiple unloading periods does not appear to drastically affect those loses.

These results do support to the hypothesis that older HU treatments will have a greater effect on the bone than HU at a younger age. However, it seems that this is true for cortical bone, which shows little effect at a young age but slight, though non-significant,

decreases at an older age. Trabecular bone shows larger decreases for BMC and lateral mechanical testing strength at older ages, but approximately the same losses of vBMD and higher failure strengths for axial testing. The total bone may attempt to adapt to the unloading environmental stimuli in order to provide a more efficient structure by increasing cortical bone density and changing the bone geometry to better support external loading. This is supported by the endocortical resorption and periosteal expansion, seen in the results of this study, which modifies the shape of the bone into a larger tube with a thicker shell.

Femoral neck strength is significantly weakened during HU, but it was hypothesized that the strength would either have slow or incomplete recovery after reloading, not the rapid recovery within two months that was seen. This study has shown that by the end of two months of recovery, both the axial and lateral testing strength values recovered to AC and BL values suggesting normal bone levels. This intensity of recovery at a mixed site such as the femoral neck was unexpected even though the lack of HU effect on the femoral midshaft was expected. The midshaft mechanical testing values match the densitometric values and continue to increase over the full study time. The midshaft geometric properties also increase for cortical area, cortical thickness, and moments of inertia which is another factor explaining the steady increase in midshaft strength over the life of the animals.

While midshaft cortical area and thickness increases, femoral neck cortical geometry decreases due to the expanding endocortical area at the cortical/trabecular interface. During HU, trabecular area rapidly increases, which causes the cortical area to decrease. Once recovery begins, trabecular area begins to decrease to return to normal levels, but it is often very fast and continues well beyond the original BL value. The cortical area on the other hand, decreases during HU as the trabecular area expands, and then increases to well above BL once the recovery periods occur. These changes in geometry may be

adaptations to maintain bone strength, but they cause the cortical bone on the inside of the shell to become less dense and similar to the trabecular bone.

The physiological responses of rat bone to age coupled with the results of this study suggest that comparing the treated HU groups to the AC is the most appropriate method of observing the effects of HU and the resulting recovery dynamics. However, comparisons to BL are likely more appropriate for astronauts because of the differences between human and rat bone physiology. Also, astronauts have very different lifestyles compared to individuals who might serve as an Earth-based control. Astronauts are typically highly active and athletic compared to the average person, and their level of activity may assist in their recovery from unloading after missions. However, it remains clear that space-flight unloading will cause detrimental effects to bone but the results of this study suggest that general recovery may occur after two months. Astronauts though, go through repeated long-term missions, and since trabecular bone recovery is questionable, it is necessary to continue to study how bone is affected by unloading. Particular focus should be paid to the quality of the bone during HU and throughout recovery especially at the interface between the cortical shell and the trabecular bone in mixed sites. Generally, cortical bone was unaffected during this study so future research may want to focus only on mixed sites such as the proximal femur, distal femur, and proximal tibia where trabecular bone is in greater quantities.

The initial HU did exacerbate the effects of the second HU for certain properties of the femoral neck. Total BMC, axial max force, and lateral max force exhibited greater reductions for 2HU10 than were seen for 1HU10. However, femoral neck total vBMD did not have greater reductions for 2HU10. Also, midshaft BMC, vBMD, and max force did not have greater reductions at 2HU10 compared to 1HU10. Therefore, the initial HU does exacerbate the effects of the second HU but only on certain properties and at mixed bone sites.

Alternatively, older animals do not appear to be more negatively affected by HU. Femoral neck total BMC, total vBMD, and axial max force are not more negatively affected by HU exposure at 1HU10. Also, midshaft BMC, vBMD, and max force are not further reduced at 1HU10. However, lateral max force does show greater reductions for the older HU compared to the younger HU. Since the densitometric and axial mechanical testing properties do not exhibit a greater negative effect at the older age, the greater decrease for lateral maximum force at 1HU10 compared to 1HU7 might be attributed to a difference in the loading condition of the femoral neck instead of the age of the animals.

The femoral neck densitometric, geometric, and mechanical properties generally have greater reductions during all of the HU exposures compared to midshaft properties. More specifically, the femoral neck exhibits greater reductions due to the second HU exposure as explained above, and the midshaft properties do not exhibit these greater reductions for 2HU10. Therefore, the femoral neck is more severely affected by multiple HU compared to the midshaft of the femur.

REFERENCES

1. Pajamaki, I., Jarvinen, T. Skeletal Effects of Estrogen and Mechanical Loading are Structurally Distinct. Bone 2008 43:748-757.
2. Morey-Holton, E.R., Globus, R. K. Hindlimb Unloading of Growing Rats: A Model for Predicting Skeletal Changes During Space Flight. Bone 1998 22(5):83S-88S.
3. Jarvinen, T.L.N., Jarvinen, M. Dual-Energy X-Ray Absorptiometry in Predicting Mechanical Characteristics of Rat Femur. Bone 1998 22(5):551-558.
4. Frost, H.M. A Determinant of Bone Architecture: The Minimum Effective Strain. Clinical Orthopedics 1983 175:286-292.
5. Goldstein, S.A. The Mechanical Properties of Trabecular Bone: Dependence on Anatomic Location and Function. Journal of Biomechanics 1987 20:1055-1061.
6. Martin, R.B. Determinants of the Mechanical Properties of Bones. Journal of Biomechanics 1991 24(Suppl.1):79-88.
7. Jarvinen, T.L.N., Kannus, P. Femoral Neck Response to Exercise and Subsequent Deconditioning in Young and Adult Rats. Journal of Bone and Mineral Research 2003 18:1292-1299.
8. Haapasalo, H., Kannus, P., Sievanen, H., Pasanen, M., Uusi-Rasi, K., Heinonen, A., Oja, P., Vuori, I. Effect of Long-Term Unilateral Activiy on Bone Mineral Density of Female Junior Tennis Players. Journal of Bone and Mineral Research 1998 13:310-319.
9. Kannus, P., Haapasalo, H., Sankelo, M., Sievanen, H., Pasanen, M., Heinonen, A., Oja, P., Vuori, I. Effect of Starting-Age of Physical Activity on Bone Mass in the Dominant Arm of Tennis and Squash Players. Annals of Internal Medicine 1995 123:27-31.
10. Osteo. Osteoporosis. 2011 http://www.nof.org/

11. Amin, S., Khosla, S. Association of Hip Strength Estimates by Finite-Element Analysis With Fractures in Women and Men. Journal of Bone and Mineral Research 2011 26(7):1593-1600.
12. Turner, R.T. Physiology of a Microgravity Environment Invited Review: What Do We Know About the Effects of Spaceflight on Bone? Journal of Applied Physiology 2000 89:840-847.
13. Lang, T., Yu, A. Cortical and Trabecular Bone Mineral Loss from the Spine and Hip in Long-Duration Spaceflight. Journal of Bone and Mineral Research 2004 19:1006-1012.
14. Bloomfield, S.A., Delp, M. D. Site- and Compartment-specific Changes in Bone With Hindlimb Unloading in Mature Adult Rats. Journal of Bone 2002 31(1):149-157.
15. NASA. Human Research Project. 2011 http://www.nasa.gov/exploration/humanresearch/
16. Shimano, M.M., Volpon, J. B. Biomechanics and Structural Adaptations of the Rat Femur After Hindlimb Suspension and Treadmill Running. Brazilian Journal of Medical and Biological Research 2009 42:330-338.
17. Morey-Holton, E.R., Globus, R. K. Hindlimb Unloading Rodent Model: Technical Aspects. Journal of Applied Physiology 2002 92:1367-1377.
18. Currey, J.D. Bones: Structure and Mechanics, 2002 vol. Princeton University Press, Princeton.
19. Institute, N.C. 2011 Structure of Bone Tissue. http://training.seer.cancer.gov/anatomy/skeletal/tissue.html
20. Baker, C. Primary Tissues: Bone Ossification and Growth. 2011 https://courses.stu.qmul.ac.uk/smd/kb/microanatomy/bone/answers/index.htm
21. Martin, R.B., Burr, D.B., Sharkey, N.A. Skeletal Tissue Mechanics, 1998 vol. Springer, New York.
22. Dalsky, G.P., Stocke, K.S., Ehsani, A.A., Slatopolsky, E., Lee, W.C., Birge, S.J. Jr. Weight-Bearing Exercise Training and Lumbar Bone Mineral Content in Postmenopausal Women. Annals of Internal Medicine 1988 108:824-828.

23. Haapasalo, H., Kontulainen, S., Sievanen, H., Kannus, P., Jarvinen, M., Vuori, I. Exercise-Induced Bone Gain is Due to Enlargement in Bone Size Without a Change in Volumetric Bone Density: A Peripheral Quantitative Computed Tomography Study of the Upper Arms of Male Tennis Players. Bone 2000 27:351-357.
24. Heinonen, A., Sievanen, H., Kannus, P., Oja, P., Vuori, I. Effects of Unilateral Strength Training and Detraining on Bone Mineral Mass and Estimated Mechanical Characteristics of the Upper Limb Bones in Young Women. Journal of Bone and Mineral Research 1996 11:490-501.
25. Berard, A., Bravo, G., Gauthier, P. Meta-Analysis of the Effectiveness of Physical Activity for the Prevention of Bone Loss in Postmenopausal Women. Osteoporosis International 1997 7:331-337.
26. Seeman, E. An Exercise in Geometry. Journal of Bone and Mineral Research 2002 17:373-380.
27. Forwood, M.R., Burr, D.B. Physical Activity and Bone Mass: Exercises in Futility? Bone and Mineral 1993 21:89-112.
28. Grey, H. Anatomy of the Human Body, 1918 vol. Lea & Febiger, Philadelphia, PA.
29. Bagi, C.M., Bertolini, D. Morphological and Structural Characteristics of the Proximal Femur in Human and Rat. Journal of Bone 1997 21(3):261-267.
30. Fowler, T.W., Gaddy, D. Reambulation After Disuse Causes Differential Age-Dependent Responses in Bone Strength and Bone Formation in Trabecular and Cortical Bone American Society of Bone and Mineral Research, 2011 vol.
31. Bagi, C.M., Miller, S.C. Effect of Estrogen Deficiency on Cancellous and Cortical Bone Structure and Strength of the Femoral Neck in Rats. Calcified Tissue International 1997 61:336-344.
32. Turner, C.H., Burr, D. B. Basic Biomechanical Measurements of Bone: A Tutorial. Bone 1993 14:595-608.

33. Allen, M.R., Reinwald, S., Burr, D.B. Alendronate Reduces Bone Toughness of Ribs without Significantly Increasing Microdamage Accumulation in Dogs Following 3 Years of Daily Treatment. Calcified Tissue International 2008 82:354-360.
34. Mashiba, T., Hirano, T., Turner, C.H., Forwood, M.R., Johnston, C.C., Burr, D.B. Suppressed Bone Turnover by Bisphosphonates Increases Microdamage Accumulation and Reduces Some Biomechanical Properties in Dog Rib. Journal of Bone and Mineral Research 2000 15:613-620.
35. Jamsa, T., Jalovaara, P. Femoral Neck Strength of Mouse in Two Loading Configurations: Method Evaluation and Fracture Characteristics. Journal of Biomechanics 1998 31:723-729.
36. Courtney, A.C., Hayes, W. C. Age-Related Reductions in the Strength of the Femur Tested in a Fall-Loading Configuration. Journal of Bone & Joint Surgery 1995 77:387-395.
37. Carpenter, R.D., LeBlanc, A.D., Evans, H., Sibonga, J.D., Lang, T.F. Long-Term Changes in the Density and Structure of the Human Hip and Spine After Long-Duraction Spaceflight. Acta stronautica 2010 67:71-81.
38. Martin, R.B. Effects of Simulated Weightlessness on Bone Properties in Rats. Journal of Biomechanics 1990 23(10):1021-1029.
39. Lang, T.F., Lu, Y. Adaptation of the Proximal Femur to Skeletal Reloading After Long-Duration Spaceflight. Journal of Bone and Mineral Research 2006 21:1224-1230.
40. Keyak, J.H., Koyama, A.K., LeBlanc, A., Lu, Y., Lang, T.F. Reduction in Proximal Femoral Strength Due to Long-Duration Spaceflight. Bone 2009 44:449-453.
41. Keyak, J.H., Skinner, H.B., Fleming, J.A. Effect of Force Direction on Femoral Fracture Load for Two Types of Loading Conditions. Journal of Orthopaedic Research 2001 19:539-544.

42. Jamsa, T., Tuukkanen, J. Femoral Neck Is a Sensitive Indicator of Bone Loss in Immobilized Hind Limb of Mouse. Journal of Bone and Mineral Research 1999 14:1708-1713.
43. Kodama, Y., Matsumoto, T. Inhibition of Bone Resorption by Pamidronate Cannot Restore Normal Gain in Cortical Bone Mass and Strength in Tail-Suspended Rapidly Growing Rats. Journal of Bone and Mineral Research 1997 12:1058-1067.
44. Allen, M.R., Hogan, H.A., Bloomfield, S.A. Differential bone and muscle recovery following hindlimb unloading in skeletally mature male rats. Journal of Musculoskeletal Neuronal Interactions 2006 6(3):217-225.
45. LeBlanc A., R., R., Schneider, V., Evans, H., Hedrick, T. Regional Muscle Loss After Short Duration Spaceflight. Aviation Space and Environmental Medicine 1995 66:1151-1154.
46. Fitts, R., Riley, D., Widrick, J. Physiology of a Microgravity Evironment Invited Review: Microgravity and Skeletal Muscle. Journal of Applied Physiology 2000 89:823-839.
47. Perrien, D.S., Akel, N.S., Dupont-Versteegden, E.D., Skinner, R.A., Siegel, E.R., Suva, L.J., Gaddy, D. Aging Alters the Skeletal Response to Disuse in the Rat. Am J Physiol Regul Integr Comp Physiol 2007 292:R988-R996.
48. Thomsen, J.S., Viidik, A. Influence of Physical Exercise and Food Restriction on the Biomechanical Properties of the Femur of Ageing Male Rats. Gerontology 2008 54:32-39.
49. Dehority, W.M.-H.E. Bone and Hormonal Changes Induced by Skeletal Unloading in the Mature Male Rat. American Journal of Physiology 1999 276:E62-E69.
50. Jaworski, Z., Uhthoff, H. Reversibility of Non-Traumatic Disuse Osteoporosis During its Active Phase. Bone 1986 7:431-439.

51. Cheng, X.G., Dequeker, J. Assessment of the Strength of Proximal Femur In Vitro: Relationship to Femoral Bone Mineral Density and Femoral Geometry. Journal of Bone 1997 20(3):213-218.
52. LeBlanc, A., Lin C., Shackelford, L., Sinitsyn, V., Evans, H., Belichenko, O., Schenkman, B., Kozlovskaya, I., Oganov, V., Bakulin, A., Hedrick, T., Feeback, D. Muscle Volume, MRI Relaxation Times (T2), and Body Composition After Spaceflight. Journal of Applied Physiology 2000 89:2158-2164.
53. McCarthy, I., Goodship, A., Herzog, R., Oganov, V., Sussi, E., Vahlensieck, M. Investigation of Bone Changes in Microgravity During Long and Short Duration Space Flight: Comparison of Techniques. European Journal of Clinical Investigation 2000 30:1044-1054.
54. Kupke, J.S. Characterization of the Femoral Neck Region's Response to the Rat Hindlimb Unloading Model Through Tomographic Scanning, Mechanical Testing and Estimated Strengths Biomedical Engineering, 2010 vol. Master of Science. Texas A&M University, College Station.
55. Davis, J.M. Characterization of the Bone Loss and Recovery Response at the Distal Femur Metaphysis of the Adult Male Hindlimb Unloaded Rat Mechanical Engineering, 2011 vol. Master of Science. Texas A&M University, College Station.
56. Cory, E., Nazarian, A., Vahid, E., Vartanians, V., Muller, R., Snyder, B.D. Compressive Axial Mechanical Properties of Rat Bones as Functions of Bone Volume Fraction, Apparent Density and Micro-CT Based Mineral Density. Journal of Biomechanics 2010 43:953-960.
57. Sogaard, C.H., Mosekilde, L. Long-Term Exercise of Young and Adult Female Rats: Effect on Femoral Neck Biomechanical Competence and Bone Structure. Journal of Bone and Mineral Research 1994 9(3):409-416.

APPENDIX A: LEFT FEMORAL NECK DENSITOMETRIC RESULTS

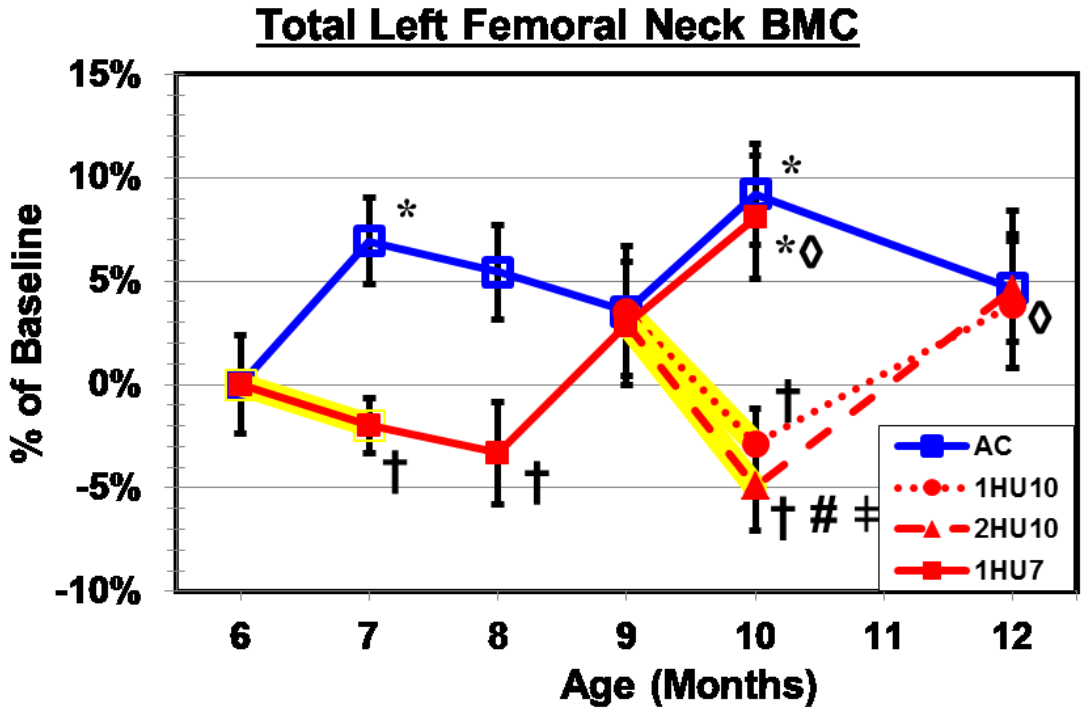

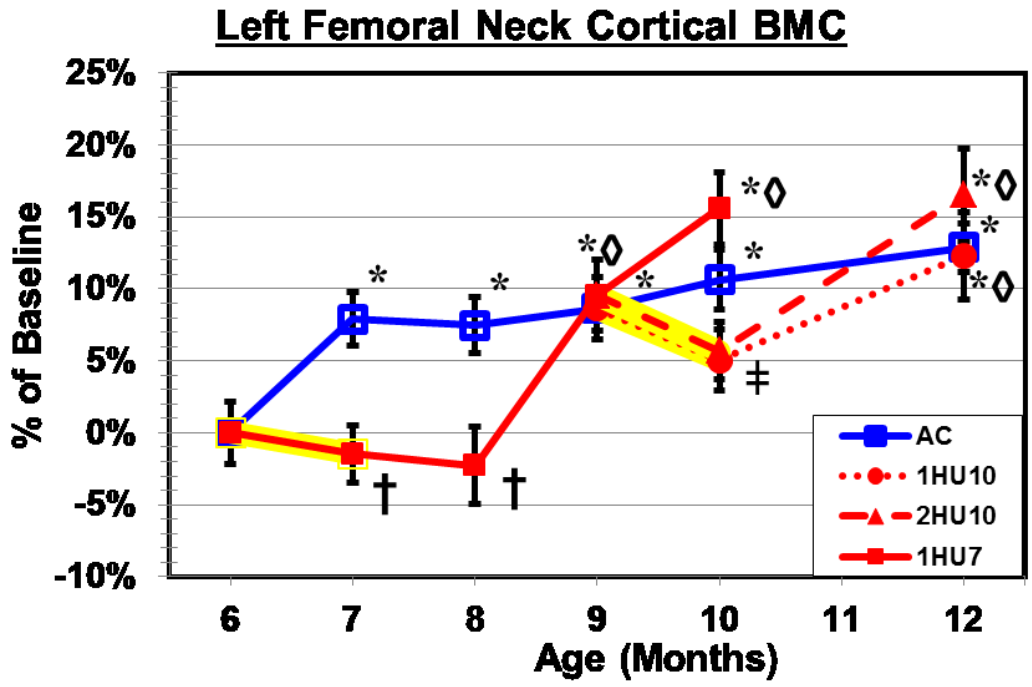

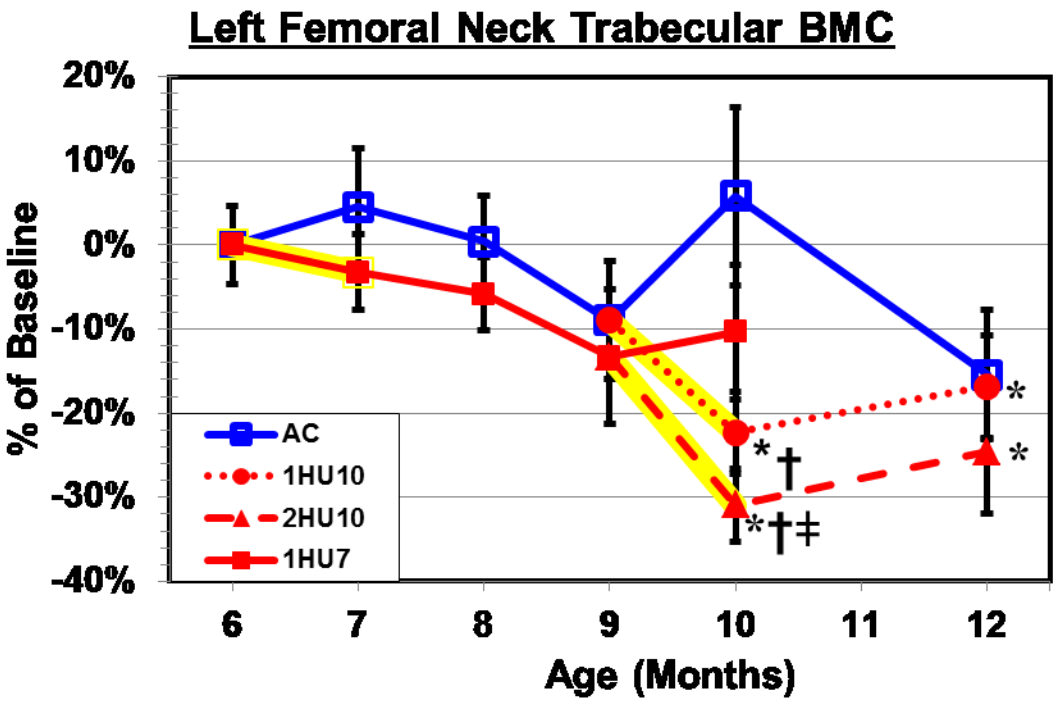
Left Femoral Neck Trabecular BMC
20%
10%
0%
-10%
-20%
-30%
-40%
% of Baseline
6
7
8
9
10
11
12
Age (Months)
AC
1HU10
2HU10
1HU7
*
*†
*†‡
*
*

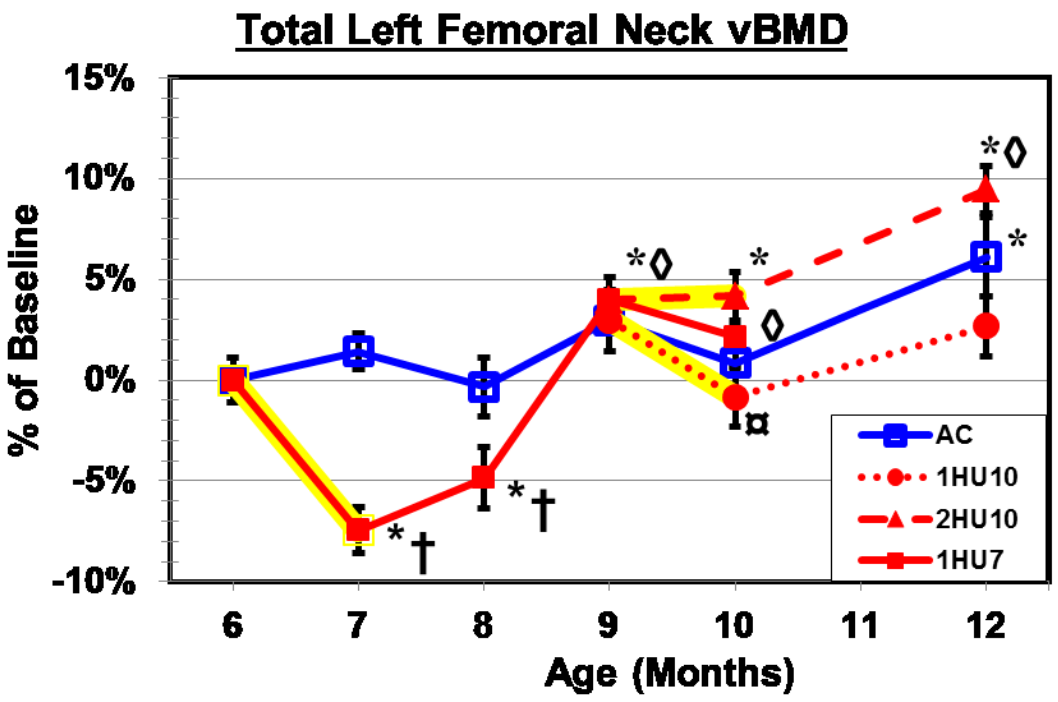
Total Left Femoral Neck vBMD
15%
10%
5%
0%
-5%
-10%
% of Baseline
6
7
8
9
10
11
12
Age (Months)
AC
1HU10
2HU10
1HU7
*†
*†
*◊
*
◊
¤
*◊
*

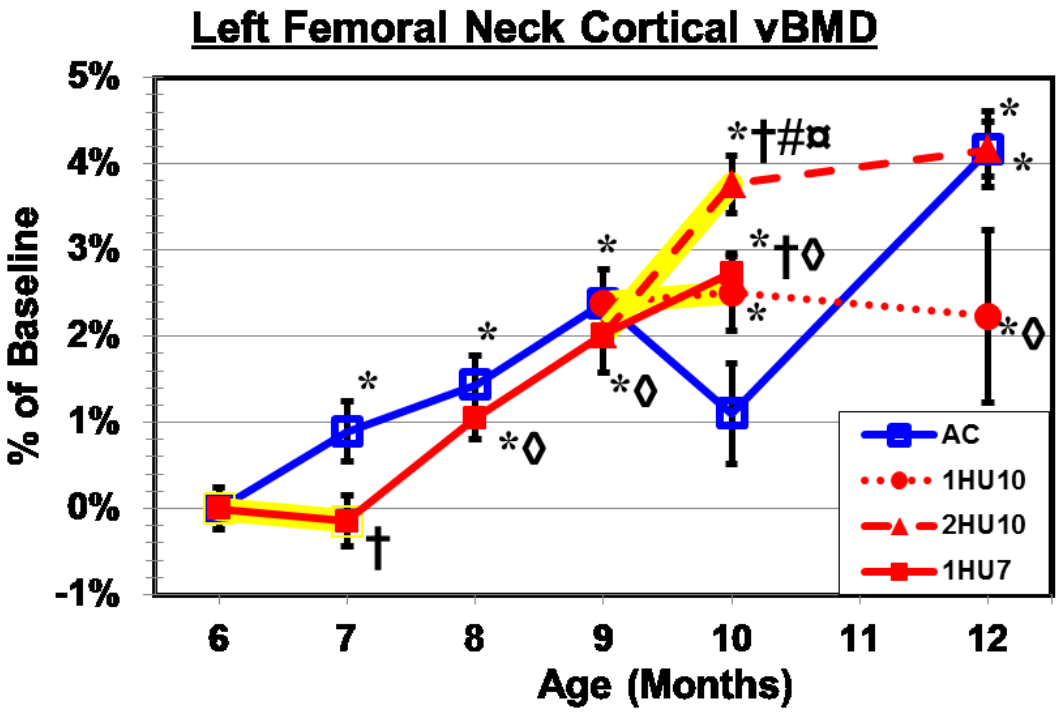
Left Femoral Neck Cortical vBMD
% of Baseline
5%
4%
3%
2%
1%
0%
-1%
6
7
8
9
10
11
12
Age (Months)
AC
1HU10
2HU10
1HU7

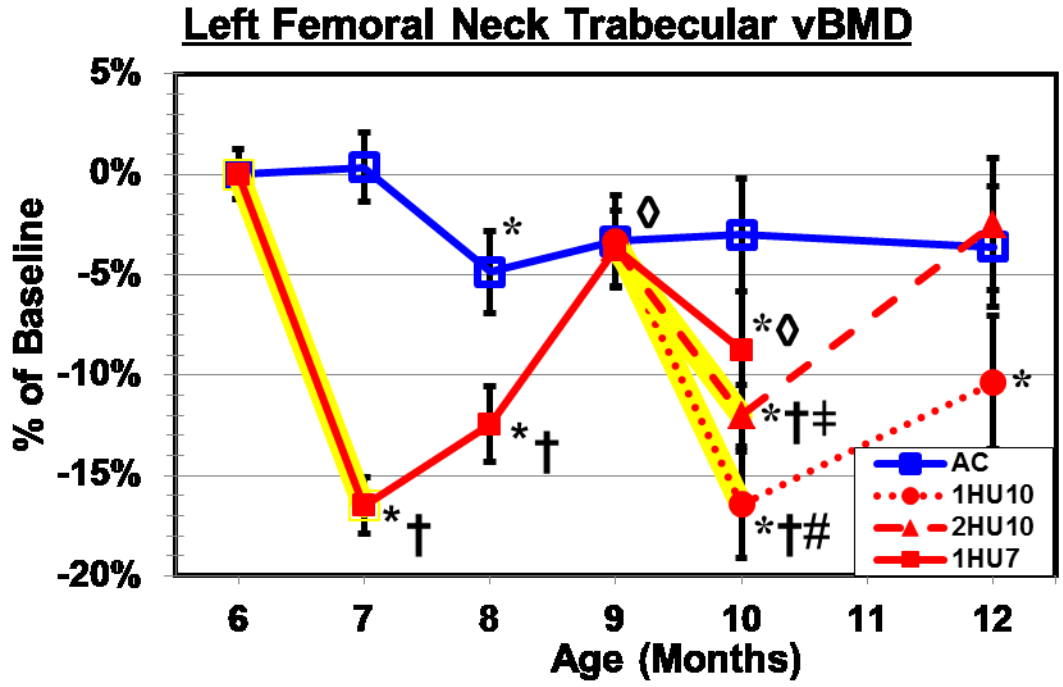
Left Femoral Neck Trabecular vBMD
% of Baseline
5%
0%
-5%
-10%
-15%
-20%
6
7
8
9
10
11
12
Age (Months)
AC
1HU10
2HU10
1HU7

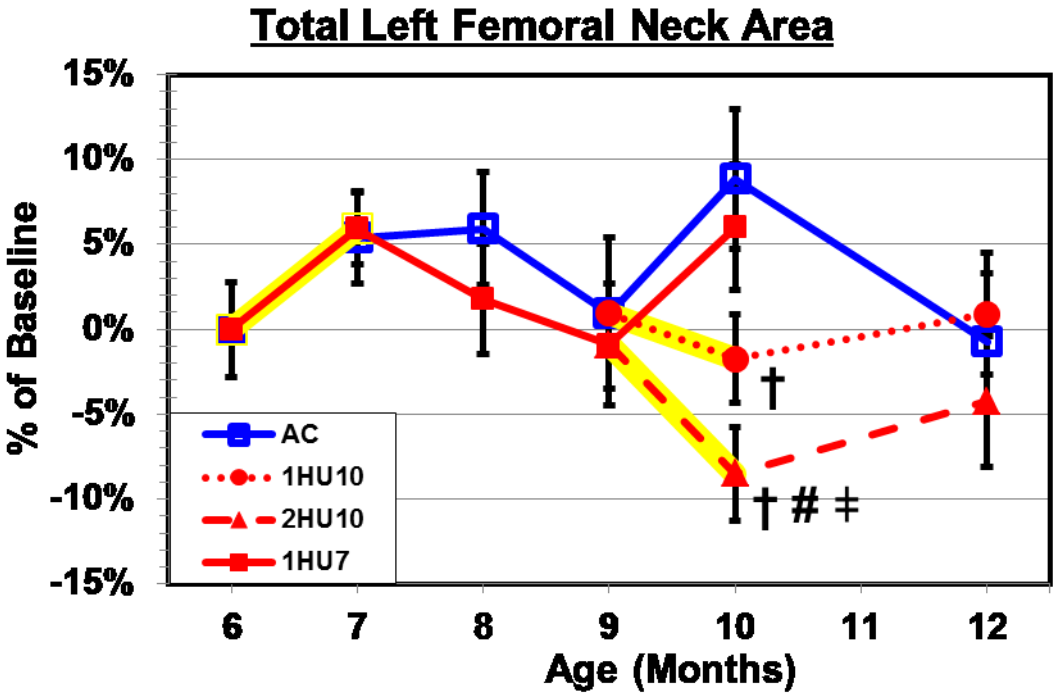
Total Left Femoral Neck Area
15%
10%
5%
0%
-5%
-10%
-15%
% of Baseline
AC
1HU10
2HU10
1HU7
6
7
8
9
10
11
12
Age (Months)

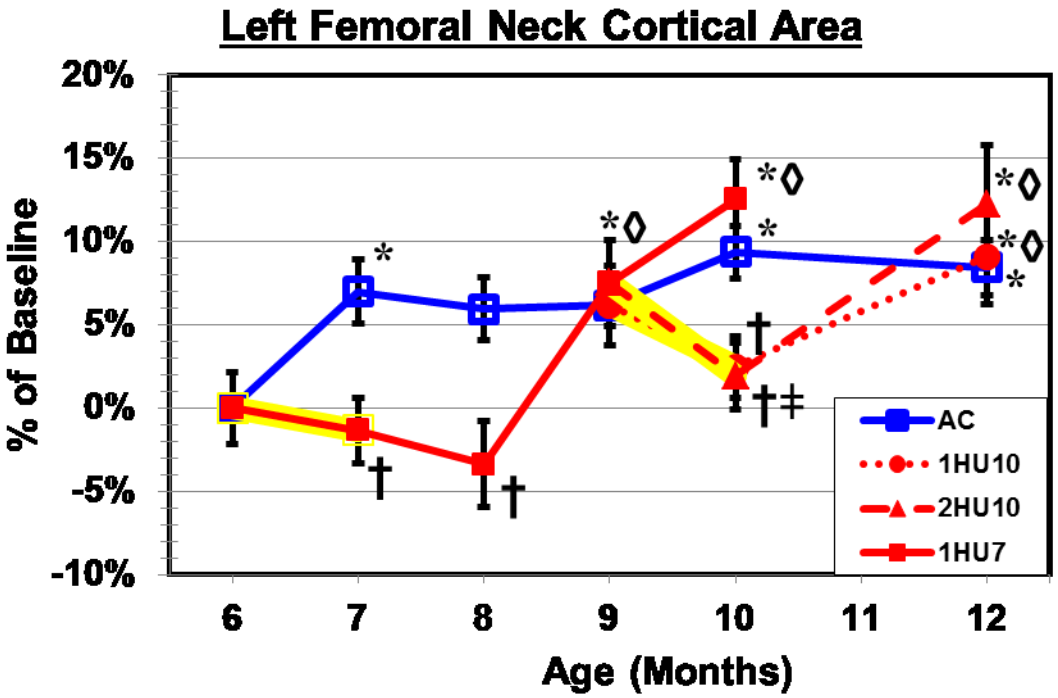
Left Femoral Neck Cortical Area
20%
15%
10%
5%
0%
-5%
-10%
% of Baseline
AC
1HU10
2HU10
1HU7
6
7
8
9
10
11
12
Age (Months)

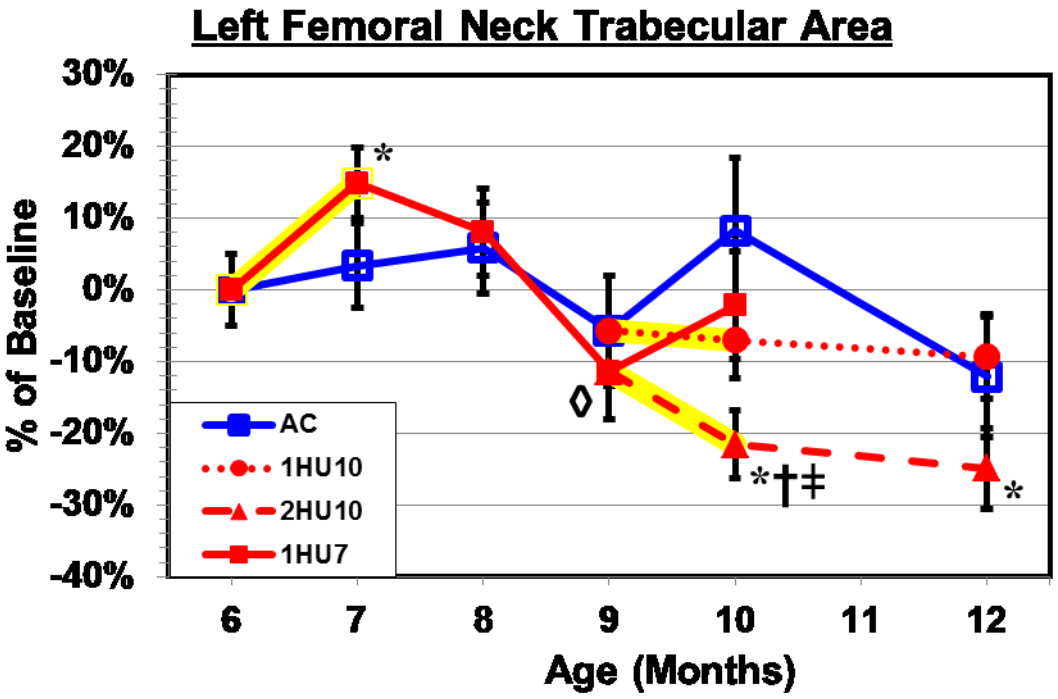
Left Femoral Neck Trabecular Area
30%
20%
10%
0%
-10%
-20%
-30%
-40%
% of Baseline
6
7
8
9
10
11
12
Age (Months)
AC
1HU10
2HU10
1HU7

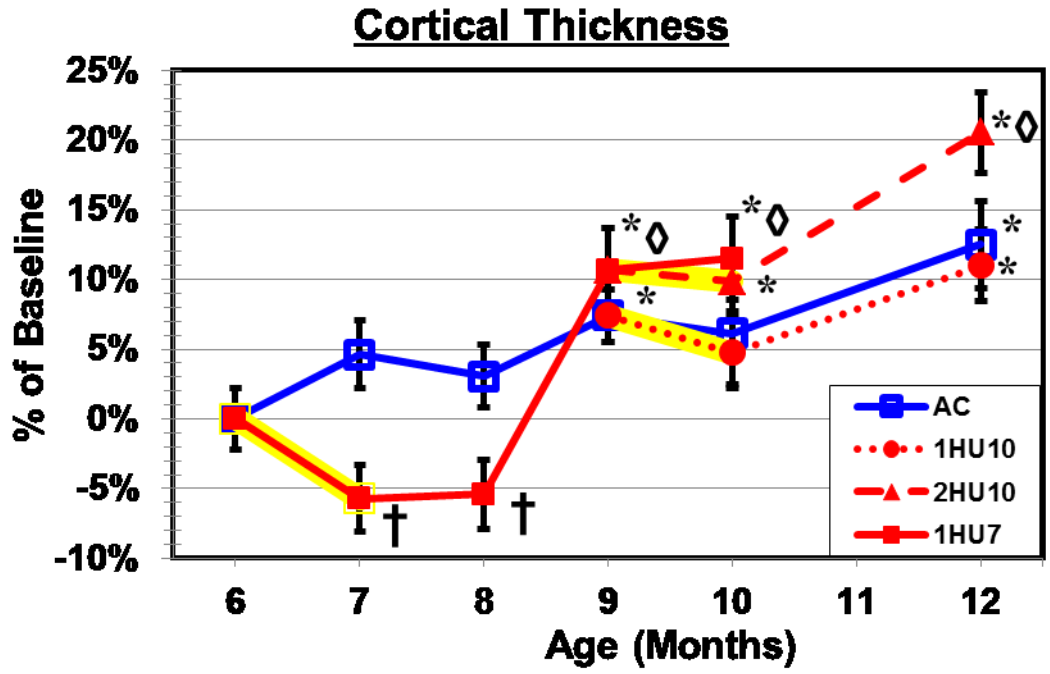
Cortical Thickness
25%
20%
15%
10%
5%
0%
-5%
-10%
% of Baseline
6
7
8
9
10
11
12
Age (Months)
AC
1HU10
2HU10
1HU7

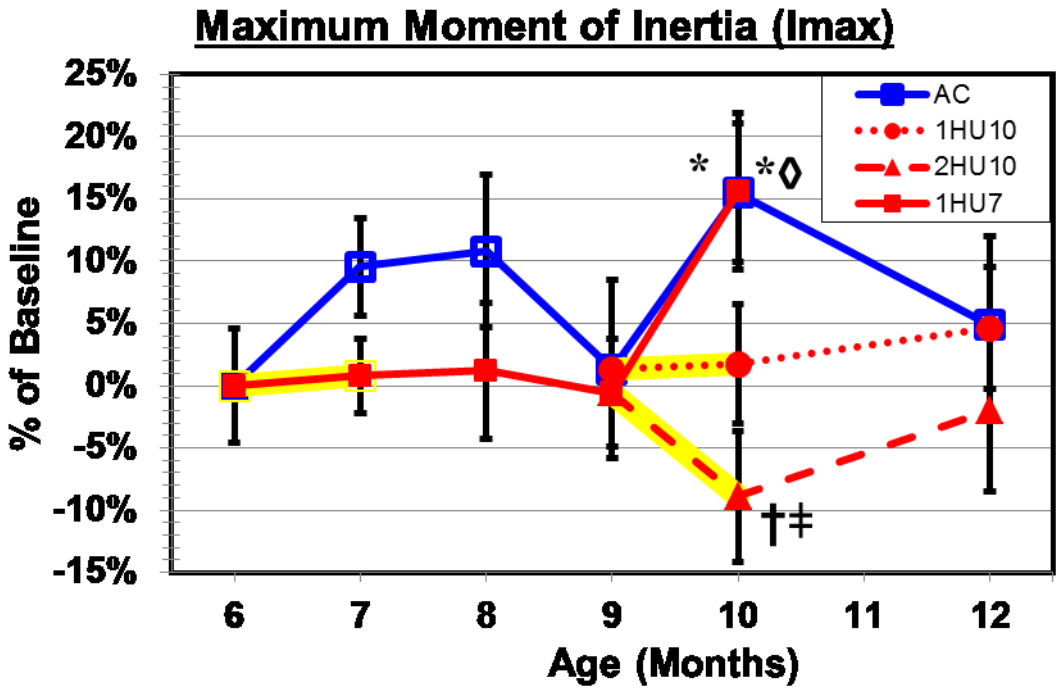
Maximum Moment of Inertia (Imax)
% of Baseline
25%
20%
15%
10%
5%
0%
-5%
-10%
-15%
6
7
8
9
10
11
12
Age (Months)
AC
1HU10
2HU10
1HU7
*
*◊
†‡

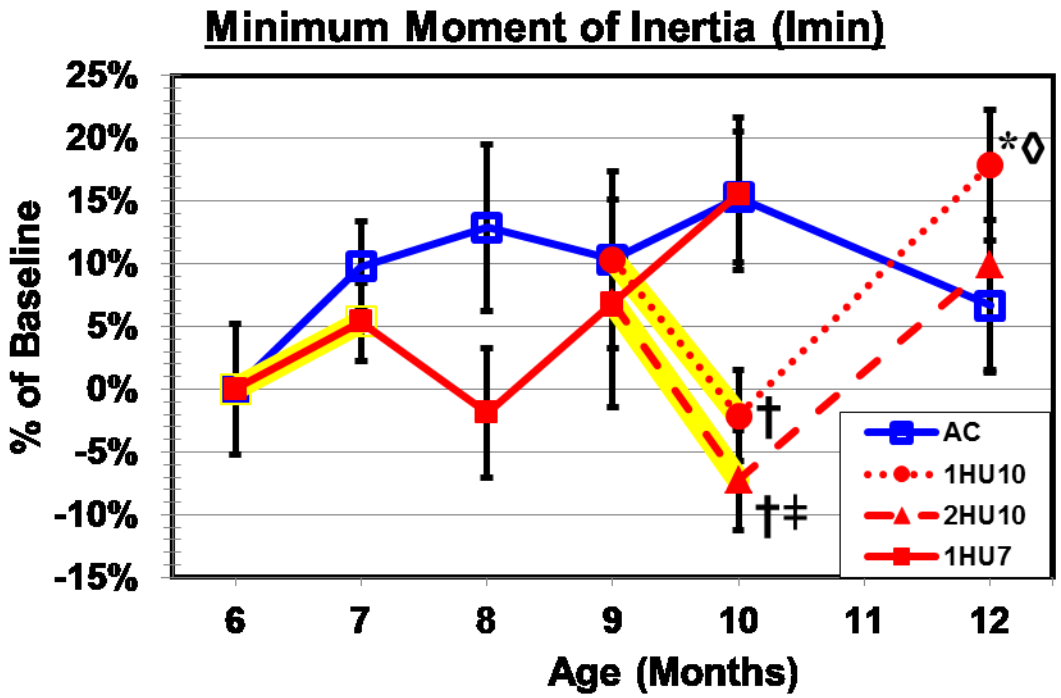
Minimum Moment of Inertia (Imin)
% of Baseline
25%
20%
15%
10%
5%
0%
-5%
-10%
-15%
6
7
8
9
10
11
12
Age (Months)
AC
1HU10
2HU10
1HU7
*◊
†
†‡

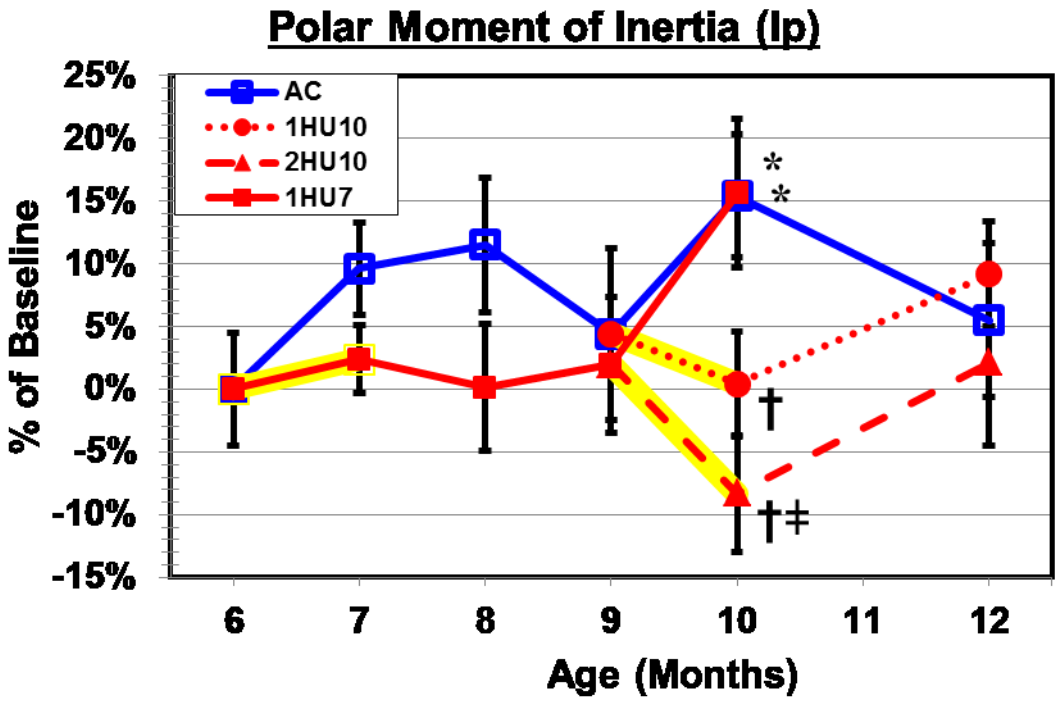
Polar Moment of Inertia (Ip)
25%
20%
15%
10%
5%
0%
-5%
-10%
-15%
% of Baseline
AC
1HU10
2HU10
1HU7
*
*
†
†‡
6
7
8
9
10
11
12
Age (Months)

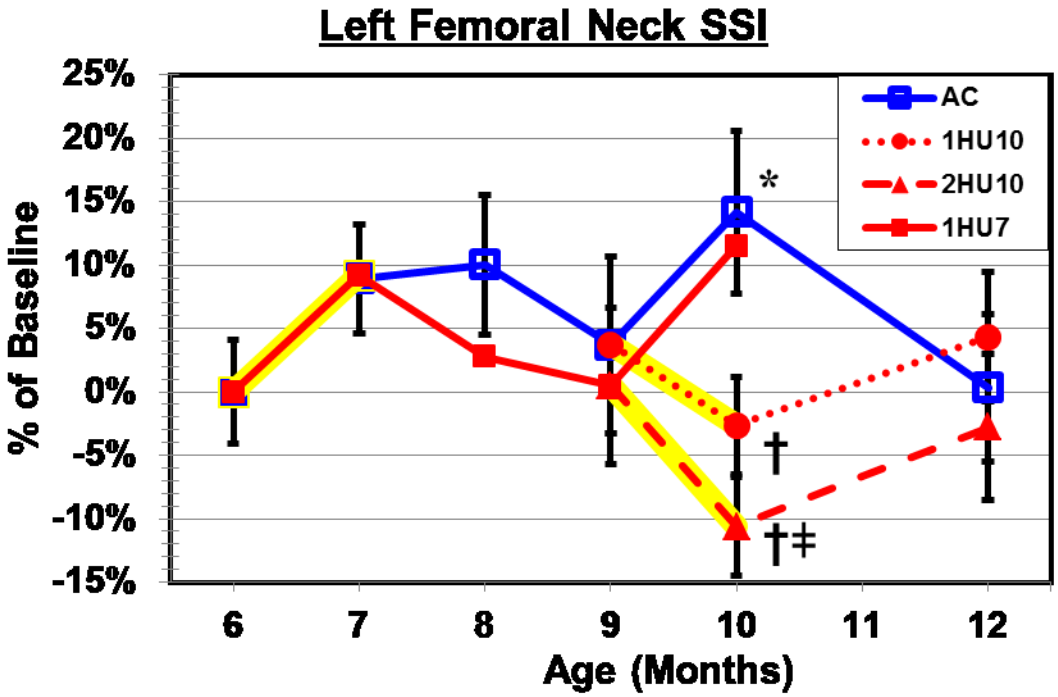
Left Femoral Neck SSI
25%
20%
15%
10%
5%
0%
-5%
-10%
-15%
% of Baseline
AC
1HU10
2HU10
1HU7
*
†
†‡
6
7
8
9
10
11
12
Age (Months)

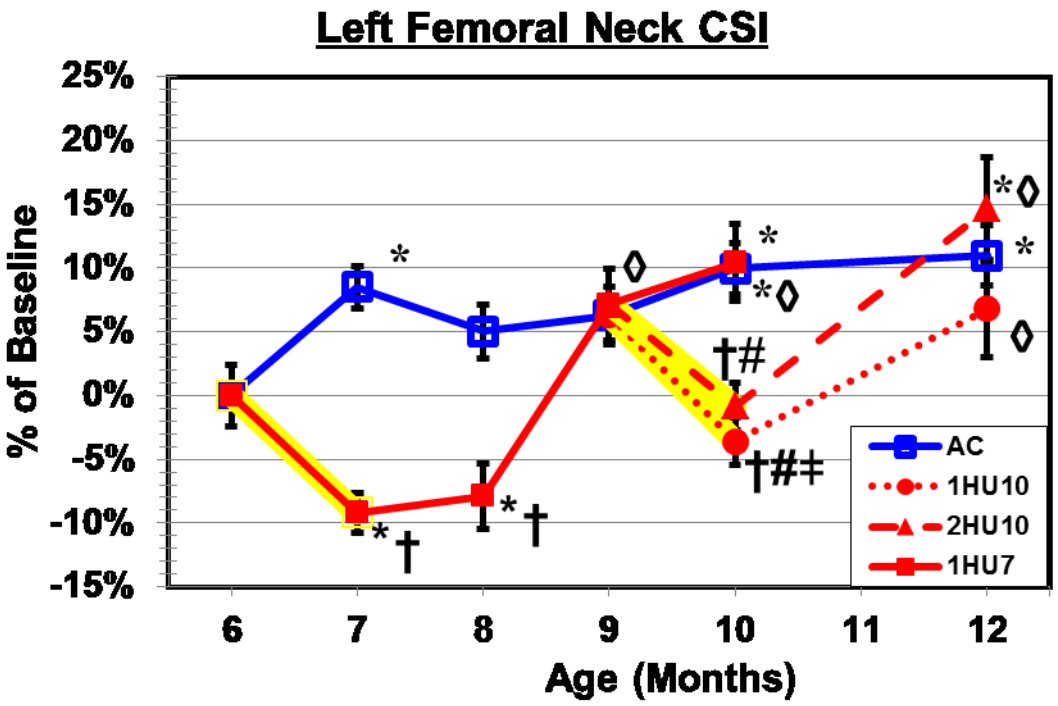
Left Femoral Neck CSI
25%
20%
15%
10%
5%
0%
-5%
-10%
-15%
% of Baseline
6
7
8
9
10
11
12
Age (Months)
AC
1HU10
2HU10
1HU7

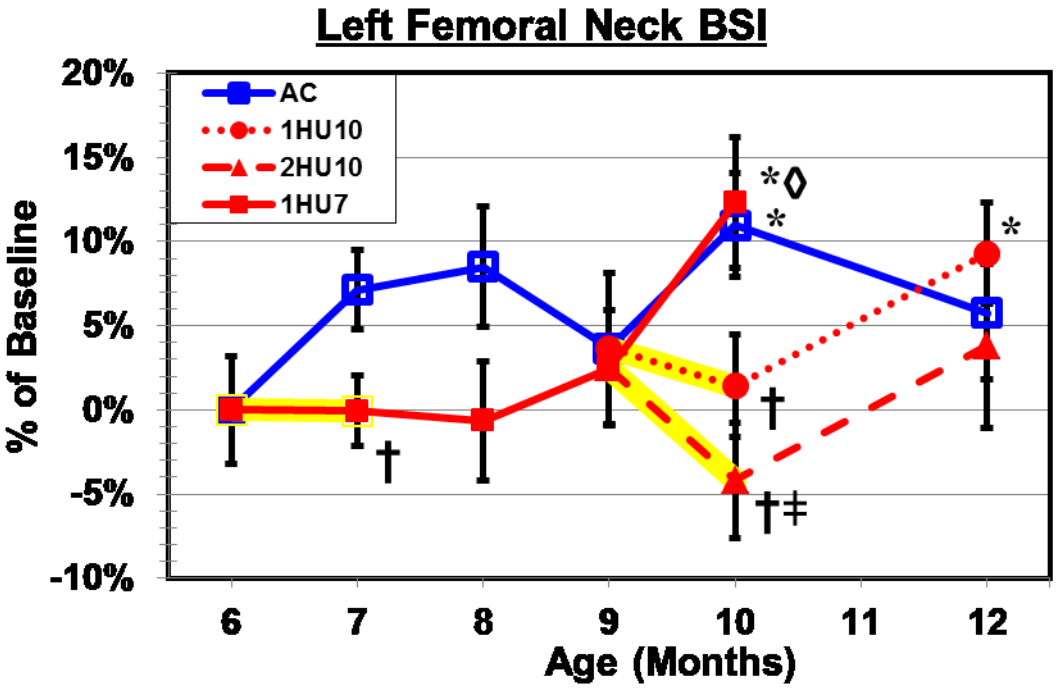
Left Femoral Neck BSI
20%
15%
10%
5%
0%
-5%
-10%
% of Baseline
6
7
8
9
10
11
12
Age (Months)
AC
1HU10
2HU10
1HU7

APPENDIX B: AXIAL V. LATERAL COMPARISONS

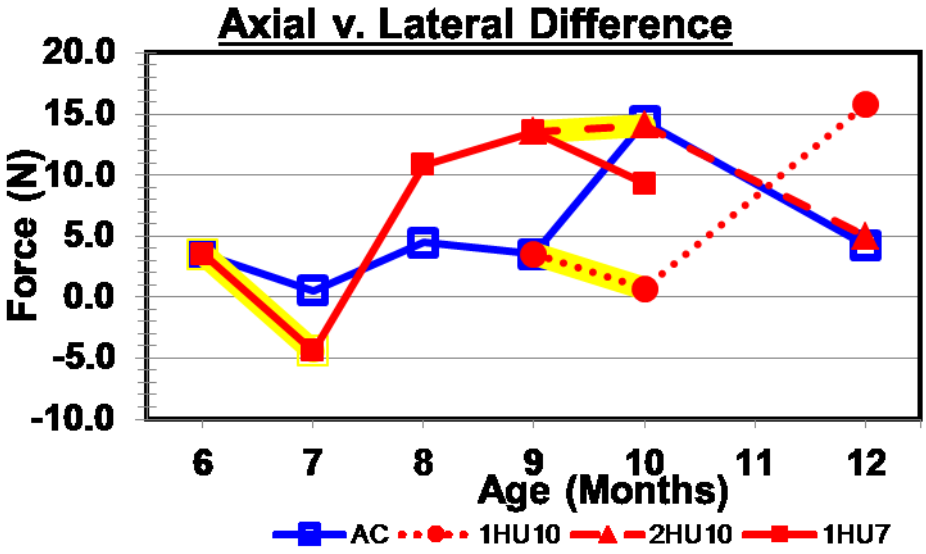

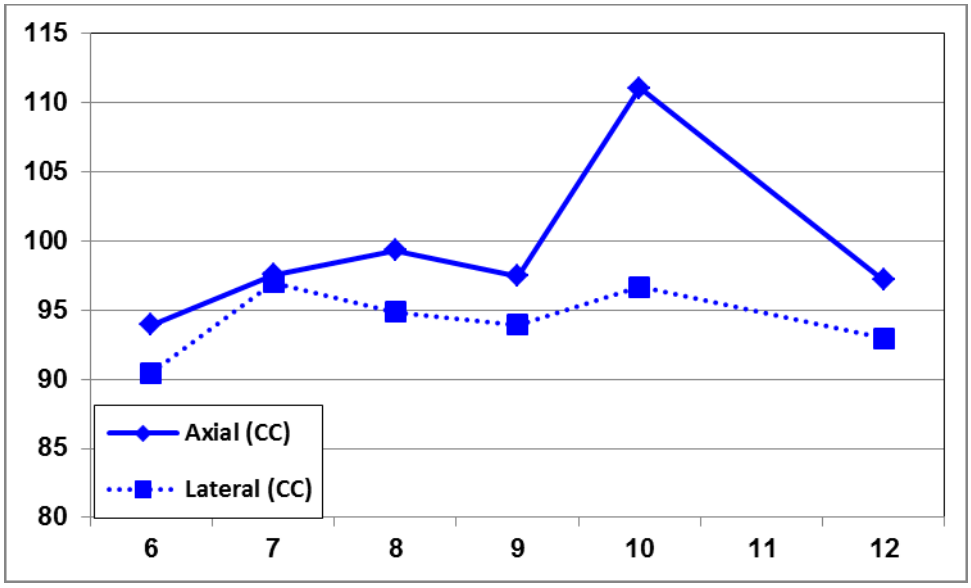

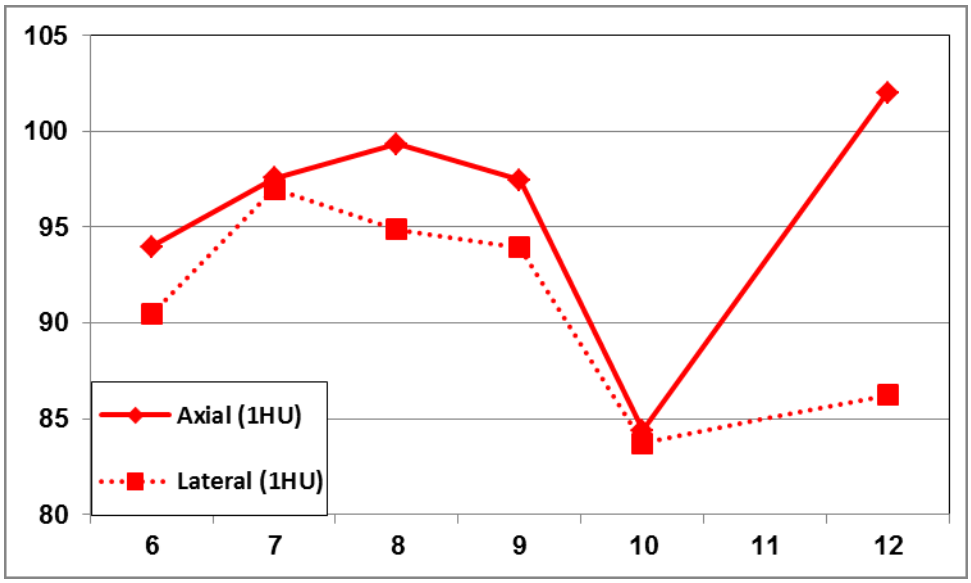
105
100
95
90
85
80
6
7
8
9
10
11
12
Axial (1HU)
Lateral (1HU)

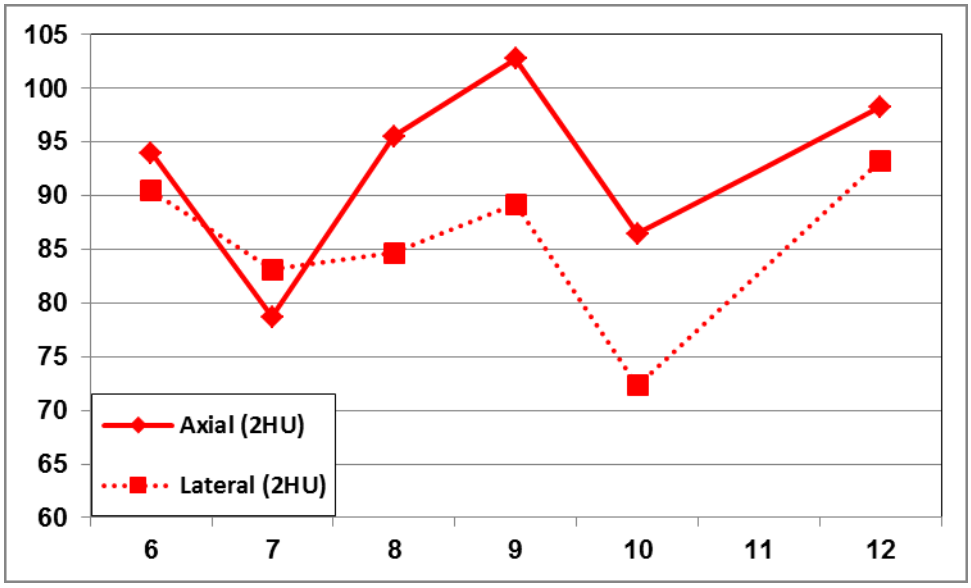
105
100
95
90
85
80
75
70
65
60
6
7
8
9
10
11
12
Axial (2HU)
Lateral (2HU)

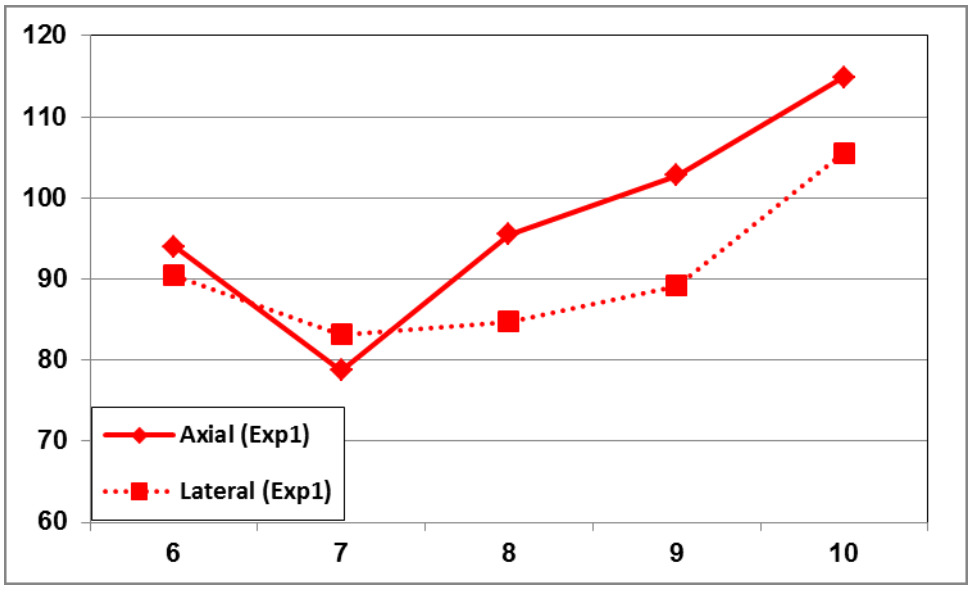
120
110
100
90
80
70
60
6
7
8
9
10
Axial (Exp1)
Lateral (Exp1)

APPENDIX C: SAMPLE EXCEL FILE GENERATED BY DATMET

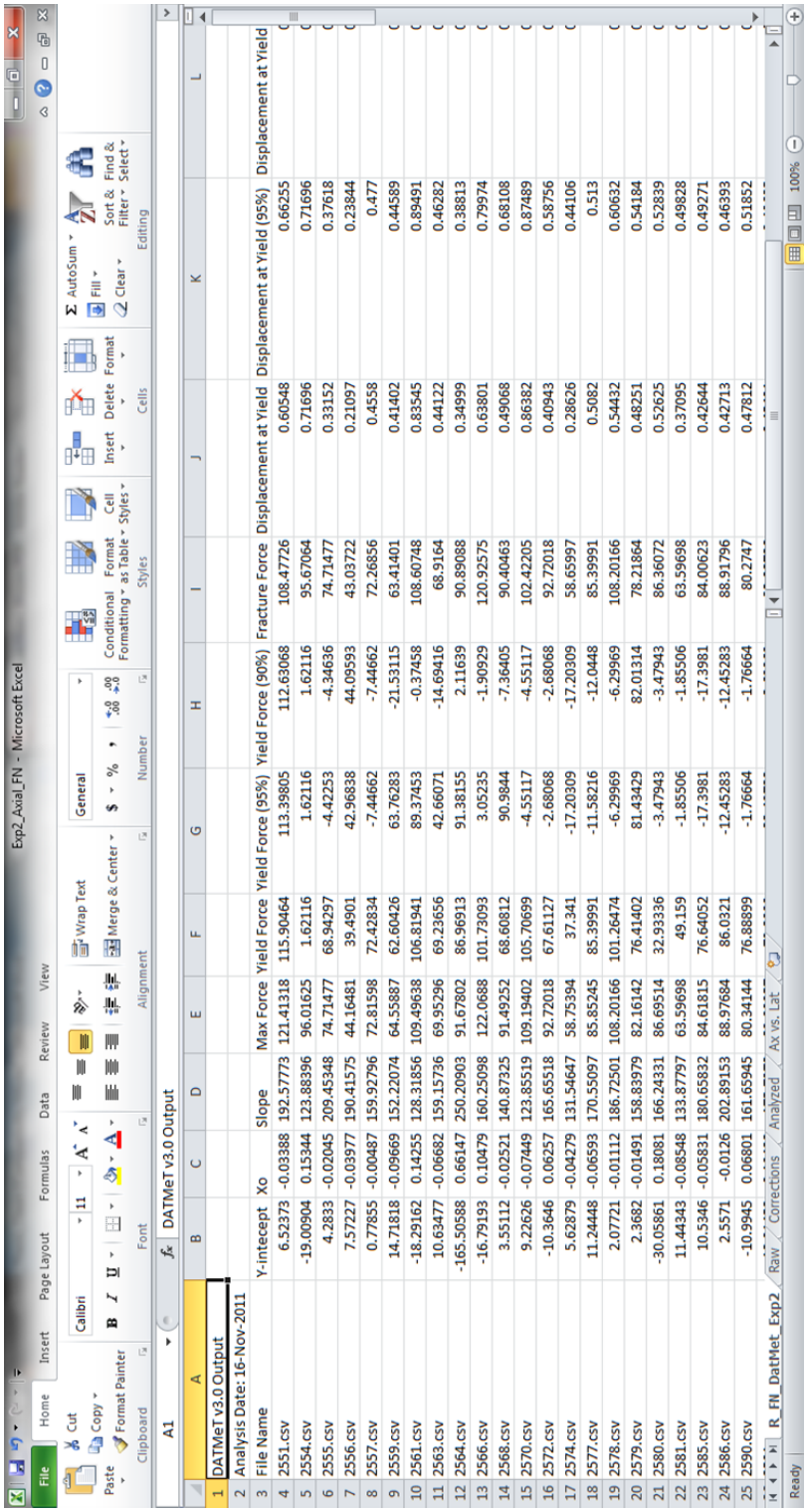

Exp2_Axial_FN - Microsoft Excel

	A	B	C	D	E	F	G	H	I	J	K	L
1	DATMeT v3.0 Output											
2	Analysis Date: 16-Nov-2011											
3	File Name	Y-intecept	Xo	Slope	Max Force	Yield Force	Yield Force (95%)	Yield Force (90%)	Fracture Force	Displacement at Yield	Displacement at Yield (95%)	Displacement at Yield
4	2551.csv	6.52373	-0.03388	192.57773	121.41318	115.90464	113.39805	112.63068	108.47726	0.60548	0.66255	C
5	2554.csv	-19.00904	0.15344	123.88396	96.01625	1.62116	1.62116	1.62116	95.67064	0.71696	0.71696	C
6	2555.csv	4.2833	-0.02045	209.45348	74.71477	68.94297	-4.42253	-4.34636	74.71477	0.33152	0.37618	C
7	2556.csv	7.57227	-0.03977	190.41575	44.16481	39.4901	42.96838	44.09593	43.03722	0.21097	0.23844	C
8	2557.csv	0.77855	-0.00487	159.92796	72.81598	72.42834	-7.44662	-7.44662	72.26856	0.4558	0.477	C
9	2559.csv	14.71818	-0.09669	152.22074	64.55887	62.60426	63.76283	-21.53115	63.41401	0.41402	0.44589	C
10	2561.csv	-18.29162	0.14255	128.31856	109.49638	106.81941	89.37453	-0.37458	108.60748	0.83545	0.89491	C
11	2563.csv	10.63477	-0.06682	159.15736	69.95296	69.23656	42.66071	-14.69416	68.9164	0.44122	0.46282	C
12	2564.csv	-165.50588	0.66147	250.20903	91.67802	86.96913	91.38155	2.11639	90.89088	0.34999	0.38813	C
13	2566.csv	-16.79193	0.10479	160.25098	122.0688	101.73093	3.05235	-1.90929	120.92575	0.63801	0.79974	C
14	2568.csv	3.55112	-0.02521	140.87325	91.49252	68.60812	90.9844	-7.36405	90.40463	0.49068	0.68108	C
15	2570.csv	9.22626	-0.07449	123.85519	109.19402	105.70699	-4.55117	-4.55117	102.42205	0.86382	0.87489	C
16	2572.csv	-10.3646	0.06257	165.65518	92.72018	67.61127	-2.68068	-2.68068	92.72018	0.40943	0.58756	C
17	2574.csv	5.62879	-0.04279	131.54647	58.75394	37.341	-17.20309	-17.20309	58.65997	0.28626	0.44106	C
18	2577.csv	11.24448	-0.06593	170.55097	85.85245	85.39991	-11.58216	-12.0448	85.39991	0.5082	0.513	C
19	2578.csv	2.07721	-0.01112	186.72501	108.20166	101.26474	-6.29969	-6.29969	108.20166	0.54432	0.60632	C
20	2579.csv	2.3682	-0.01491	158.83979	82.16142	76.41402	81.43429	82.01314	78.21864	0.48251	0.54184	C
21	2580.csv	-30.05861	0.18081	166.24331	86.69514	32.93336	-3.47943	-3.47943	86.36072	0.52625	0.52839	C
22	2581.csv	11.44343	-0.08548	133.87797	63.59698	49.159	-1.85506	-1.85506	63.59698	0.37095	0.49828	C
23	2585.csv	10.5346	-0.05831	180.65832	84.61815	76.64052	-17.3981	-17.3981	84.00623	0.42644	0.49271	C
24	2586.csv	2.5571	-0.0126	202.89153	88.97684	86.0321	-12.45283	-12.45283	88.91796	0.42713	0.46393	C
25	2590.csv	-10.9945	0.06801	161.65945	80.34144	76.88899	-1.76664	-1.76664	80.2747	0.47812	0.51852	C

Sheet tabs: R_FN_DatMet_Exp2 | Raw | Corrections | Analyzed | Ax vs. Lat

VITA

Name:	Derrick Scott Morgan
Address:	Department of Mechanical Engineering 3123 TAMU College Station, TX 77843, C/O Dr. Harry Hogan
Email Address:	dscottmorgan84@gmail.com
Education:	B.S., Mechanical Engineering, Baylor University 2007 M.S., Biomedical Engineering, Baylor University 2009